A CORRECTION METHOD FOR COINCIDENCE LOSSES IN NEUTRON ACTIVATION ANALYSIS WITH SHORT-LIVED NUCLIDES

NIMALASIRI K. DESILVA

The thing that teases the mind over and over for years, at last gets itself put down rightly on paper - whether little or great, it belongs to Literature.

- Sarah Orne Jewett

DEDICATION

To my late parents,

and

to Shantha

ABSTRACT

Development of instrumental neutron activation analysis (INAA) methods for simultaneous determination of multielement concentrations is reported in this thesis. Emphasis is placed on the use of short-lived nuclides.

A correction method for count losses (coincidence losses) due to both *analyser dead-time* and *pulse pile-up* in gamma-ray spectrometry of short-lived nuclides was developed. The method consists of simultaneous measurements of two time variables using a multichannel scaler: the ADC dead-time and the total count rate at the single channel analyser output of the ADC. This correction method was successfully applied to nuclides with half-lives as short as 0.72 *s* (^{38m}Cl) at rapidly varying initial total count rates as high as 60,000 *cps*.

A pseudo-cyclic INAA (PCINAA) method which can be used to improve the sensitivity of short- and medium-lived nuclides with half-lives longer than approximately 10 *s* was developed. An automated rapid cyclic transfer system is described for the measurement of very short-lived (half-life < 10 *s*) activities by cyclic INAA (CINAA). A mathematical formula is proposed and used to correct for coincidence losses in CINAA. This procedure considerably simplifies data manipulation without sacrificing the accuracy.

An epithermal INAA (EINAA) method to reduce interfering activities of thermal neutron activation products is reported. A novel boron shield to cut off thermal neutrons was developed. This shield can be constructed easily in any chemical laboratory and applied advantageously over conventionally used cadmium foils.

Precision and accuracy of the above INAA methods were evaluated by analysing several standard reference materials. These methods were successfully applied to several other matrices of biological and environmental interest. Further improvements are proposed.

Theoretical aspects of the limits in high count rate gamma-ray spectrometry are described.

ACKNOWLEDGEMENTS

Academic satisfaction derived from this thesis was plentiful, frustrations and stresses were as those usually associated with a doctoral thesis. Had not been for the cooperation and assistance of friends and colleagues, this probably would not have been a success. Should I omit mention of any, I owe my apologies to them.

I express my deepest gratitude to Dr. Amares Chatt for all the encouragement and guidance. He was always willing to help me academically or otherwise. It was a pleasure to work in Dr. Chatt's research group under his able direction and it was a wonderful experience.

Presence of my group members in the lab certainly created a friendly and a pleasant atmosphere to work.

Assistance of Dr. Robert Guy and helpful discussions with Dr. James A. Pincock are highly appreciated.

The successful use of electronic circuitry in this thesis work is mostly attributed to the excellent course instructions of Dr. Louis Ramaley and Dr. A. Simpson.

I thank Dr. Jiri Holzbecher, Dr. D.C. Stuart, Mr. David Read and Mrs. Diedry Brooks for sample irradiation work, again Dr. Holzbecher for helpful discussions.

Dr. C.S. Tse's voluntary assistance in computer work was invaluable.

Machine shop instructions of Reg, cooperation and assistance of Jurgen, Chris and stock room staff are appreciated.

I would also like to thank Dr. R. Shaw and Mr. C. Wiseman, Environment Protection Service, Halifax, and Mr. P.J. Leblanc, Nova Scotia Power Corporation for providing me with samples. Volutary assistance of Mr. Dwight Veinot and Danny Morehouse, Defence Research Laboratory, Halifax, is appreciated.

It is a pleasure to acknowledge fellowship of close friend Dr. Palitha Wickramanayake. Long and close association with Palitha during my graduate and undergraduate days has been beneficial.

I am indebted to my brothers and sisters who looked after me in all respects during my early education without whom graduate studies would have only been a dream.

My wife Shantha's never ending patience and comments contributed in large to the successful completion of this thesis. Amidst her own studies she found the time and did the painful job of typing the entire thesis. She was also successful in pulling me out of frustrated moments.

Finally, I gratefully acknowledge the Izaak Walton Killam and Dalhousie University Graduate Fellowships. This research was supported by NSERC and AES, Environment Canada funds.

TABLE OF CONTENTS

CHAPTER VII

LIST OF FIGURES

Figure Page

LIST OF TABLES

Table Page

Table | Page

LIST OF SYMBOLS

A - activity after a decay time

A_o - initial absolute activity

ADC - analog to digital converter

AF - advantage factor

b - barns

C - measured number of counts

C_o - number of counts expected (free of losses)

CR - cadmium ratio

d - dead-time per pulse

DT - fractional dead-time

DUSR - Dalhousie University Slowpoke Reactor

E - energy

eV - electron volt

f - frequency

FL_d - fractional loss due to dead-time

FL_p - fractional loss due to pile-up

FU_p - fraction of undistorted pulses

Hz - hertz

i - channel number

I - resonance integral

K - dead-time and pile-up correction factor

K_c - correction factor for coincidence losses for cumulative counts

K_d - dead-time correction factor (C/C_o)

K_n - correction factor for coincidence losses for nth cycle

K_p - pile-up correction factor

m - mass of element

M - atomic mass

MCS - multichannel scaler

n - number of cycles, number of pulses, neutrons

N - measured total number of counts

p - probability

P_o - true photopeak count rate

PHA - pulse height analyser

psi - pounds per square inch

R - regression coefficient

R - measured count rate

R_a - output count rate of the amplifier

R_o - absolute input count rate

R_s - output count rate at single channel analyser output of ADC

SCA OUT - single channel analyser output of ADC

T - cycle period

$t_{\frac{1}{2}}$ - half-life

t_c - count time (clock time)

t_d - decay time

t_{dead} - dead-time

t_i - irradiation time

t_l - live-time

t_s - set count time

v - velocity

ϕ - neutron flux

ε - detector efficiency

λ - decay constant

μ_B - background counts

θ - isotopic abundance

σ - cross-section

τ - pulse resolving time

CHAPTER I

INTRODUCTION

Nuclear activation analysis is being continually developed as an analytical technique since the first neutron activation experiment reported by Hevesy and Levi in 1936 (36H1). With the development of high-resolution radiation detectors and computerized multichannel analysers, activation analysis has become a very sensitive analytical tool especially for simultaneous multielement determinations. Increasing popularity of the detection of minute quantities of elements by activation analysis is evidenced by the continuous growth of the number of papers published in the literature. Non-destructive activation analysis using gamma-ray spectroscopy has been applied to various fields such as archaeological, biological, criminological, environmental and geological sciences.

Basically, in activation analysis a sample is irradiated in a flux of elementary particles, such as neutrons, protons, *etc.*, or in radiations such as bremsstrahlung (photons), and the intensity of induced radioactivity is measured with an appropriate detector-analyser system. Various nuclides produced in the sample possess characteristic parameters such as half-life, type and energy of emitted radiation which enable one to perform qualitative as well as quantitative

analyses for more than 70 elements in an equally varied number of matrices.

A. Neutron Activation Analysis (NAA) in General

Among the activation analysis techniques, neutron activation analysis (NAA) is the most common type where neutrons are employed as the bombarding particles to induce radioactivity. With the development of nuclear reactors capable of producing neutron fluxes of the order of 10^{12} to 10^{15} $n\ cm^{-2}\ s^{-1}$, sensitivity of this technique for quantitative determinations of elemental concentrations has been improved to as low as picogram, or parts per trillion levels in some cases.

Neutron activation analysis can be performed in a variety of ways depending on the nature of the background matrix and the nuclides of interest. In some cases, the element of interest is concentrated from an interfering matrix prior to irradiation with neutrons; the technique is then termed as preconcentration neutron activation analysis (PNAA). In opposite instances, the irradiation is followed by a chemical separation of the desired element; this procedure is then known as radiochemical neutron activation analysis (RNAA). Application of these techniques to natural matrices involves a number of steps such as digestion of the sample followed by wet chemical separations. Therefore, both PNAA and RNAA are time-consuming and hence inconvenient for routine analysis. Furthermore, in RNAA special precautions (such as addition of carriers) have to be taken in order

to correct for errors due to loss of the elements of interest whereas PNAA does not take advantage of the capability of *reagent blank free* determinations of NAA. Moreover, RNAA has an added disadvantage of not being able to make use of short-lived nuclides due to relatively long experimental times involved. However, PNAA and RNAA can be very useful for analyzing certain matrices.

In contrast to PNAA and RNAA, non-destructive (*i.e.*, no pre- or post-irradiation chemical separations) or instrumental neutron activation analysis (INAA) technique offers the advantage of multi-element analysis without any physical destruction of the sample by using recently developed high-resolution detectors. When high-resolution Ge(Li) detectors are used, the specificity of INAA is usually excellent as the purity of the nuclide measured can be checked by its characteristic half-life and the energy of the gamma-ray emitted. Thus the primary advantages of INAA over most of the other analytical techniques are its non-destructive nature, freedom from reagent blanks, excellent selectivity and sensitivity, high accuracy and precision, and capability of simultaneous measurement of multielement concentrations.

In recent years, these advantages of INAA have been utilized in developing nuclear analytical methods for solving a diverse type of analytical problems. Several INAA methods have been developed and subsequently applied to study the translocation of trace elements in agricultural (74C1), atmospheric (74G1, 75P1) and aquatic (77E1)

environments.

The basic activation equations are applicable to all types of NAA procedures. The induced activity at the end of an irradiation, A_o, depends on (i) abundance of the target isotope (θ), (ii) cross section (σ), which is a measure of probability for the particular reaction, (iii) decay constant of the nuclide being measured (λ), (iv) flux of bombarding neutrons (ϕ), and (v) irradiation time (t_i). For grams of the element with the atomic mass, M, the induced activity can be given as:

$$A_o = \frac{\phi \sigma m \theta}{M} 6.023 \times 10^{23} (1 - e^{-\lambda t_i}) \qquad \text{I-1}$$

The activity, A, after an elapsed time, t_d, is given by:

$$A = A_o e^{-\lambda t_d} \qquad \text{I-2}$$

Assuming a 100% efficient pulse processor, the number of counts, C, accumulated in the photopeak area within a counting time, t_c, is given by:

$$C = \gamma \varepsilon A \int_0^{t_c} e^{-\lambda t} dt$$

$$= \gamma \varepsilon A (1 - e^{-\lambda t_c}) / \lambda \qquad \text{I-3}$$

Where γ and t_c are the branching ratio of the particular gamma-emission and the efficiency of the detector, respectively. Combining equations

I-1, I-2, and I-3, one obtains:

$$C = \gamma \frac{\varepsilon \phi \sigma m \theta}{\lambda M} 6.023 \times 10^{23} (1 - e^{-\lambda t_i})(e^{-\lambda t_d})(1 - e^{-\lambda t_c}) \quad \text{I-4}$$

By measuring C for known timing parameters, *viz.* t_i, t_d and t_c, the amount of the element present, m, can be calculated. A reliable determination of m requires prior knowledge of accurate values for θ, σ, λ, ϕ and ε. Since these parameters are not generally known with a high degree of accuracy, this absolute activity treatment does not provide a highly reliable value for m.

Quantitative determinations of superior accuracy in NAA are normally done using the *comparator method* where the specific activity of a nuclide in a sample is compared with that of a sample of known composition (called a comparator standard) under identical experimental conditions.

A complex material, after irradiation with neutrons, contains a mixture of nuclides with varying half-lives (Fig. I-1). In order to detect a desired nuclide of a given half-life, timing parameters need to be carefully selected. The choice of timing parameters depends on, among other factors, the half-lives of the background activities and that of the nuclide of interest. It is evident form Fig. I-1 that in the presence of background activities it may not always be advantageous to irradiate a sample to the saturation activity of the nuclide of interest and count until it decays almost completely. Irradiation

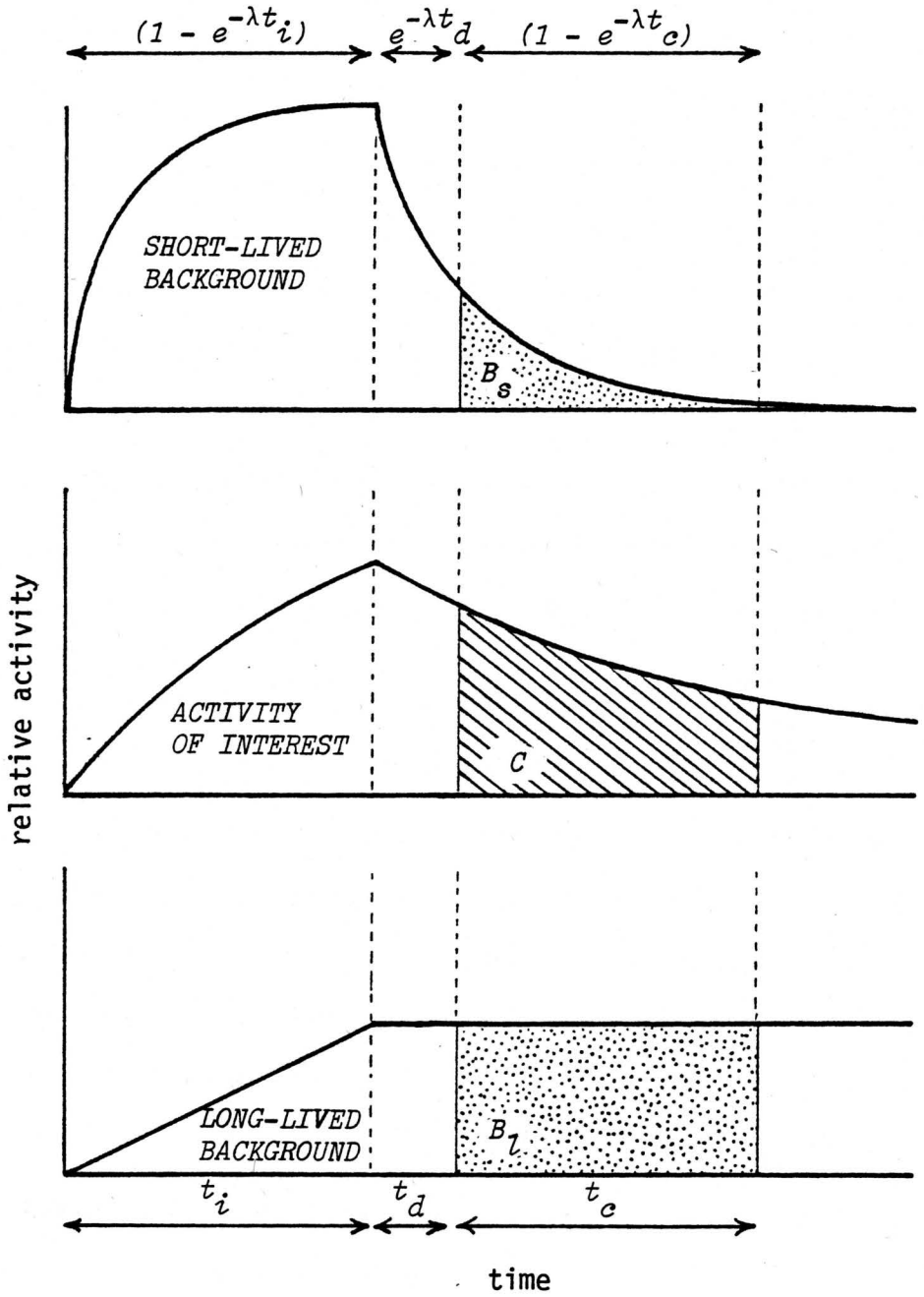

Figure I-1. Effect of half-life on selection of timing parameters

for a long time enhances the activity of interest with respect to a shorter lived background which attains saturation activity sooner. At the same time, activity of interest relative to the long-lived background diminishes because the latter activity increases almost linearly with irradiation time. On the other hand, irradiation for a short t_i has the exactly opposite effects. Similar effects are possible when t_c is changed. In the presence of high background activities due to short-lived nuclides, making the decay time t_d as short as possible may not be advantageous. Particular attention should therefore be focussed on selecting optimum timing parameters so that maximum possible sensitivity (number of counts), C, with a minimum possible background activity ($B_s + B_l$) can be achieved.

There are several elements which produce fairly long-lived nuclides (half-lives longer than several days) whose determinations require lengthy irradiation, decay and counting times leading to total experimental times of several weeks. Alternatively, short-lived isomers of the long-lived nuclides can be assayed. For the purpose of this thesis, *short lived nuclides* are referred to as those with half-lives less than approximately one minute. Since the total analysis time is of much importance in cases such as medical and environmental research, there has been a growing interest in the utilization of short-lived nuclides in INAA.

B. Instrumental NAA Using Short-Lived Nuclides

1. Advantages

At a given neutron flux, the activity A_o of a particular nuclide produced is directly proportional to its reaction cross-section (σ) and the saturation factor.

$$A \propto \sigma (1 - e^{-0.6932 t_i / t_{1/2}})$$

The maximum attainable activity for a given value of σ is achieved when the irradiation factor, $(1 - e^{-0.6932 t_i / t_{1/2}})$, attains its maximum value of unity for which t_i has to be several times larger than $t_{1/2}$. For $t_i / t_{1/2}$ equal to 1, 2, 3, 4, . . . , the corresponding values for the irradiation factor are 1/2, 3/4, 7/8, 15/16, . . . 1. Therefore, for a short-lived nuclide one can easily extend the irradiation time so as to approach its saturation factor within seconds to minutes in contrast to a long-lived nuclide (with a half-life of the order of several days) where very long irradiations are required for achieving the same value of saturation factor.

Depending on the available sample transfer facility, short half-lives can offer greater flexibility in selecting the timing parameters when discrimination of half-lives is necessary to avoid interferences. This can best be illustrated by considering an example, say, determination of Ag in the presence of relatively large amounts

of As. The nuclide ^{110}Ag has a half-life of 24 seconds and its most populated gamma-ray is at 658 *keV*. This photopeak can be interfered with by the 657-*keV* gamma-ray of ^{76}As which has a half-life of 1.12 *d*. After a short irradiation, the activity of the short-lived ^{110}Ag can be measured; if any interference from ^{76}As is suspected, it can be quantitatively determined by counting the sample again after a decay for a few minutes when this gamma-ray is emitted by only ^{76}As. On the other hand, the long-lived counterpart of ^{110}Ag, ^{110m}Ag with a half-life of 120 days also emits the same 658-*keV* gamma-ray which is its most abundant gamma-ray. Therefore, if Ag is to be determined via the long-lived ^{110m}Ag isomer, one has to wait for several days or weeks until the ^{76}As activity decays almost completely.

In general, nuclides produced by short irradiations also have short half-lives. Consequently, the irradiated sample becomes virtually inactive after few minutes or hours depending on the composition of the matrix. Then, the same sample can be re-irradiated and analysed under identical conditions in situations where the evaluation of the precision of measurement or where standard addition techniques are desired. Furthermore, under these conditions, as the sample activity is short-lived and hence virtually free from radioactivity after a short time, one may use the same sample for other experiments which may or may not involve radioactivity. The production of short-lived nuclides in ordinary nuclear analytical laboratories essentially eliminates the problem of radioactive sample waste management.

For some elements, INAA via short-lived nuclides is the only or the most sensitive method available; *e.g.* determinations of F, O, Se and Pb. For elements where both short- and long-lived neutron activation products exit, the use of short-lived nuclides offers not only time saving but also considerable financial saving.

Some of the major as well as interfering elements, such as Na, Mn, Br and La which are generally present in most matrices analysed by INAA, do not create serious problems in measurements of trace elements via short-lived nuclides. In situations where the decay time is over 2-3 seconds, even Cl does not offer much interference.

Some research reactors can be operated in the pulse-mode thereby producing very high flux of neutrons momentarily. Consequently, the activity enhancement for short-lived nuclides is higher than that for long-lived ones. This phenomenon has been advantageously utilized to improve sensitivities of short-lived nuclides (76M1).

Although there are many advantages, if the problems associated with the measurements of short-lived activities are not carefully attended to, unreliable results can outweigh the favourable aspects as commented earlier.

2. Analytical Problems

The sensitivity of measurement depends on the number of counts C accumulated under a photopeak. The factors that limit one

from obtaining the maximum value of C for a particular analysis can be recognized from the expression derived for C (equation I-4). Assuming that all components of the analyser-system other than the detector are 100% efficient:

$$C = \varepsilon A_o \int_{t_d}^{(t_d + t_c)} e^{-0.6932t/t_{1/2}} \, dt$$

$$= \varepsilon A_o \, e^{-0.6932t_d/t} \, (1 - e^{-0.6932t_c/t_{1/2}}) \qquad \text{I-5}$$

where ε is the detector efficiency and A_o is the activity of the nuclide corresponding to the photopeak under consideration at the end of irradiation and counted for a time t_c after a decay time of t_d.

The counting factor $(1 - e^{-0.6932t_c/t_{1/2}})$ approaches unity as $t_c/t_{1/2}$ is maximized. This does not create much problems for short half-lives, except when t_c has to be optimized in order to suppress unnecessary accumulation of long-lived background activity. In contrast, the decay factor $(e^{-0.6932t_d/t_{1/2}})$ reaches its maximum value as $t_d/t_{1/2}$ tends to zero. Since t_d is practically finite for reactor irradiation one has to make $t_d/t_{1/2}$ as small as possible. Therefore, the lower limit of half-lives that can be successfully handled depends mainly on how rapidly one is able to transfer the sample from the irradiation site to the detector position; and hence it is

essential to have a fast as well as a reproducible transfer system. Moreover, the need for the timing parameters t_i, t_d and t_c to be of the order of the half-life of interest - which can range from milliseconds to seconds - demands precision timing of very short time intervals in order to obtain reproducible results. Next consideration is the maximization of the most critical parameter, A_o. Obviously, for an optimum irradiation time, A_o can be increased by increasing the sample size or the neutron flux. However, the analyser should be able to cope with the high activity. This becomes a serious problem when the average time interval between two pulses to be processed approaches the pulse resolving time of the analyser where significant coincidence losses of pulses can occur due to pulse pile-up and multichannel analyser dead-time. A satisfactory solution to these problems becomes very complicated especially when there is a rapidly decaying high activity due to a mixture of long- and short-lived nuclides. These important phenomena of coincidence losses due to pulse pile-up and dead-time are explicitly treated in Chapter III and IV.

C. Objectives

In this thesis, development of INAA methods is considered with an emphasis on the improvement of sensitivity of determination using short-lived nuclides. Hence, the primary objective is to develop a correction method, for both dead-time and pulse pile-up losses, which can be applied to short-lived nuclides at rapidly varying count rates

so that high activities can be properly treated. Once the correction method is successfully developed, one does not have to restrict total count rates to considerably low values; thereby sacrificing the sensitivity and the precision of measurement, in order to minimize errors due to coincidence losses.

However, even if one has a highly accurate correction method or an ideal analyser with a 100% efficiency (*i.e.* with no coincidence losses), still the question remains that whether or not these measures can solve all the problems in INAA. Even if the analyser accurately processes each and every detector event, in the presence of a high background activity, photopeaks with small number of counts diminish in relative size due to random fluctuation of the high background counts. In fact, in order to make a proper correction one has to first *detect* the photopeak of interest at high activities. The masking effect on the photopeak by high background activity is common in INAA. INAA mehods which enhance the relative activity of nuclides of interest with respect to the background are needed. Hence, another objective of this work was to develop methods for such an enhancement. Two different approaches will be taken. One approach deals with the development of pseudo-cyclic and cyclic INAA (PCINAA and CINAA) methods for measuring elemental content through highly active short- and very short-lived nuclides. The other approach involves the reduction of interfering activities contributing to high background by developing epithermal INAA (EINAA) methods.

CHAPTER II

PRINCIPLES OF CYCLIC AND EPITHERMAL NEUTRON ACTIVATION ANALYSIS

In modern times, CINAA and EINAA methods have become popular for the discrimination of undesirable activities against to those of nuclides of interest. For the relative enhancement of the desired activities the fundamental criterion used in CINAA is the differences in half-lives, whereas EINAA makes use of the fact that the variation of cross-section with the neutron energy is different for different nuclides.

A. Pseudo-Cyclic and Cyclic INAA of Short-Lived Nuclides

1. Evolution

Cyclic instrumental neutron activation analysis (CINAA) technique is used to enhance the sensitivity of short-lived nuclides by improving counting statistics of the photopeaks of interest. This is done by repeating *irradiation - transfer - counting* process of a sample for a suitable number of cycles; the gamma-ray spectrum of each cycle is recorded to finally yield a cumulative spectrum. Using a pneumatic sample transfer system, this approach was first introduced to activation analysis by Anders (60A1) who used the $^{19}F(n,\alpha)^{16}N$ reaction to

determine fluorine via the 7.4 second-^{16}N nuclide. Anders (61A1) later used the same technique for measuring a few other selected elements. The term *cyclic activation analysis* was originally given by Caldwell and co-workers (66C1, 70G1) to a technique of electronic cycling of activation and counting for neutron activation analysis with a pulsed neutron generator. This term is currently used for repeated analysis by mechanical transfer (69G1, 71J1, 69W1); the mathematical treatment is basically the same in both types of recycling. The theory of CINAA has been well described by Givens *et al.* (70G1), more recently by Spyrou and Kerr (79S2). Recently, Spyrou *et al.* (74S1, 76E1) Grass *et al.* (77G1, 78G1) and Chatt *et al.* (80C1, 81C1) have applied CINAA technique for trace analysis using reactors as neutron sources. The CINAA technique often requires rather expensive automated equipment which are not commonly available in most nuclear analytical laboratories. During the initial stages of this work a non-automated pseudo-cyclic instrumental neutron activation analysis (PCINAA) method (79C2) was developed and successfully applied to biological materials for detecting nuclides with half-lives ranging between 10 *s* and 65 *s*. In the PCINAA method, dead-time corrections were carried out by reading the average dead-time from a meter and subsequently calculating a correction factor for each cycle. Possible errors, due to not using an elaborate correction method were minimized by maintaining the dead-time at a low value ($\lesssim$10%). However, after the design and installation of an automated sample recycling system (described in section V.B)

which can handle much shorter half-lives (of the order of milliseconds), the need for a more reliable correction method for coincidence losses was immediately recognized. Moreover, most CINAA methods reported in the literature use the average dead-time method for calculating correction factors where significant errors may be encountered at rapidly varying dead-times. A correction method for dead-time and pile-up losses in CINAA has been developed in this study and described in section VI.D.2. Before going into details of the correction method developed, it is imperative at this point to describe the basic theory common to CINAA and PCINAA.

2. Theory

a. *Basic Equation*

In simple terms, a sample containing the element to be determined is irradiated in a source of neutrons, transferred onto a detector and counted, and the process is repeated for an optimum number of cycles in PCINAA and CINAA.

Let us consider a cycle of period T, where T is defined by

$$T = t_i + t_d + t_c + t_{d'} \qquad \text{II-1}$$

where,

t_i = irradiation time;

t_d = decay time between the end of irradiation and the start of counting;

t_c = counting time;

$t_{d'}$ = delay between end of counting time and the start of irradiation.

The definitions of these timing parameters and the variation of a short-lived activity are shown in Fig. II-1.

Assuming that there are no coincidence losses for the first cycle, the expression for the detector response (number of counts accumulated) is the same as equation I-4, derived for the conventional case. Thus, using the same parameters as before, the detector response $C_o(1)$, for the first cycle can be written as:

$$C_o(1) = Q\,(1 - e^{-\lambda t_i})\,(e^{-\lambda t_d})\,(1 - e^{-\lambda t_c}) \qquad \text{II-2}$$

where,

$$Q = \frac{\varepsilon\,\phi\,\sigma\,m\,\theta}{\lambda\,M} \times 6.023 \times 10^{23} \qquad \text{II-3}$$

The accumulated number of counts, $C_o(2)$ is due to the activity produced during the second cycle and that remained from the first cycle. Therefore, $C_o(2)$ can be given as

$$C_o(2) = C_o(1)\,(1 + e^{-\lambda T}) \qquad \text{II-4}$$

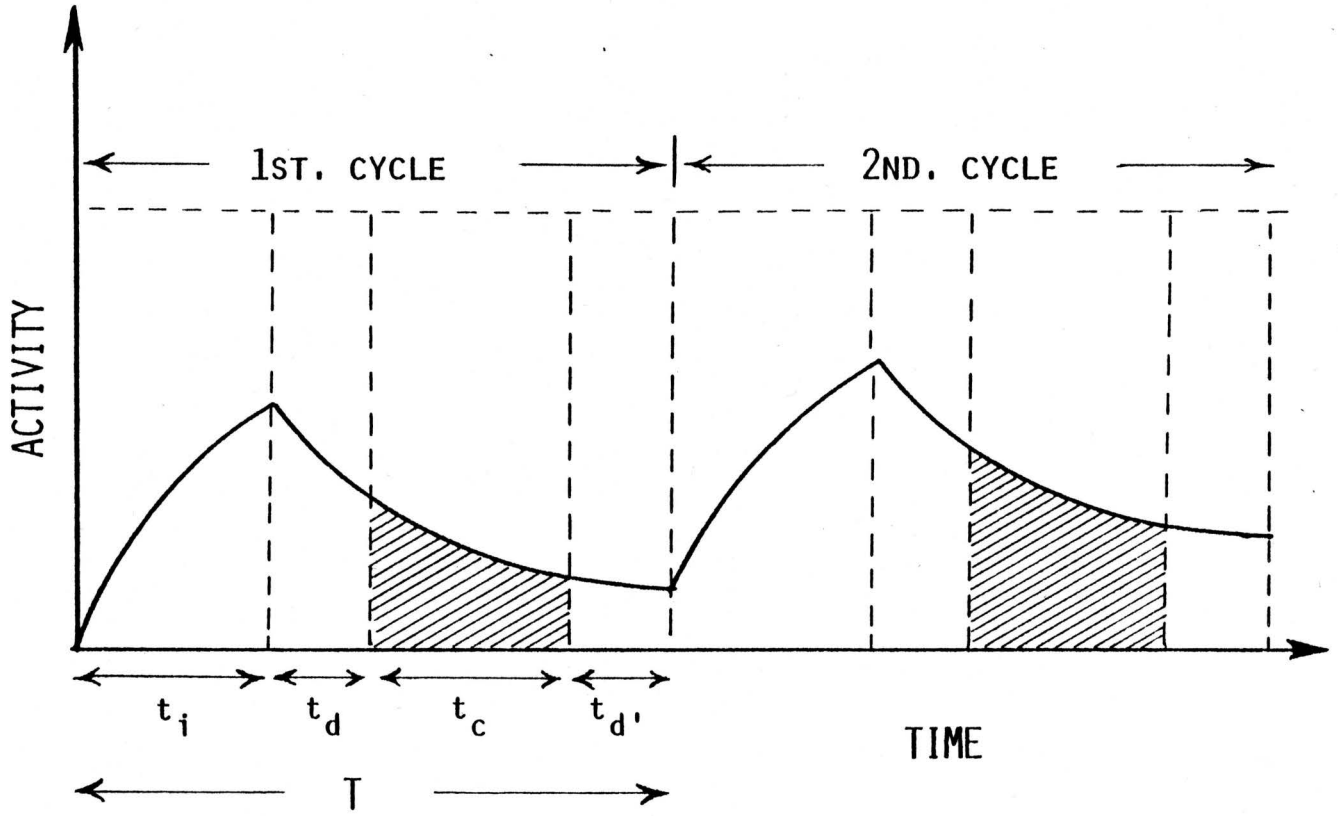

Figure II-1. Definition of a cycle period T

Similarly, the detector response at the nth cycle, $C_o(n)$ is given by:

$$C_o(n) = C_o(1)\ (1 + e^{-\lambda T} + e^{-2\lambda T} + ... + e^{-n\lambda T}) \qquad \text{II-5}$$

$$= C_o(1)\left(\frac{1 - e^{-n\lambda T}}{1 - e^{-\lambda T}}\right) \qquad \text{II-6}$$

The cumulative detector response after n cycles will be:

$$C_o(c) = C_o(1) + C_o(2) + ... + C_o(n) \qquad \text{II-7}$$

Combining equations II-6 and II-7 one can arrive at an expression for $C_o(c)$:

$$C_o(c) = C_o(1)\left\{\frac{1}{1-e^{-\lambda T}}\left[n - e^{-\lambda T}\left(\frac{1-e^{-n\lambda T}}{1-e^{-\lambda T}}\right)\right]\right\} \qquad \text{II-8}$$

Then the final expression becomes:

$$C_o(c) = \frac{\varepsilon\ \phi\ \sigma\ m\ \theta}{\lambda\ \ M} X\ 6.023\ X\ 10^{23}\ (1-e^{-\lambda t_i})(e^{-\lambda t_d})(1-e^{-\lambda t_c}) X\left\{\frac{1}{1-e^{-\lambda T}}\left[n - e^{-\lambda T}\left(\frac{1-e^{-n\lambda T}}{1-e^{-\lambda T}}\right)\right]\right\} \qquad \text{II-9}$$

To obtain the maximum $C_o(c)$, one has to select suitable timing parameters and number of cycles. In the presence of interfering back-

ground, these parameters should be optimized to achieve maximum signal to background ratio. Mathematical treatments (79T1, 71J1) and computer simulations (81T1) for the optimization of timing parameters have been reported.

B. Epithermal Neutron Activation Analysis

1. Epithermal (Resonance))Neutrons

Neutrons produced in a fission reactor can generally be classified according to their energies as thermal neutrons ($E < 0.4\ eV$), epithermal neutrons ($0.4\ eV < E < 1\ MeV$) and fast neutrons ($E > 1\ MeV$). The typical shape of a moderated reactor neutron spectrum is shown in Fig. II-2 (70C1). In spite of the relatively low magnitude of the flux, in some cases epithermal neutrons can be advantageously used for elemental determinations.

The formation rate of a nuclide depends, among other factors, on the magnitude and the distribution of the neutron flux as well as the variation of its cross-section with neutron energy. Generally, majority of the nuclides in the thermal neutron region follow the so-called $1/v$ law, which means that their activation cross-section is inversely proportional to neutron velocity or the square root of neutron energy. Several other nuclides possess large resonances in the epithermal region, which means that the cross-sections of these nuclides can reach very high values within small neutron energy intervals. For

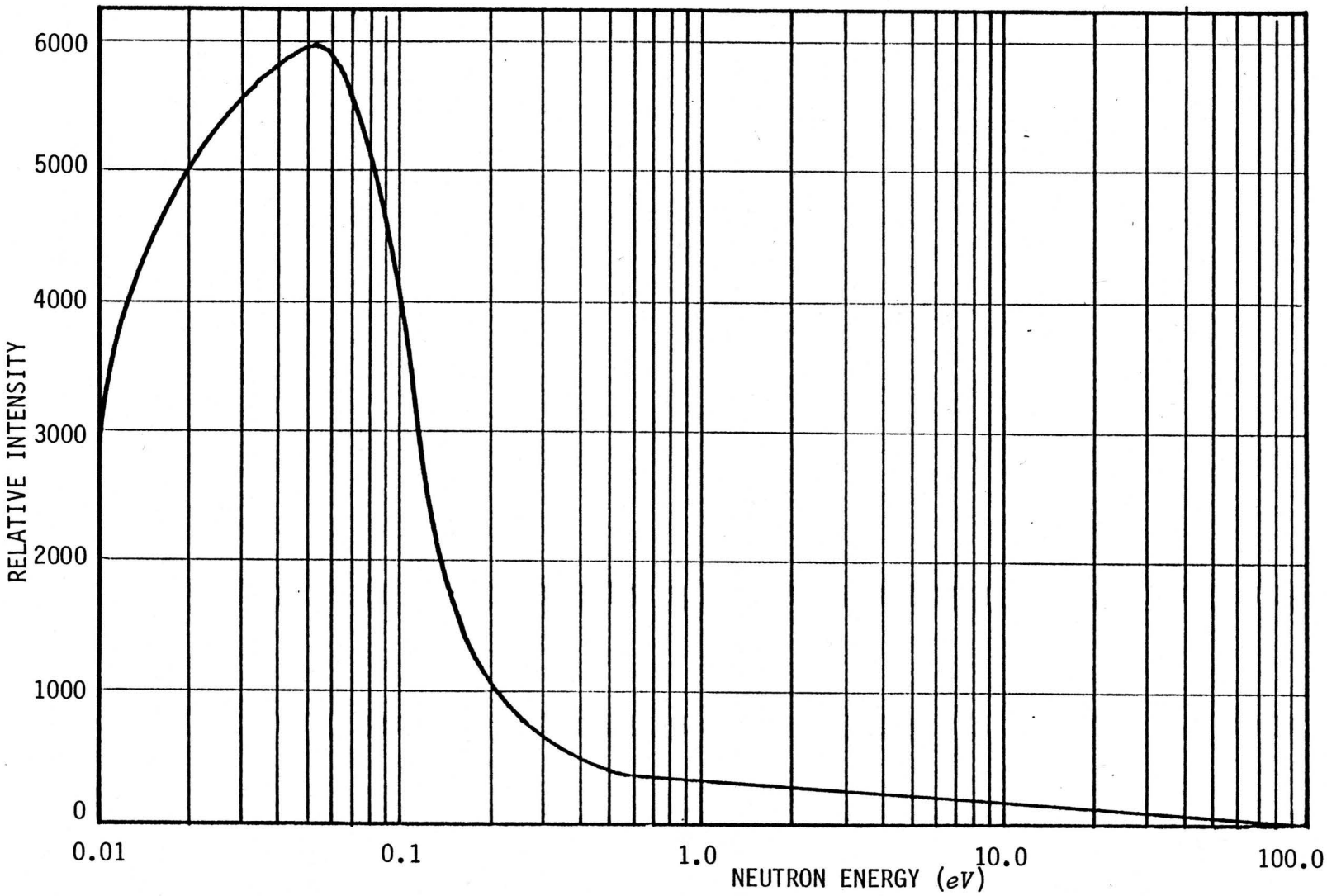

Figure II-2. A typical spectrum of moderated fission neutrons (70C1)

this reason epithermal neutrons are sometimes referred to as *resonance neutrons*. Thus, for these nuclides, activities can be selectively enhanced relative to those with higher thermal cross-sections by screening the thermal neutrons during irradiation.

2. Cadmium Ratio

Cadmium has a very high absorption cross-section of about 20,000±300 barns (72D2) for neutrons with energies less than 0.4-0.5 *eV* due to the reaction $^{113}Cd(n,\gamma)^{114}Cd$. Cadmium is virtually transparent for the neutrons with higher energies. The product nuclide ^{114}Cd is not radioactive. The effective Cd cut-off energy depends on the foil thickness and the geometry. If a sample is covered during irradiation with a Cd-foil of thickness 0.5-1.0 *mm*, the thermal neutrons can be screened out so that the nuclear reactions are only possible with *epicadmium* neutrons. If the sample is not shielded with cadmium, activation occurs due to thermal as well as epithermal neutrons. The measured ratio of the two activities produced with and without Cd shield, for a given irradiation position is called the *cadmium ratio (CR)* of the nuclide of interest, which can also be used as a measure of epithermal (resonance) to thermal flux ratio at the irradiation position.

$$CR = \frac{Activity\ without\ \text{Cd}\ foil}{Activity\ with\ \text{Cd}\ foil} \qquad \text{II-10}$$

It is obvious that the measured *CR* depends on the relative sensitivities of the monitor for resonance and thermal neutrons. The *CR* value is often measured using gold as the monitor. In DUSR, *CR* values have been measured to be 2.2 for the inner irradiation sites and 5.3 for the outer sites (78R1).

3. Advantage Factors

The enhancement of the activity of interest against that of the interfering background elements is generally described by means of the so called *advantage factor*, which as defined by Brune and Jirlow (64B1) is given by:

$$AF = \frac{(CR)_b}{(CR)_i} \qquad \text{II-11}$$

where $(CR)_i$ and $(CR)_b$ denote the two cadmium ratios measured with respect to nuclide under investigation and background nuclides, respectively. In situations where a number of interfering nuclides are considered, the expression II-11 becomes fairly complicated as the value of *AF* then depends on the relative contributions from each background nuclide. In an attempt to avoid this difficulty, a simplified form of advantage factor is commonly used as described below.

It has already been stated that cross-section varies considerably with the energy of bombarding neutrons. However, the principles and activation equations derived in earlier sections for thermal

neutrons apply equally well to EINAA. The total activation reaction rate R_r of an isotope at infinite dilution is given by:

$$R_r = \phi_{th}\,\sigma_{th} + \phi_{res}\,I \qquad \text{II-12}$$

where,

σ_{th} = cross-section for thermal neutrons;
ϕ_{th} = conventional thermal flux;
ϕ_{res} = epithermal flux for unit $ln\ E$;
I = resonance integral which is defined as:

$$I = \int_{E_c}^{\infty} \sigma\,(E)\,\frac{dE}{E} \qquad \text{II-13}$$

E_c is the lower cut-off energy generally set at 0.4 eV.

Since I is a measure of the probability of reaction with epithermal neutrons, one would expect nuclides with higher I/σ_{th} ratios to be advantageously determined by EINAA. Thus, in a simplified form, advantage factor for a particular nuclide can be expressed by means of its I/σ_{th} ratio. Table II-1 shows the nuclear data and advantage factors for some selected nuclides of varying half-lives (77R2). It should be noted that several interfering elements such as Al, V, Na, Cl and Mn, which are commonly present in most matrices analysed by INAA, have relatively low advantage factors. Therefore, EINAA can be used

Table II-1. Nuclear data for several elements of interest in epithermal instrumental neutron activation analysis (77R2)

element	nuclide	half-life	resonance activation integral, (*b*)	thermal neutron cross section, (*b*)	advantage factor, I/σ_{th}
Cl	^{38}Cl	37.3 *min*	0.17	0.43	0.40
Sc	^{46}Sc	84 *d*	11	25	0.44
Cr	^{51}Cr	27.8 *d*	8.5	16	0.53
V	^{52}V	3.8 *min*	2.7	4.9	0.55
Na	^{24}Na	15 *h*	0.31	0.528	0.59
Al	^{28}Al	2.3 *min*	0.17	0.232	0.73
Mg	^{27}Mg	9.5 *min*	0.030	0.038	0.79
Ca	^{49}Ca	8.8 *min*	0.90	1.1	0.82
K	^{42}K	12.5 *h*	1.28	1.48	0.86
Ba	^{139}Ba	83 *min*	0.30	0.35	0.9
Cu	^{66}Cu	5.1 *min*	2.5	2.2	1.1
Fe	^{59}Fe	45 *d*	1.20	1.14	1.1
Mn	^{56}Mn	2.58 *h*	14.0	13.3	1.1
La	^{140}La	40.2 *h*	11	9.0	1.2
Co	^{60}Co	5.25 *a*	75	37.5	2.0

Table II-1. (continued)

element	nuclide	half-life	resonance activation integral, (*b*)	thermal neutron cross section, (*b*)	advantage factor, I/σ_{th}
Zn	^{69m}Zn	13.8 *h*	0.24	0.07	3.4
Sr	^{87m}Sr	2.83 *h*	4	0.8	5.0
Se	^{75}Se	120 *d*	500	55	9.1
Th	^{233}Th	22.2 *min*	82	7.4	11
W	^{187}W	23.9 *h*	420	37	11
Cs	^{134m}Cs	2.9 *h*	30	2.6	12
As	^{76}As	26.5 *h*	63	4.4	14
Sm	^{153}Sm	47 *h*	2900	210	14
Ba	^{135m}Ba	29 *h*	24	0.16	15
Br	^{80}Br	17.6 *min*	125	8.4	15
In	^{116m}In	54 *min*	2600	161	16
Tb	^{160}Tb	72.1 *d*	400	25	16
Tm	^{170}Tm	130 *d*	1700	106	16
Br	^{82}Br	35.5 *h*	50	3.0	17
Rb	^{88}Rb	17.8 *min*	2.3	0.12	19

Table II-1. (continued)

element	nuclide	half-life	resonance activation integral, (*b*)	thermal neutron cross section, (*b*)	advantage factor, I/σ_{th}
Gd	^{159}Gd	18 *h*	80	3.5	23
I	^{128}I	25 *min*	150	6.2	24
Sb	^{122}Sb	67.2 *h*	180	6.2	29
Lu	^{176m}Lu	3.69 *h*	600	18	33
Ti	^{51}Ti	5.8 *min*	5.5	0.179	37
Nb	^{94m}Nb	6.3 *min*	8.0	0.15	53
Mo	^{99}Mo	66.7 *h*	7.5	0.14	54
Sn	^{125m}Sn	9.7 *min*	9	0.14	64
Zr	^{97}Zr	17.0 *h*	5.0	0.05	100
U	^{239}U	23.5 *min*	280	2.72	103
Y	^{90m}Y	3.1 *h*	0.9	0.001	900

advantageously for analyzing matrices such as, coal, coal- and oil-fly-ash and air particulates, which consist of elements such as Al and V in percentage amounts. The advantages of epithermal over conventional thermal neutron activation for elemental analysis of geological materials have been well reviewed by Steinnes (71S1).

4. Shields for Epithermal Neutron Activation

In the past, EINAA technique has been used by wrapping samples with Cd foils for determining a few selected elements in biological, geological and coal fly-ash samples (79G1, 77H1, 75A1, 76S1). Although the product nuclide, ^{114}Cd of neutron absorption reaction $^{113}Cd(n,\gamma)^{114}Cd$ is non-radioactive, the Cd-shield becomes highly radioactive after irradiation due to formation of nuclides from other isotopes of Cd. Hence, it is necessary to take the sample out of the Cd-shield before counting. One has to allow decay times of at least several minutes for opening of the capsule, removal of sample and placing it in a proper counting geometry. Consequently, EINAA where the sample is wrapped in Cd-foil cannot be used for detecting short-lived nuclides. For this reason, application of EINAA has been limited to nuclides with half-lives longer than several minutes, except where specially designed and installed facilities for epithermal neutron irradiations are available (79G1, 76M1). Therefore, if EINAA of short-lived nuclides is to be performed using normal irradiation facilities, one should have a shield which does not become highly radioactive so that counting can be done immediately after irradiation and without the removal of the sample

from the shield.

Boron is also an efficient absorber of thermal neutrons for which the absorption cross-section follows a $1/v$ relationship and reaches a small value at approximately 280 eV (72R1). Dependency of absorption cross-section on neutron energy for Cd and B are shown in Fig. II-3 (72D2). Table II-2 gives the possible nuclear reactions and relevant nuclear data for these two elements. The added advantage of B over Cd is that a few seconds after irradiation, B becomes virtually non-radioactive and hence non-interfering. Therefore, B has the potential of being a thermal neutron shield for short-lived nuclides.

Although the most commonly used shield material for thermal neutrons is Cd, B has also been used by several authors (79G1, 77H1, 79J1). For the analysis of biological materials, Hanna and Shahristani (77H1) shielded both the sample and the standard by a boron compound and placed in an irradiation container for simultaneous activation. Then the standards and the samples were counted separately. In this method irreproducibility or non-uniformity of the shield does not cause significant errors because the standards and the samples are irradiated simultaneously inside the same shield. However, this approach cannot be adopted for short decay intervals as the sample and the standards have to be taken apart before counting, and measured separately. Gladney and Perin (79G1) analysed silicates by conventional EINAA using boron filtered epithermal neutrons. They irradiated samples inside a permanently installed epithermal irradiation facility. This approach

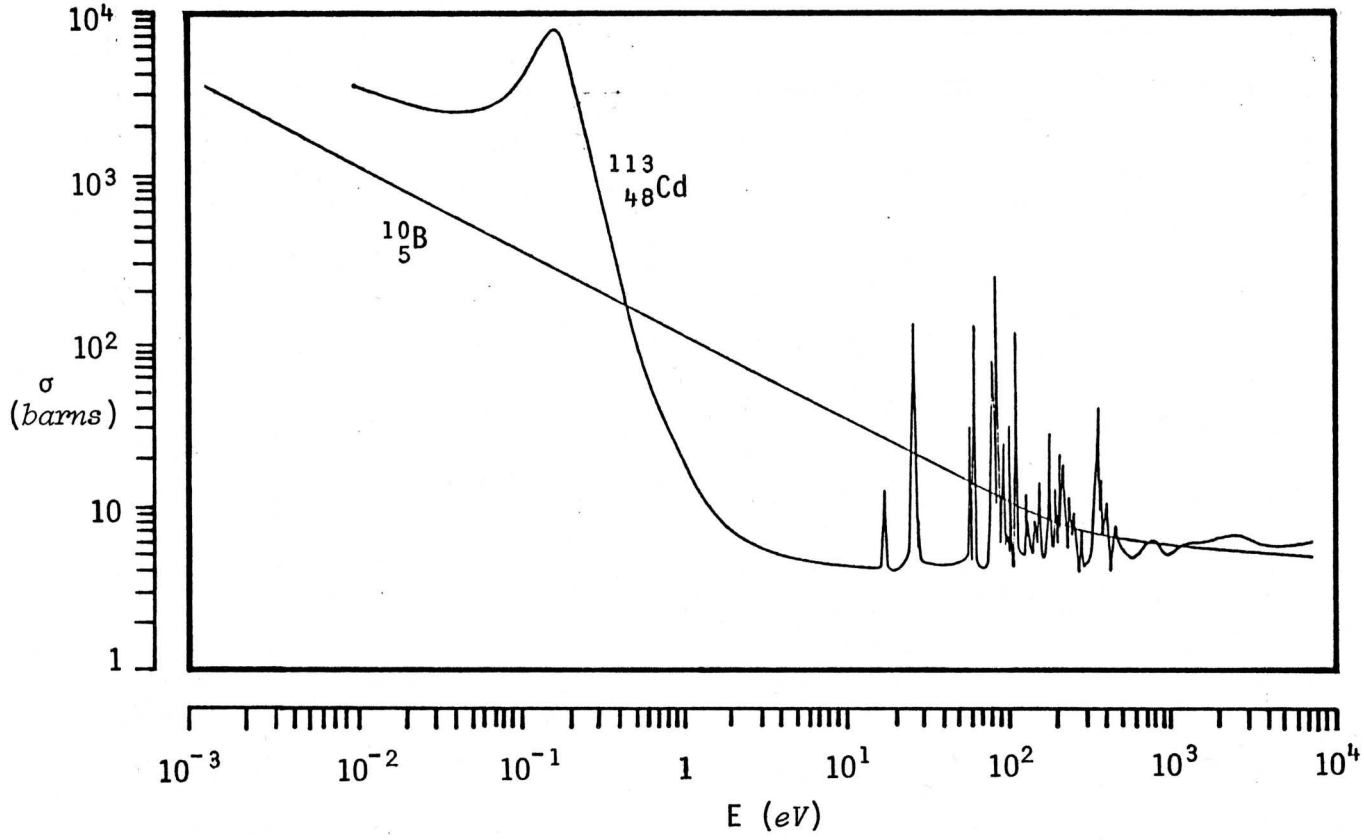

Figure II-3. Neutron absorption cross-sections of Cadmium and Boron (72D2)

Table II-2. Nuclear data for thermal neutron reactions of B and Cd (64F1)

parent isotope	abundance (%)	cross-section (*b*)	nuclear reaction	$t_{1/2}$ of product nuclide	decay mode
$^{10}_{5}B$	19.7	4017	$^{10}B(n,\alpha)^{7}_{3}Li$	...	stable
		...	$^{10}B(n,\gamma)^{11}B$	...	stable
		...	$^{10}B(n,p)^{10}_{4}B$	7.5 x 10 *y*	β^-
^{11}B	80.3	0.005	$^{11}B(n,\gamma)^{12}B$	20 *ms*	β^-, γ
		...	$^{11}B(n,p)^{11}_{4}Be$	13.6 *s*	β^-, γ
		...	$^{11}B(n,\alpha)^{8}_{3}Li$	0.84 *s*	β^-
		...	$^{11}B(n,2n)^{10}B$	...	stable
$^{106}_{48}Cd$	1.22	1.0	$^{106}Cd(n,\gamma)^{107}Cd$	6.7 *h*	EC, β^+, γ
^{108}Cd	0.87	...	$^{108}Cd(n,\gamma)^{109}Cd$	470 *d*	EC
^{110}Cd	12.39	0.2	$^{110}Cd(n,\gamma)^{111m}Cd$	49 *m*	IT, γ
			$^{110}Cd(n,\gamma)^{111}Cd$	...	stable

Table II-2. (continued)

parent isotope	abundance (%)	cross-section (b)	nuclear reaction	$t_{1/2}$ of product nuclide	decay mode
^{111}Cd	12.75	...	$^{111}Cd(n,\gamma)^{112}Cd$	...	stable
^{112}Cd	24.07	0.03	$^{112}Cd(n,\gamma)^{113m}Cd$	14 y	β^-
			$^{112}Cd(n,\gamma)^{113}Cd$	...	stable
^{113}Cd	12.26	20000	$^{113}Cd(n,\gamma)^{114}Cd$	...	stable
^{114}Cd	28.86	0.14	$^{114}Cd(n,\gamma)^{115m}Cd$	43 d	β^-, γ
		1.1	$^{114}Cd(n,\gamma)^{115}Cd$	2.3 d	β^-, γ
^{116}Cd	7.58	1.5	$^{116}Cd(n,\gamma)^{117m}Cd$	2.9 h	β^-, γ
			$^{116}Cd(n,\gamma)^{117}Cd$	50 m	β^-, γ

EC - electron capture

IT - internal transition

can be used for short-lived nuclides. However, it needs considerable modification of the irradiation facility. Furthermore, during irradiation, the sample cannot be completely covered with the shield material to obtain maximum filtering efficiency, as a passage for the sample insertion and withdrawal has to be kept open. Jones *et al.* (79J1) used a sample capsule fabricated from hot-pressed boron nitride for the determination of Si in plant materials. Although this technique can be used for short-lived nuclides, in addition to being expensive, contamination is possible during fabrication (machining) of the shield. There exists a necessity for developing a suitable shield which should be relatively free from contaminants and can be used for EINAA of short-lived nuclides.

CHAPTER III

COINCIDENCE LOSSES

There is a finite time interval in any instrument which outputs information after receiving some input data. While processing a pulse, some circuitry in the analyser system may be inactive for further input data thereby resulting in loss of information only on the subsequent pulses. On the other hand, there are some components of the system that are always active to any input data. In the latter case, if more than a single pulse approaches the device within the resolving time, then all the pulses would be subjected to distortion and hence would consequence in loss of correct information about all the pulses. In order to understand the causes and effects of these two types of *coincidence losses*, *viz. dead-time* and *pulse pile-up losses*, it is perhaps pertinent to briefly describe the basic components of a spectrometric system.

A. Origin of Dead-Time and Pulse Pile-Up Losses

A block diagram of the basic components of a gamma-ray spectrometer is shown in Fig. III-1. The interaction of photons with the semiconductor detector promotes electrons from the valence band to the conduction band or to higher energetic bands. This excitation takes place in a very short time, *viz.* of the order of 10^{-12} *s* (70C1),

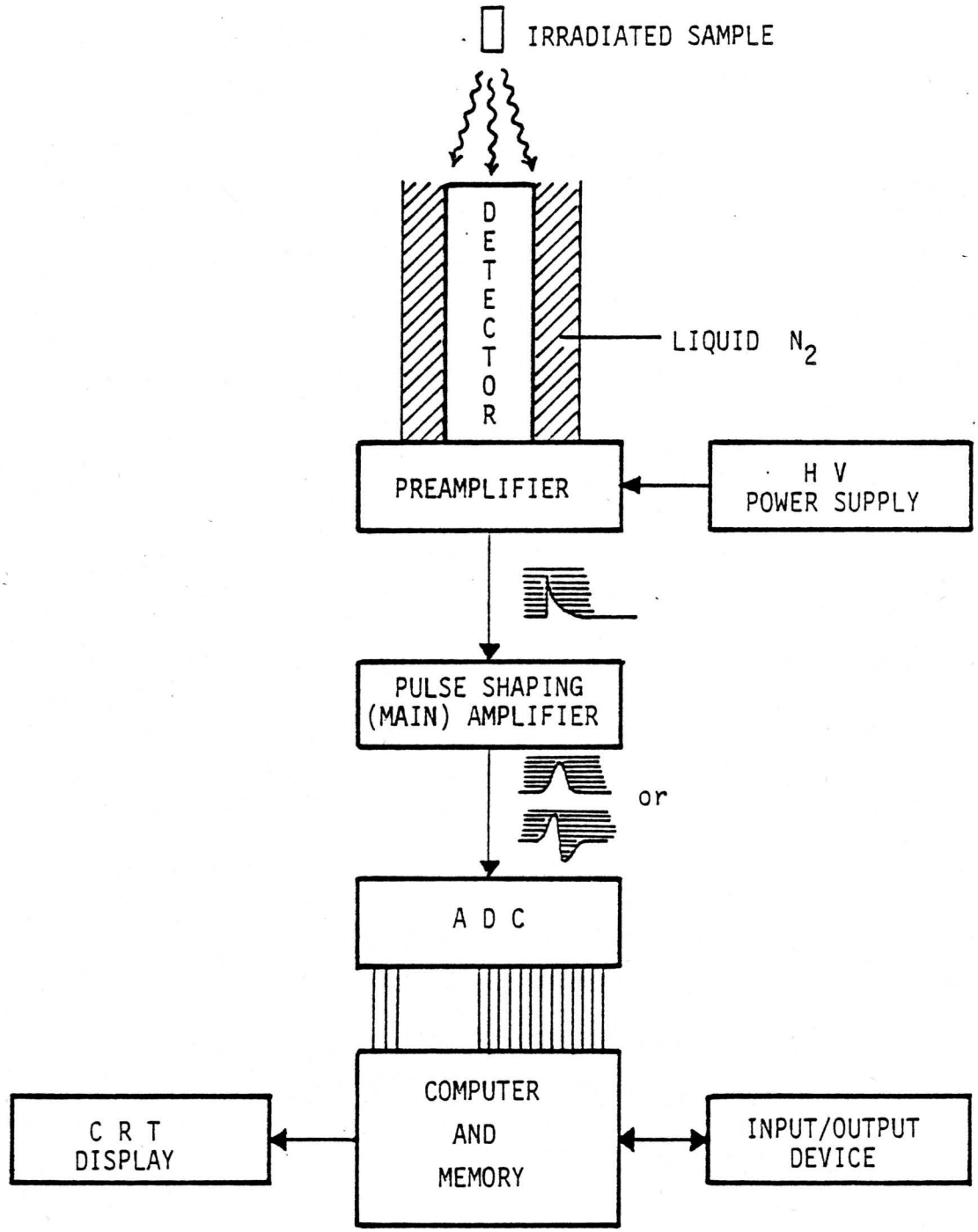

Figure III-1. A block diagram of a basic gamma-ray spectrometer

which produces a number of *electron-hole* pairs in the intrinsic region of the detector. The number of charge carriers produced depends on the energy of the interacting photon. These charges are swept through the material by an applied electric field, and then an electric pulse is produced corresponding to the detection of a single photon. The collection time of pulses may be of the order of 10^{-9} *s* depending on the design of the detector (70G3). Incidence of another photon, while one photon is being processed, will produce additional charge carriers as the detector is always sensitive to any incident photons. Assuming a 100% efficient collection, the above process will be equivalent to the detection of a single photon with an energy equal to the sum of the energies of two photons. Thus, the overlap of two or several discrete events will result in a distortion of the gamma-ray spectrum. This phenomenon is known as *pulse pile-up*.

The primary purpose of the preamplifier is to integrate the burst of charges collected from the detector and convert it into a voltage pulse which maintains a constant proportionality to the photon energy. After sufficient amplification, the voltage pulse is passed onto the main amplifier which performs two major functions. The first and the most obvious task is to provide a continuously adjustable linear gain over a wide range of photon energies. The second and the one that receives greatest attention is the process of pulse shaping which is important to enhance the signal to noise ratio - hence the resolution - in order to fully exploit the high resolving power of Ge(Li) detectors. In addition to yielding a high

signal to noise ratio, shaping operation reduces the total duration of a pulse so that pulses can be packed close together without riding on top of one another.

Similar to the detector, at no time are both the preamplifier and main amplifier insensitive to an input signal. Hence, pulse pile-up losses can also take place at the preamplifier and main amplifier. Most preamplifiers used in conjunction with semiconductor detectors are generally fast output devices having typical rise times of the order of 10^{-7} s (70C1). However, pulse shaping networks used in the main amplifier to improve resolution increase the processing time; typical shaping time constants range from 0.05 to 12 μs (It should be mentioned that the magnitudes of the pulse resolving time and the corresponding shaping time constant are different - the former being larger). Higher the value of time constant, better is the performance of pulse shaping networks - hence improved resolution. It is evident from the above time constants that the major contribution to pulse pile-up originates at the main amplifier. Thus for high count rates, there is often a conflict between selecting a short time constant and obtaining a good resolution. In such situations a compromise is necessary.

The distortion of pulses in the linear (main) amplifier is frequently due to the occurence of a second pulse before the baseline completely returns to its original value. Fig. III-2a shows, for bipolar pulses, the effect of overshoot of the first pulse to the

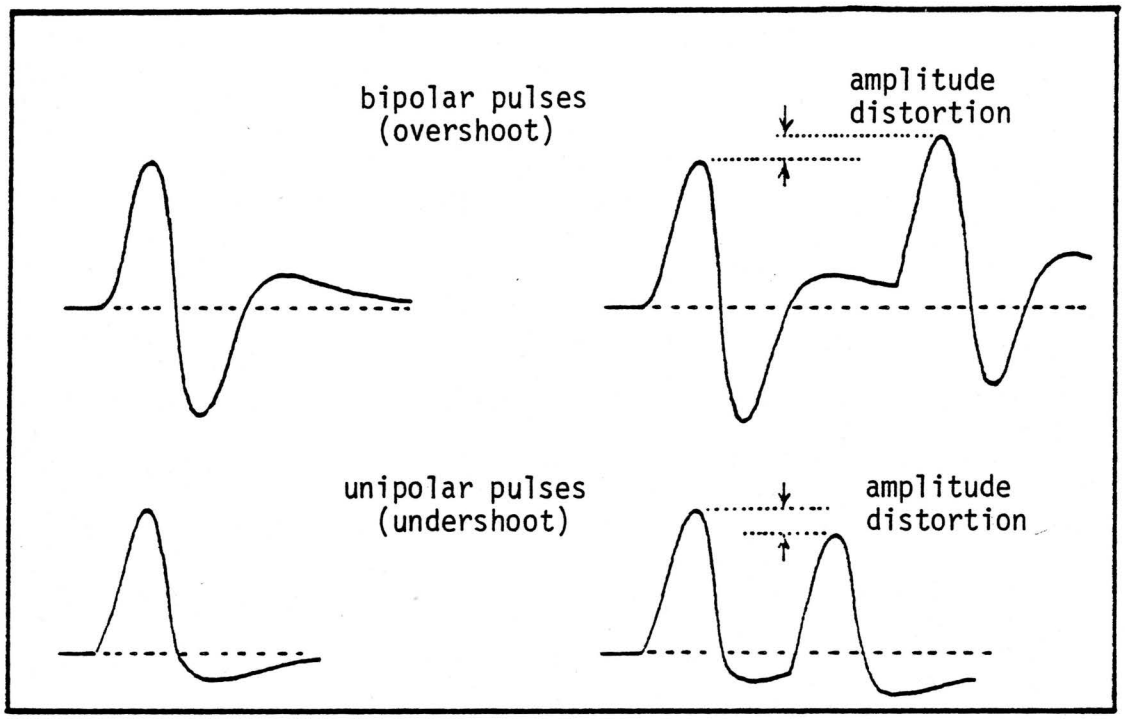

III-2a

Effect of base line restoration

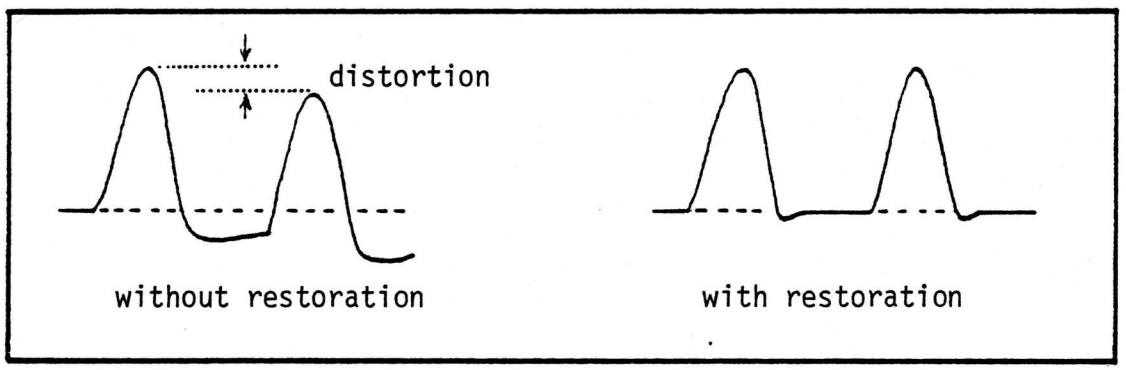

III-2b

Figure III-2. Amplitude distortion of unipolar and bipolar pulses

amplitude of the second. If unipolar pulses are used, an opposite distortion (due to undershoot) of the base line is encountered. This difficulty of base line distortion has been considerably overcome (as shown in Fig. III-2b) by modern electronic techniques such as base line restoration (68W1) and pole zero cancellation (65N1). However, they do not eliminate the problem of pulse pile-up. In order to avoid recording of distorted pulses that leads to distortion of the spectrum, a device known as *pulse pile-up rejector* has been developed. It consists mainly of an additional fast amplifier and a pile-up inspector (70C1). The pile-up rejector prevents distorted pulses from entering into the *analog to digital converter* (ADC) for further processing. However, this system does not correct for the pulses that are lost due to distortion and subsequent rejection.

The ADC used in this study employs the familiar Wilkinson conversion technique. In this method a capacitor is charged to the peak amplitude of an analog input pulse which comes from the output of the main amplifier after careful shaping and a linear amplification. At the end of the charging process, the capacitor is linearly discharged to zero. Fig. III-3 shows the typical timing diagram of the ADC used in this study (73T1). During the linear discharge a periodic pulse train (typically a 50 or 100 *MHz* clock) is scaled into a binary scaler. The scaled total number of clock pulses or the binary address is directly proportional to the peak amplitude of the analog pulse since the scaling time is directly proportional to the peak amplitude.

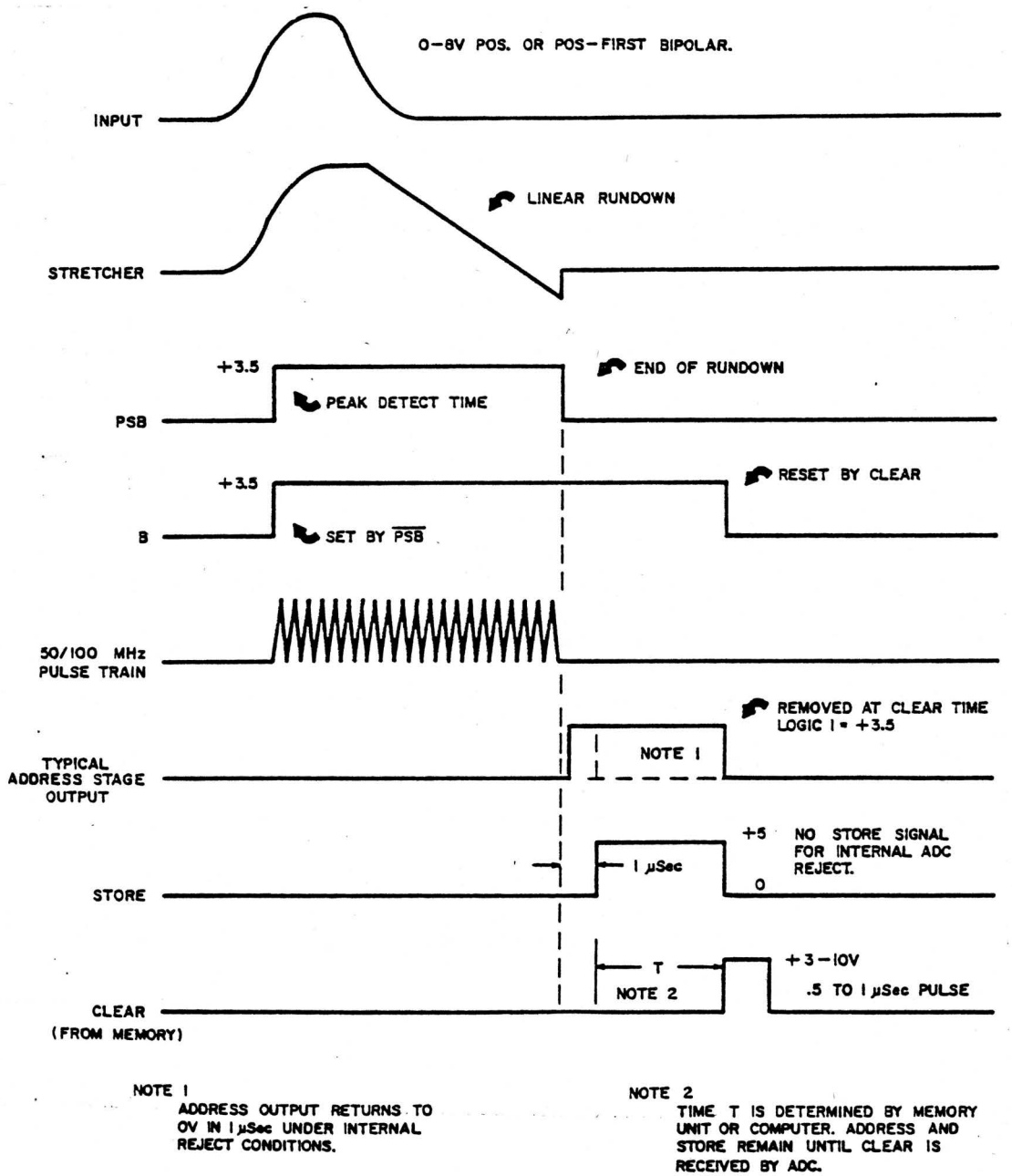

Figure III-3. ADC timing (75T1)

Consequently, the number of pulses, recorded in the memory unit for the channel corresponding to this digital signal is raised by one. Thus one obtains the distribution of all the recorded pulses with respect to their energies.

If the channel number into which the signal is assigned is i, and the frequency of the ADC clock is f, the time taken for scaling during the linear run-down is i/f. For a signal that is assigned to the channel number 1000 (*e.g.*, if the instrument is calibrated at 1 *keV/channel*, it corresponds the energy of 1000 *keV*), and ADC with a clock frequency of 50 *MHz* has a scaling time of 20 μs. In addition to the scaling operation, ADC has to perform several logic functions which last for a constant duration, a, independent of the channel number. The constant, a, can have typical values in the range of 5 - 15 μs depending on the characteristics of the computer interfaced with the ADC. Unlike the detector, preamplifier and main amplifier, the ADC does not respond to any subsequent input signals while one signal is being processed. This time interval during which the ADC is inactive to input data is referred to as ADC *dead-time*, $d(i)$. It can be expressed as:

$$d(i) = a + i/f \qquad \text{III-1}$$

In summary, one may state that, in a typical gamma-spectrometer, the chief contributor to the pile-up losses is the main amplifier. Using short pulse shaping time constants, consequently sacrificing

the resolution, pulse pile-up losses can be partially reduced. Also, when the ADC is *busy*, a significant portion of pulses may be lost at high count rates due to dead-time. Therefore, in dealing with short-lived nuclides at high count rates, significant corrections would be necessary for both types of coincidence losses.

B. Magnitudes of the Two Effects

1. Dead Time Losses

With the knowledge of parameters a and f(equation III-1) and the number of counts in each channel one can make an approximate estimation of the dead-time. Then a satisfactory correction can be made provided that there is no change in shape of the spectrum during the counting period. However, this is valid only for gamma-ray spectra of long-lived activities. In reality, particularly for short-lived nuclides, a gamma-ray spectrum corresponds to nuclides of different half-lives comparable to the counting time. In such situations, the total activity - therefore the dead-time and the composition of the spectrum - may change significantly during counting time,thereby necessitating the determination of dead-time experimentally.

For comparison purposes, however, fractional loss of pulses due to ADC dead-time can be approximately estimated in the following manner. For the simplicity of calculation all the channels of the spectrum can be considered equivalent to a weight-averaged single channel (for a typical spectrum with 4096 channels, weight-averaged

channel number can be assumed to be 1000). The dead-time due to a single pulse, d, can be calculated from equation III-1 by selecting typical values for parameters a and f. The relationship between the input pulse rate, R_o, measured rate, R, and the fractional dead-time, DT, can be expressed as:

$$R = R_o (1 - DT) \qquad \text{III-2}$$

Then,

$$DT = d \; X \; R$$

$$= d R_o (1 - DT) \qquad \text{III-3}$$

The fractional loss due to dead time, FL_d, is related to R_o by the following expression obtained by combining equation III-2 and III-3:

$$FL_d = (R_o - R) / R_o$$

$$= d R_o / (1 + d R_o) \qquad \text{III-4}$$

Equation III-4 enables one to approximately estimate the fractional count losses due to dead-time at different input count rates.

2. Pulse Pile-Up Losses

For a quantitative treatment of pulse pile-up losses, one cannot avoid selecting a suitable statistical model due to the random nature of the photon emission process from a radioactive source. Assuming Poisson Statistics (78W1) the following formula is proposed in section IV.A.2 to estimate fractional loss due to pile-up, FL_p, for an analyser with a pulse resolving time, τ, and for an input count rate, R_o:

$$FL_p = (1 - e^{-\tau R_o}) \qquad \text{III-5}$$

The magnitudes of these two kinds of coincidence losses calculated according to equation III-4 and III-5 for different pulse rates using typical values for different parameters (a, i, f, τ) are shown in Fig. III-4. At low pulse rates and small resolving times of the amplifier, coincidence losses are mainly due to the dead-time. In such situations only dead-time corrections may be sufficient. However, if one uses larger values for the amplifier shaping time constant - therefore larger values for τ - losses due to pulse pile-up become important, especially at high count rates. It should be noted that these calculated values can only be used as a rough guide line. For accurate results, the parameters in the above equations should be determined experimentally.

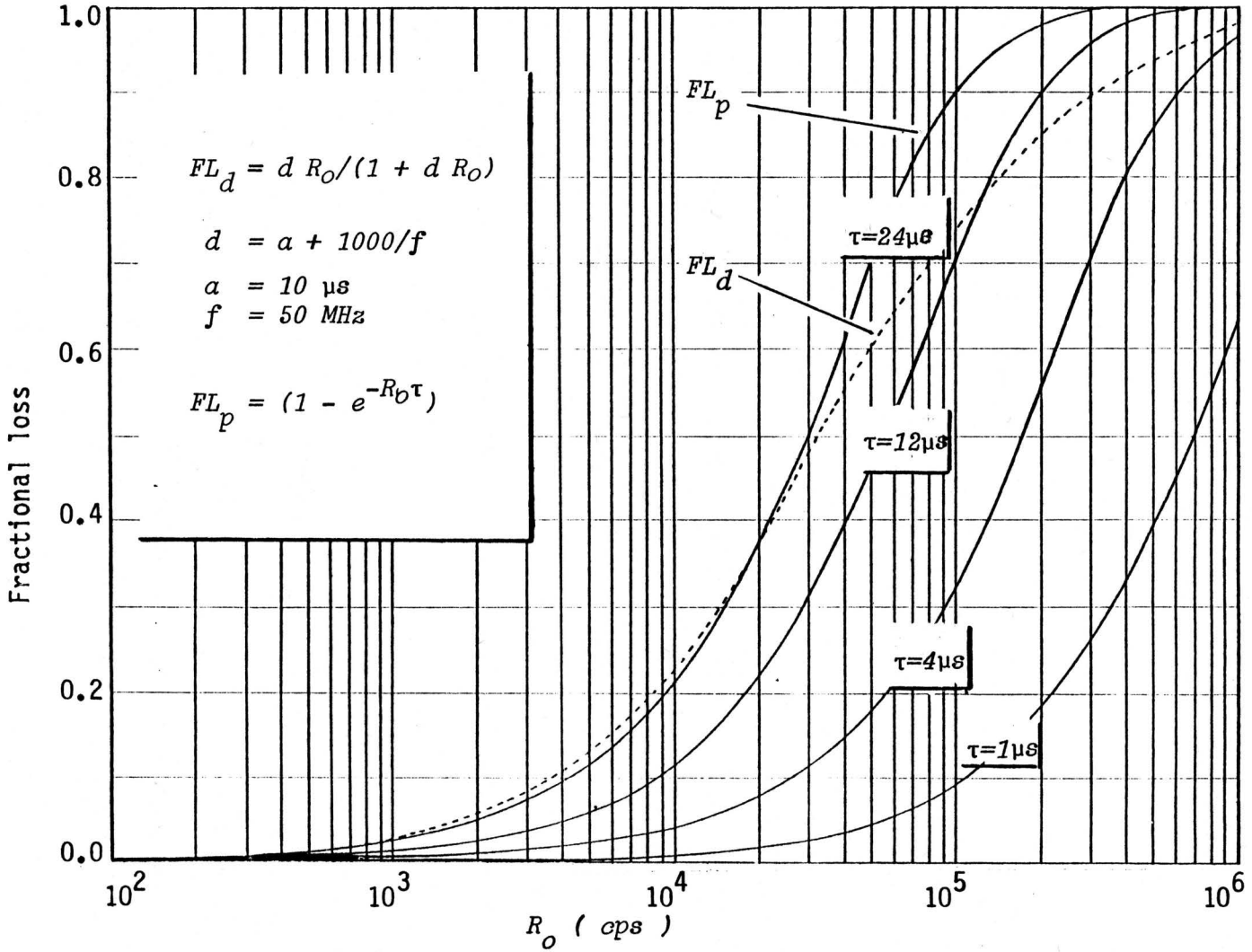

Figure III-4. Magnitudes of dead-time and pulse pile-up losses at different total absolute count rates

C. Available Correction Methods for Coincidence Losses

It is possible to minimize problems concerning dead-time and pulse pile-up by restricting the total incident rate of photons to such an extent that the coincidence losses are negligible. Such an approach will lead to poor counting statistics and therefore sensitivity and precision would be considerably reduced. In order to avoid sacrifice of sensitivity and precision arising from restricted low count rates, attempts have been made to correct for coincidence losses in gamma-ray spectrometry. Recent work in this area has generated numerous correction techniques. It should be noted that the necessity of correction methods for coincidence losses is not unique to INAA of short-lived nuclides. In fact, absolute count rate measurements of longer lived nuclides have initiated research in this area. In the following sections a brief account will be given about the available methods that are considered to be most applicable for short-lived nuclides. The reader is referred to the literature for further details regarding any individual technique.

1. Methods for Dead-Time Correction

In pulse height analysis, automatic correction for dead-time is almost always carried out by counting in the live-time mode where the counting interval is automatically extended to compensate for any dead-time thoughout the measurement. The live-time method can be expected to yield an accurate compensation for losses due to dead-time as long as the activity of interest does not decay significantly

during the entire counting period. This is because for short-lived nuclides, the activity of interest would not be the same during the dead-time and the extended time intervals (Fig.III-5). The above method, therefore, is certainly inadequate for short-lived nuclides where the counting time may be several times longer than the half-life of the desired nuclide. However, if the fractional dead-time, *DT*, remains constant throughout the measurement (*i.e.* the dead-time is mainly due to a long-lived background), appropriate correction factors can be mathematically calculated if the half-life or the decay constant of the desired short-lived nuclide is known.

The basic equation for *C*, the measured net counts in the photopeak area, can be expressed for the general case as derived by Schönfeld (66S1):

$$C = \int_{o}^{t_c} P_o \, e^{-\lambda t} \, (1 - DT) \, dt \qquad \text{III-6}$$

where,

P_o = true photopeak count rate at the beginning of the counting interval;

λ = decay constant of the nuclide of interest;

DT = instantaneous fractional dead-time;

t_c = clock time, *i.e.* counting time after extending to compensate for dead-time.

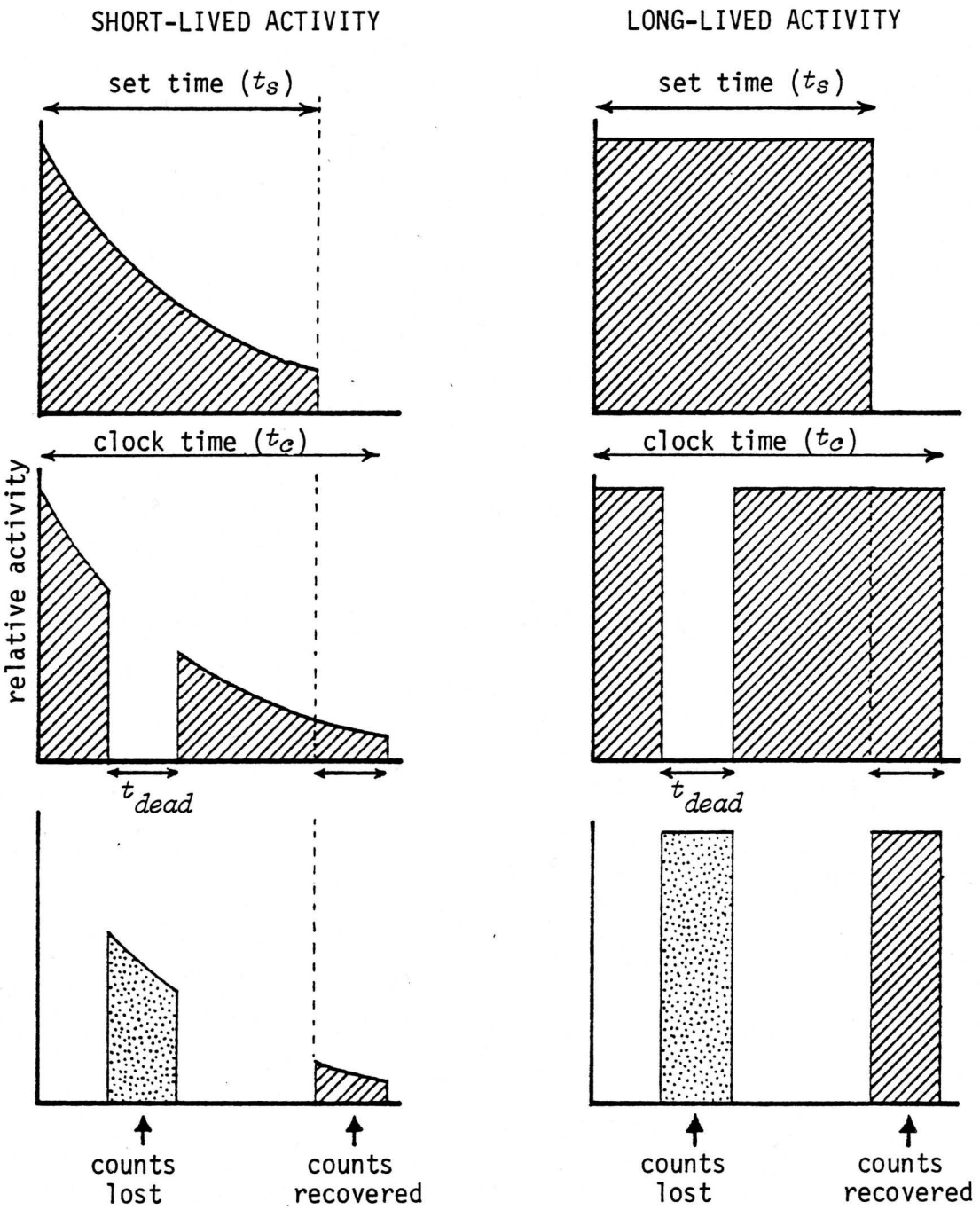

Figure III-5. Counting in live time mode for short- and long-lived nuclides

If DT remains constant, the relationship between t_c and the preset time t_s is given by:

$$t_s = t_c\ (1 - DT) \qquad \text{III-7}$$

Since DT is assumed to be a constant, a simple integration of equation III-6, and then substitution for t_c from equation III-7 gives:

$$C = P_o\ (1 - DT)\ (1 - e^{-\lambda t_s/(1 - DT)}\ )\ /\ \lambda \qquad \text{III-8}$$

If there is no dead-time (*i.e.* $DT = 0$), the corresponding expected counts in the photopeak, C_o - the quantity of ultimate interest - is then given by (substituting $DT = 0$ in equation III-8):

$$C_o = P_o\ (1 - e^{-\lambda t_s}\ )\ /\ \lambda \qquad \text{III-9}$$

From equations III-8 and III-9 it follows that the dead-time correction factor, K_d, which can be defined as the ratio C/C_o is related to DT by the following equation where λ has been replaced by $0.693/t_{1/2}$.

$$K_d = C\ /\ C_o \qquad \text{III-10}$$

$$= \frac{(1 - DT)\ (1 - e^{-0.693\ t_s/t_{1/2}\ (1 - DT)}\ )}{(1 - e^{-0.693\ t_s/t_{1/2}})} \qquad \text{III-10}$$

Fig. III-6 shows variation of K_d in relation to different ratios of $t_{1/2}/t_c$ at different constant dead-times, calculated according to equation III-10. The figure suggests that if the half-life is very small compared to t_s then even by counting the sample in the live-time mode, the relative error can be as much as the magnitude of fractional dead-time unless an additional mathematical correction is included using equation III-10. On the other hand, since K_d approaches unity as the ratio $t_{1/2}/t_s$ gets larger, the live-time method becomes satisfactory for long-lived activities where $t_{1/2}$ is several times larger than t_s.

In practice, however, this live-time correction technique has been found by several authors (72B3, 60C1, 74C2) to be erroneous even for long-lived activities. An under-compensation for dead-time arises due to the finite width of timing pulses of the live-time clock (72B3, 60C1). This effect is explained in Fig. III-7. Also, an over-compensation is introduced by ADC electronics (74C2). The relative magnitudes are such that the net effect of these two counteracting errors is an over-compensation for ADC dead-time. To correct for the error caused by the finite width of the clock pulses, a simple electronic circuit has been proposed by Bartošek *et al.* (72B3) whereas Cohen (74C2) has proposed a modification to the ADC electronics in order to eliminate the dead-time caused by pulses that are digitized by the ADC but are not stored in the memory.

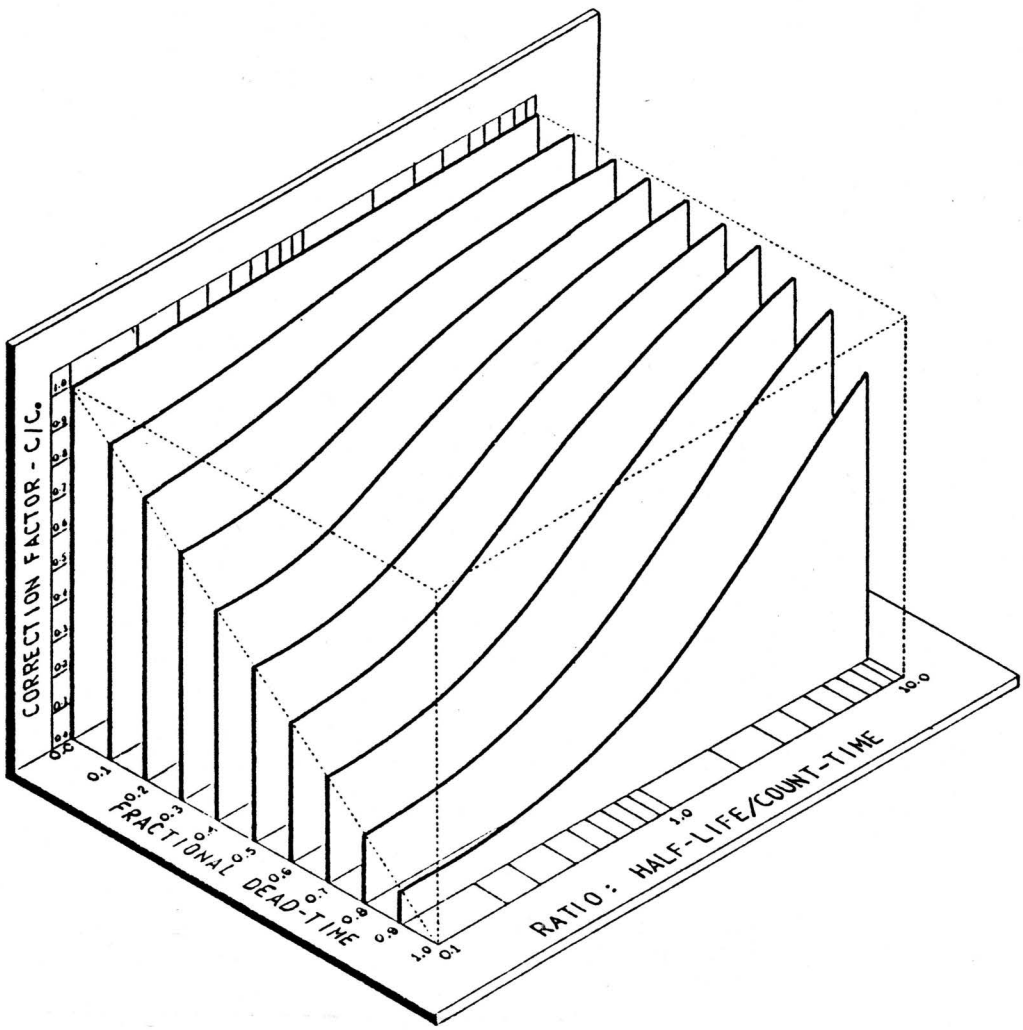

Figure III-6. Variation of the dead-time correction factor with $t_{1/2} / t_s$ ratio at different constant dead-times (for counting in the live-time mode)

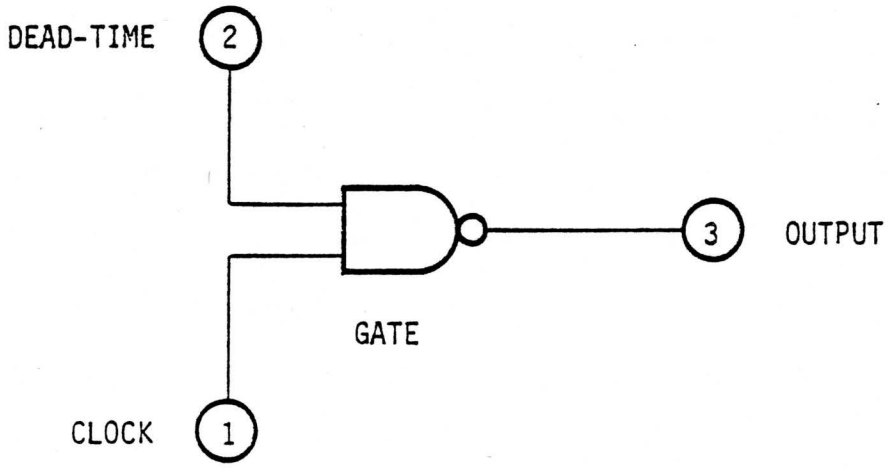

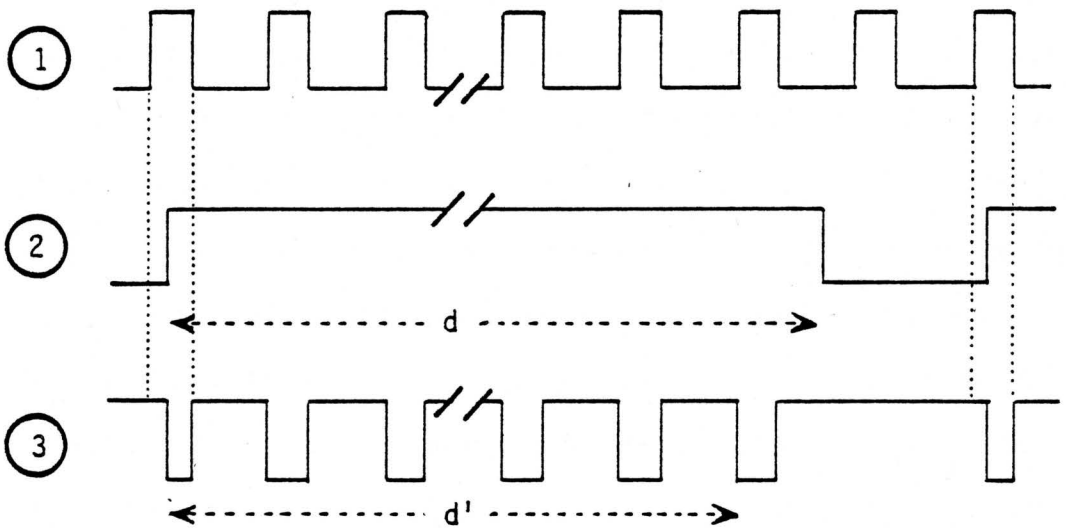

d - actual dead-time signal

d'- dead-time measured by the clock

d'<d (under-compensation)

Figure III-7. Dead-time compensating circuit - Effect of finite width of the clock pulse

A more complicated situation arises when DT varies during the counting time, *i.e.* the integration of equation III-6 becomes complicated when DT is a function of time. Several authors (72D1, 74J1, 64L1, 69W1) have proposed mathematical correction methods. Each of these methods is limited to dead-time correction only and assumes that the dead-time is due to one short-lived activity with a long-lived background (a detailed evaluation of this assumption will be given in section VI.D.1). In some methods activity is measured at different time intervals to estimate the time dependent dead-time which would be impractical if t_c is of the order of seconds, which is the case for short-lived nuclides. In cyclic activation analysis, corrections for dead-time have been done by Spyrou and Kerr (79S1) and Wiernik and Amiel (69W1) using the average dead-time in each cycle. Also in this laboratory, the average dead-time correction method was used for cyclic and pseudo-cyclic INAA before development of the elaborate correction method described in this thesis. In order to minimize possible errors in the average dead-time method the sample activity has to be restricted to low levels and the activity should not considerably change during measurement. Wiernik (71W2) has reviewed the methods available for dead-time correction in gamma-ray spectrometry.

Another approach that has been taken to circumvent the problem of time variable dead-time is to keep the dead-time at a constant value throughout the measurement by external means. This constant value is used for mathematical integration of equation III-6.

For this purpose, a dead-time stabilizer using a voltage controlled pulse generator was suggested by De Bruin *et al.* (74D1). In their system, frequency of the pulse generator is controlled by the dead-time signal from the ADC in such a way that the ADC dead-time remains constant. One major drawback of this method is the fact that generated pulses which are fed into the preamplifier create additional dead-time and pile-up losses despite maintaining a constant dead-time. Bartošek *et al.* (72B1) have proposed a method based on automatic creation of an additional dead-time at the end of very short measuring intervals so as to keep the total dead-time constant. Both the above methods have the advantage of being able to be applied to rapidly decaying activities with the latter being free from introduction of additional pile-up losses. However, both methods sacrifice the sensitivity and precision of the analysis due to unnecessary additional dead-time. To partially eliminate these problems, Görner and Höhnel (70G2) have used a modified live timer to correct for analyser dead-time where the frequency of the live-timer clock is made to decay with the half-life of the nuclide of interest, which enables one to calculate appropriate correction factors by a simple mathematical treatment. This approach, however, has the limitation that it cannot be applied to multielement analysis where several activities with different half-lives are measured.

Schönfeld (66S1) plotted the value of instantaneous dead-time read from the dead-time meter of the ADC, versus elapsed time and corrected the results by numerical integration. A similar

approach was taken by Woittiez *et al.* (79W2) by reading the dead-time at different time intervals and fitting the data into a mathematical equation. However, for these procedures half-life of the measured nuclide - as well as counting time - should be larger than several minutes. Based on Schonfeld's approach, a method was proposed by Miller and Guinn (76M1) where ADC dead-time is electronically monitored with a very small sampling time throughout the measurement. Although this method can be applied to short-lived nuclides, here a correction is done only for dead-time losses and not for pulse pile-up.

Harms (67H1) described a very promising approach for automatic correction for dead-time losses. He measured the number of pulses that are lost while the ADC is busy by means of an auxiliary counter. Correction is performed by storing compensating pulses distributed over all channels with the same distribution as that of the measured pulse-height. As long as the pulse-height distribution remains constant this method provides a satisfactory solution even for varying count rates. However, if both the count rate and pulse-height distribution vary, dead-time correction cannot be accurate for short-lived nuclides. Based on this principle, a fast digital processor has been proposed by Westphal (79W1), which he used to determine the true count rate by measuring the observed total counts and the live-time. Proper weighting factors to each channel were estimated by using only the clean pulses which are free from distortion due to pile-up. Despite the fact that this method is applicable

to very short-lived nuclides, it does not provide a satisfactory solution to pile-up losses.

2. Combined Methods for Dead-Time and Pile-Up Correction

Cohen (74C2) proposed the following relationship between the measured count rate, P, of the photopeak and its true count rate, P_o.

$$P_o = \frac{P}{1 - \tau N / t_l} \qquad \text{III-11}$$

where τ is the pulse resolving time of the amplifier and N is the total number of pulses detected. The ADC live-time, t_l, can be calculated from the clock-time, t_c, and dead-time, t_{dead}, using the following equation.

$$t_l = t_c - t_{dead} \qquad \text{III-12}$$

Since the number of counts in each channel and the appropriate parameters for the particular ADC can be known, t_{dead} can be estimated using equation III-1. The main disadvantage of applying this method to short-lived nuclides is that the formula is valid only for non-varying count rates; *i.e.* for long-lived activities. For variable count rates, Roscoe and Furr (77R1) proposed a mathematical solution for both dead-time and pile-up losses applying Cohen's formula (equation III-11) for pile-up correction. Their method

involves reading the dead-time at different time intervals and fitting the data into a mathematical equation which assumes that the measured dead-time is the sum of a dead-time varying with an average half-life and a constant dead-time. Even for a single short-lived nuclide in the presence of a long-lived background, the above assumption is not valid for high dead times since the activity does not follow a direct proportionality to the dead-time which depends on the measured count rate but not on the true count rate. Furthermore, they assumed N/t_l of Cohen's formula to be directly proportional to the measured dead-time. If the composition of the gamma-ray spectrum varies, this assumption would be erroneous due to the fact that the dead-time depends not only on the number of processed counts but also on the energy of the pulses or the channel number (equation III-1). However, at relatively low count rates, the assumptions may be sufficient for a satisfactory correction. Yet, the method can only be applied to medium-lived nuclides (half-lives longer than several minutes) due to manual recording of dead-time from the meter.

A pulser peak method to correct for losses in the entire pulse processing and recording system was introduced by Strauss *et al.* (68S1) and Anders (69A1). The basic principle of this method is that the losses suffered by pulses that are injected into the analyser at a known frequency and a precise amplitude should be equal to those suffered by any other photopeak. As long as the total activity and the composition of the spectrum do not change, this

method can be expected to yield a satisfactory correction. However, this is not applicable to the instances where the counting time exceeds the half-life of the activity of interest and to the case of varying activities.

Bolotin *et al.* (70B1) extended the above method to correct for coincidence losses at variable count rates using a random pulser with a variable pulse rate which is maintained at a fixed fraction of the nuclear event rate. In the case of mixed activities, their method is not applicable since the composition of the spectrum generally varies during measurement. Moreover, they recognized that the nuclear events suffered losses due to coincidence with both nuclear event as well as pulser events, whereas the pulser events suffered losses due to coincidence only with nuclear events. The reason for the above observation is that the overlap of pulser events among themselves did not occur in their random pulser. Bolotin *et al.* suggested that the above difference between overlaps for the pulser events and nuclear events could be minimized if the pulser rate is kept relatively low. Weirnik (71W2) studied possible systematic errors associated with the corrections for losses using a regular pulser and concluded that the errors can be avoided if the dead-time caused by the pulser event is kept an order of magnitude lower than that caused by nuclear events. He also demonstrated that a random pulser could reduce the systematic errors to a certain extent. Debertin (71D1) also showed that the errors due to non-overlap of pulser event with each other are

negligible if the nuclear event rate is relatively high.

Wyttenbach (71W3) extended the pulser idea to determine pile-up correction factors by simultaneously measuring the clock-time and live-time of the analyser. Then the measured clock-time and live-time were used to estimate the total count rate which was used to mathematically calculate the pile-up correction factor. His correction method appears to be effective up to a total count rate of 40,000 *cps*.

Although the pulser techniques described above are satisfactory for long-lived activities, they have limited applicability to short-lived nuclides where the composition of the spectrum and the count rate change rapidly during counting.

In addition to the loss of pulses, another problem caused due to pile-up effects is the feeding of unnecessary distorted pulses into the ADC for further processing. This problem has been overcome by incorporating the so-called pile-up rejectors (72B2, 67S1) into modern analysers. In a pile-up rejector, which consists of a fast amplifier and a pile-up inspector, each and every pulse is electronically inspected before input to the ADC, and the pulses subjected to distortion due to pulse-overlap are rejected, thereby eliminating the distortion of the total spectrum due to the storage of wrong information (Fig. III-8). However, this does not make any correction for the lost information but also introduces additional losses due to its finite inspection time.

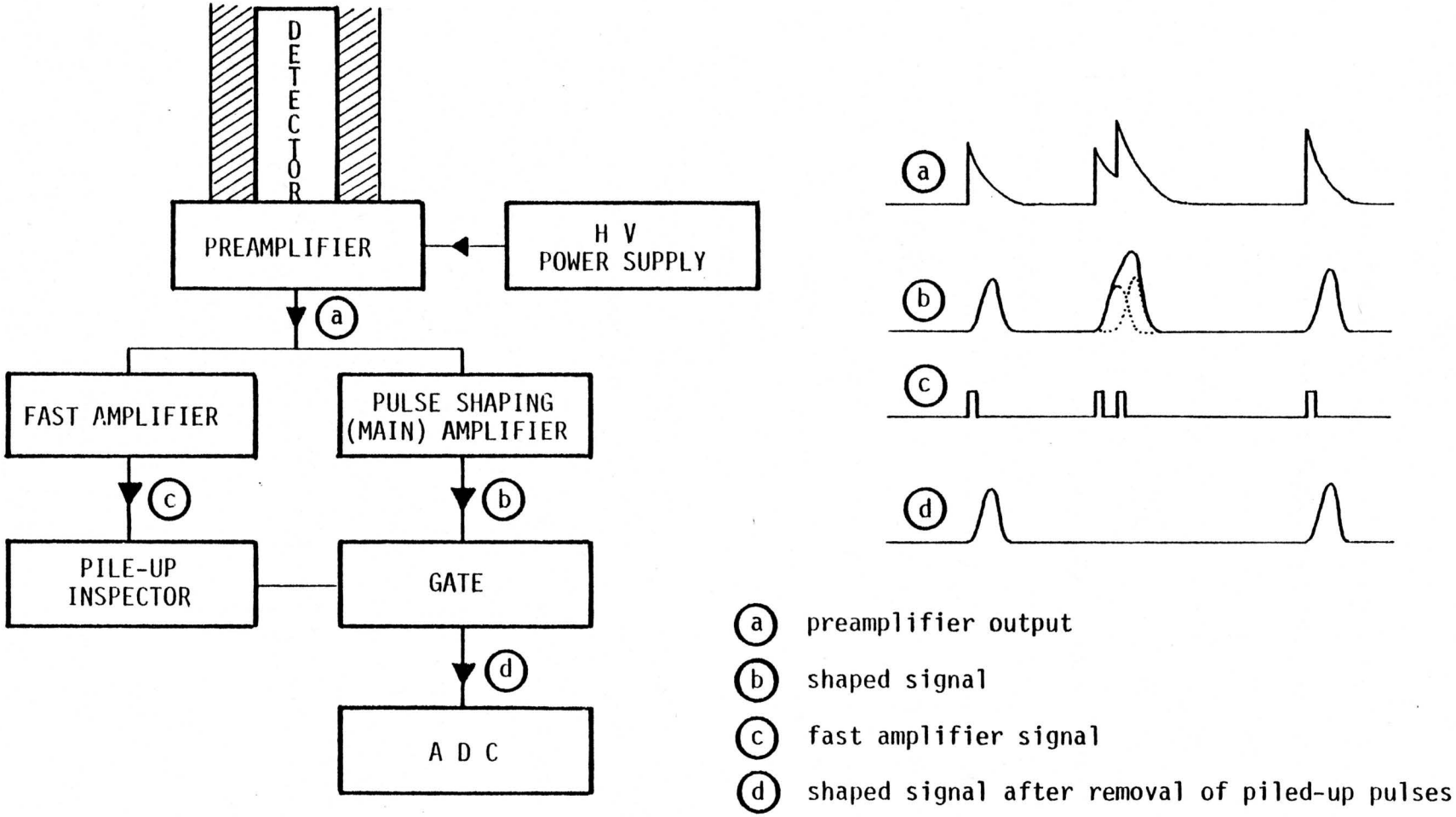

Figure III-8. Schematic representation of pile-up rejection

In conclusion to the brief review given above, one can note that there have been many possible approaches to correct for coincidence losses in gamma-ray spectrometry. None of them offers an ideal solution; each and every method has its own advantages and limitations. The choice of a particular method depends on available instruments and the nature of the analytical problem. Most of the methods described above are not applicable to short-lived nuclides with half-lives ranging from a fraction of a second to a few seconds. For details about experimental comparison of some of the above methods, the reader is referred to the studies carried out by, most notably, Wiernik (71W1), Huysmans *et al.* (74H1) and Dryak *et al.* (78D1).

During the earlier developments of PCINAA and CINAA (79C2, 81C1) methods in this laboratory, the dead-time corrections were performed using the average dead-time measured in each cycle. In order to minimize errors, the dead-time of the analyser had to be maintained below $\sim$ 10% or the standards also had to be analysed under similar dead-time conditions. In some cases, the sensitivity of the methods could not be exploited at its best as the total activity sensed by the detector had to be restricted by employing shorter irradiations, lower fluxes, smaller sample sizes or less efficient geometries.

In several instances severe problems were encountered, even in conventional INAA using medium-lived nuclides (half-lives of the order of minutes) in the presence of interfering nuclides such as ^{28}Al and ^{52}V. These interferences were observed in a wide variety of

matrices, such as coal (79S1), coal fly-ash, oil fly-ash and atmospheric particulate matter (81D1), biological (80T1, 79C1), geological materials (78C1), and suspended particulate matter (80K1), analysed in this laboratory.

It was recognized that a satisfactory solution to the problem of coincidence losses for half-lives ranging from a fraction of a second to several minutes was essential; especially for CINAA methods developed in this study for nuclides with half-lives less than few seconds. This led to the development of the correction technique, described in this thesis for both dead-time and pile-up losses, which was later successfully applied to short-lived nuclides in the presence of rapidly varying activities. The correction method developed is described in Chapter IV.

CHAPTER IV

PROPOSED CORRECTION METHOD FOR COINCIDENCE LOSSES

Chapter III expects to acquaint the reader with the nature of problems arising from dead-time and pulse pile-up losses. Theoretical treatments developed to obtain an expression for the correction factor in terms of experimentally determinable parameters, considering both types of coincidence losses are dealt in this chapter. Also discussed are the methods to determine quantities along with the mathematics developed for their manipulation.

A. Theoretical Aspects

1. Ideal Case

If the true count rate at the beginning of counting of a photopeak is P_o then the measured number of counts, C_o - assuming no coincidence losses in the photopeak - is ideally given by:

$$C_o = \int_o^{t_s} P_o \, e^{-\lambda t} \, dt \qquad \text{IV-1}$$

$$= P_o \, (1 - e^{-\lambda t_s}) \, / \, \lambda \qquad \text{IV-2}$$

However, it is impossible to measure the true count rate of a

random process by means of a physical instrument due to its finite time resolution. If the pulses are subjected to coincidence losses, the measured number of counts, C, should be appropriately corrected so that it accurately represents the expected value C_o. Thus, the success of a correction method depends on how close the corrected value is to the exact value.

2. Incorporation of Pile-Up Correction

It was mentioned earlier (Section III.B.2) that for quantitative treatment of pile-up losses, one cannot avoid a statistical treatment due to the random nature of photon emission from a radioactive source. One of the axioms of nuclear science, since the original proposition in 1905 by von Schweidler (05S1), has been that radioactive decay is a Poisson process. This has often been confirmed (32C1, 62E1, 10R1) and also, there has been some observations that measured counts do not strictly follow Poisson statistics in beta and gamma counting systems (72A1, 74F1). However, the magnitude of this difference is such that it is a reasonable approximation for the situation considered below. The principles used in the following derivation can be equally applied to any other statistical model. It is worth noting that the quantitative treatment of pile-up losses should be different depending on whether or not a pulse pile-up rejector is used in an analyser system. The use of a pile-up rejector results in only the clean pulses arriving at the ADC for conversion. On the other hand, when a pile-up rejector is not used, two or more pulses coming together

within the resolving time appear as a single distorted pulse at the ADC input. Both the above cases are considered separately in deriving an expression for a pile-up correction factor K_p in terms of experimentally determinable parameters as given below.

a. *Case I - when a pile-up rejector is used*

According to Poisson statistics (78W1), the probability distribution of the Poisson random variable, X, representing the number of successes, x, occuring in a given time interval or specified region is:

$$p\ (x,\ \mu) \quad = \quad \frac{e^{-\mu}\ \mu^{x}}{x!} \qquad\qquad x = 1,\ 2,\ 3,\ \ldots \qquad \text{IV-3}$$

where μ is the average number of successes in the given time interval or specified region.

Applying this concept to photon counting, the probability for n pulses occuring together in a time τ can be given as:

$$p\ (n,\ R_o\tau) \quad = \quad \frac{e^{-R_o\tau}\ (R_o\tau)^{n}}{n!} \qquad\qquad \text{IV-4}$$

where R_o is the true average pulse rate. If τ is taken as the pulse resolving time of the amplifier, in such a situation information about n pulses would be lost. Therefore, all pulses with $n \geq 2$ entering

the amplifier within time τ would be rejected from entering the ADC.

The average number of pulses that can come with $n \geq 2$ in the time interval, τ, N_{lost} can be given as:

$$N_{lost} = \sum_{n=2}^{\infty} \frac{e^{-R_o\tau} (R_o\tau)^n n}{n!} \qquad \text{IV-5}$$

$$= e^{-R_o\tau}\left[\sum_{n=1}^{\infty} \frac{(R_o\tau)^n n}{n!} - \sum_{n=1}^{1} \frac{(R_o\tau)^n n}{n!}\right]$$

$$= e^{-R_o\tau} (R_o\tau\, e^{R_o\tau} - R_o\tau)$$

It follows that:

$$N_{lost} = R_o\tau (1 - e^{-R_o\tau}) \qquad \text{IV-6}$$

Since $R_o\tau$ is the average number of pulses entering during time τ, fractional loss due to pulse pile-up, FL_p is given by:

$$FL_p = \frac{N_{lost}}{R_o\tau} = (1 - e^{R_o\tau}) \qquad \text{IV-7}$$

Therefore, the fraction of unaffected pulses, FU_p can be given as:

$$FU_p = e^{-R_o\tau}$$

If R_a is the output rate from the amplifier-pile-up rejector system, fraction unaffected would be same as R_a/R_o. Therefore,

$$R_a / R_o = e^{-R_o\tau} \qquad \text{IV-8}$$

The above equation provides a means to estimate R_o if the pulse resolving time τ and measured rate at the output of the amplifier, R_a, are known. Then the correction for instantaneous peak count rate can be derived from:

$$P / P_o = e^{-R_o\tau} \qquad \text{IV-9}$$

where, P - measured count rate of the photopeak

P_o - true count rate of the photopeak

b. *Case II - when a pile-up rejector is not used*

Here the distinction from *case I* arises in the observation that when n pulses come together within time τ, they are recorded as a single pulse instead of being completely rejected. Therefore, the number of counts lost will be $(n-1)$ compared to n in *case I*.

Hence, the average number of pulses lost during time τ would be

$$N_{lost} = \sum_{n=2}^{\infty} \frac{e^{-R_o\tau} (R_o\tau)^n (n-1)}{n!} \qquad \text{IV-10}$$

$$N_{lost} = \sum_{n=2}^{\infty} \frac{e^{-R_o\tau}(R_o\tau)^n\, n}{n!} - \sum_{n=2}^{\infty} \frac{e^{-R_o\tau}(R_o\tau)^n}{n!}$$

which reduces to (in a similar manner as equation IV-6 was simplified)

$$N_{lost} = R_o\tau + e^{-R_o\tau} - 1 \qquad \text{IV-11}$$

The number of pulses coming out of the amplifier within time τ (N_a) is given by

$$N_a = R_o\tau - N_{lost}$$

$$= 1 - e^{-R_o\tau} \qquad \text{IV-12}$$

However, the fraction of pulses recorded in the photopeak, P/P_o, will still take the same relationship as in *case I*. This is because although a pulse corresponding to the photopeak is recorded even after distortion, it would be recorded in another channel, which is equivalent to rejection of that pulse from the photopeak. Therefore, the ratio P/P_o still bears the relationship given by equation IV-9 appeared in *case I*.

Combining equations IV-9 and IV-12, one obtains

$$P / P_o = (1 - N_a) \qquad \text{IV-13}$$

Since N_a is the average number of pulses coming out of the amplifier within time τ and R_a is the average pulse rate at the output of the amplifier, N_a in the above equation can be replaced by $R_a\tau$. Then equation IV-13 can be rewritten as:

$$P / P_o = (1 - R_a\tau) \qquad \text{IV-14}$$

The above equation is similar to the relationship (equation III-11) derived using a different approach, by Cohen (74C2) who only considered *case II*.

The choice of equation IV-9 or IV-13 will depend on whether or not a pile-up rejector is incorporated in the analyser system. The use of equation IV-9 (for cases when pile-up rejectors are used) would require further mathematical treatment. However, since in this study a pile-up rejector was not used, only equation IV-14 will be considered.

$(R_a\tau)^2$ and $(R_a\tau)^3$ terms:

There are several ways by which $(R_a\tau)^2$ and $(R_a\tau)^3$ terms could appear in equation IV-14. These terms may be significant at very high count rates. An incoming pulse can overlap with the previous one on the negative side or the positive side of the base line. This overlap results in a higher background of the gamma-ray spectrum on either side of the photopeak than under the peak, which would lead to over-

estimation of the true background and would take away some peak counts in addition to the real background. Another reason for the appearence of these additional terms (*viz.* $(R_a\tau)^2$, $(R_a\tau)^3$) is that R_a is derived from "SCA OUT" of the ADC, which will be described later in detail (section IV.A.3). Moreover, other factors such as possible deviation from Poisson statistics and the possibility of having variable values for τ in extreme cases, due to overlap of several pulses to give a very large pulse which can affect τ, may also contribute to these terms. Consequently, equation IV-14 should be modified as:

$$P / P_o = \{1 - c_1 R_a \tau - c_2 (R_a \tau)^2 - c_3 (R_a \tau)^3\} \qquad \text{IV-15}$$

where c_1, c_2, c_3 are constants. By incorporating c_1, c_2 and c_3 with τ in another set of constants, *i.e.* C_1, C_2, C_3, the above equation can be rewritten as:

$$P / P_o = (1 - C_1 R_a - C_2 R_a^2 - C_3 R_a^3) \qquad \text{IV-16}$$

Consequently, the expression for the number of counts measured in the photopeak by the ideal equation IV-1 can be modified using equation IV-16, to incorporate the pile-up correction terms. Then the resultant equation becomes:

$$C = \int_0^{t_s} P_o (1 - C_1 R_a - C_2 R_a^2 - C_3 R_a^3) e^{-\lambda t} dt \qquad \text{IV-17}$$

3. Incorporation of Dead-Time Correction

Due to its finite processing time (dead-time), an ADC does not process all the incoming pulses that come out of the amplifier per unit time (*i.e.* R_a in equation IV-17). However, generally all ADC's have a "SCA OUT" (single channel analyser output) which gives a logic pulse for each pulse processed by the ADC. Therefore the number of pulses processed by the ADC in a unit time would be the same as the rate of logic pulses given out by SCA output, R_s. If the fractional dead-time is DT, R_s and R_a can be related by:

$$R_a = R_s / (1 - DT) \qquad \text{IV-18}$$

It should be noted that this relationship is valid only if the discriminators are properly set. The lower level discriminator (LLD) should be set just above the noise level and the upper level discriminator (ULD) should be as high as possible. If the ULD is set too low, then the pulses going above this level would not be included in R_s, which would result in lower values for R_a in equation IV-18. However, when ULD is properly adjusted, pulses going above this level would be negligible. At extremely high count rates, even though there is a greater probability of piled-up pulses going above the set ULD, their effects have already been taken into account by $(R_a\tau)^2$ and $(R_a\tau)^3$ factors in deriving equation IV-17.

The second term which should be corrected in equation IV-17 for ADC dead-time is dt. During a small clock (real) time dt, the ADC is sensitive to incoming pulses only for a duration $(1-DT)dt$. Therefore, dt should be replaced by $(1-DT)dt$.

Furthermore, if the counting is performed in the live-time mode, t_s in the integration term of equation IV-17 should be replaced by t_c since the analyser automatically extends the clock-time to t_c so that live-time of the analyser still has the value of set-time t_s.

When the terms R_a, dt, and t_s in equation IV-17 are replaced by $R_s/(1-DT)$, $(1-DT)dt$, and t_c, respectively, (*i.e.* the terms corrected for ADC dead-time) it becomes:

$$C = P_o \int_o^{t_c} \left[1 - C_1\left(\frac{R_s}{1-DT}\right) - C_2\left(\frac{R_s}{1-DT}\right)^2 - C_3\left(\frac{R_s}{1-DT}\right)^3\right] X\ (1-DT)\ e^{-\lambda t}\ dt \qquad \text{IV-19}$$

Consequently, the final correction factor K for both pulse pile-up and dead-time losses can be obtained by dividing equation IV-2 by equation IV-19:

$$K = C / C_o$$

$$K = \frac{\int_o^{t_c} \left[1 - C_1\left(\frac{R_s}{1-DT}\right) - C_2\left(\frac{R_s}{1-DT}\right)^2 - C_3\left(\frac{R_s}{1-DT}\right)^3\right](1-DT)\ e^{-\lambda t}\ dt}{(1 - e^{-\lambda t_s}) / \lambda} \qquad \text{IV-20}$$

It should be noted that R_s and DT in the above equation are instantaneous values since they are time dependent quantities for varying count rates. Now, according to the above expression, the combined correction factor K for dead-time and pile-up losses can be determined by simply knowing R_s and DT as time variables, coefficients C_1, C_2 and C_3, and the clock time t_c.

B. Experimental Procedures

1. Measurement of Parameters

a. R_s - *logic pulse rate at "SCA OUT"*

The time dependent variable R_s can be obtained by measuring logic pulse rate from "SCA OUT" of the ADC at properly selected sampling intervals using another analyser operated in the multichannel scaling mode. A multichannel scaler (MCS) uses each channel as a separate counter and counts are recorded in one channel for a preset time (*i.e.* a sampling time which can generally range from μs to ms). Then the analyser switches automatically to channel two and so on. From these successively accumulated counts in each channel the variation of R_s with time can be derived.

b. DT - *time dependent dead-time*

Whenever the ADC is processing and storing a pulse, it outputs a *busy* signal. This signal is monitored as a function of time using

an electronic circuit (which has been designed in this work and described in Appendix A) that gives out a number of pulses proportional to the length of the *busy* signal or the dead-time. This operation is performed by using the *busy* signal to enable a gate to allow passage of clock pulses from a 5 MHz crystal controlled oscillator to a MCS. The principle of this operation is depicted in Fig. IV-1.

It has been described above that both time variable quantities R_s and DT have to be measured using multichannel scalers. The requirement of two multichannel scalers is avoided by storing both the signals alternately in the same analyser with the aid of a data selector circuit (designed in this project and described in Appendix B) run at a suitable toggle frequency.

The complete arrangement of the analyser system including the components designed for measuring R_s and DT are shown in Fig. IV-2.

c. t_c - *counting time*

The clock time t_c would be equal to the set-time t_s when an analyser is operated on clock-time mode. Even when it is operated in the live-time mode, if the dead-time is negligibly small, t_c would be almost same as t_s. However, if the dead-time is appreciable, t_c would be larger than t_s (equation IV-21) so that the live-time of the analyser would remain equal to t_s.

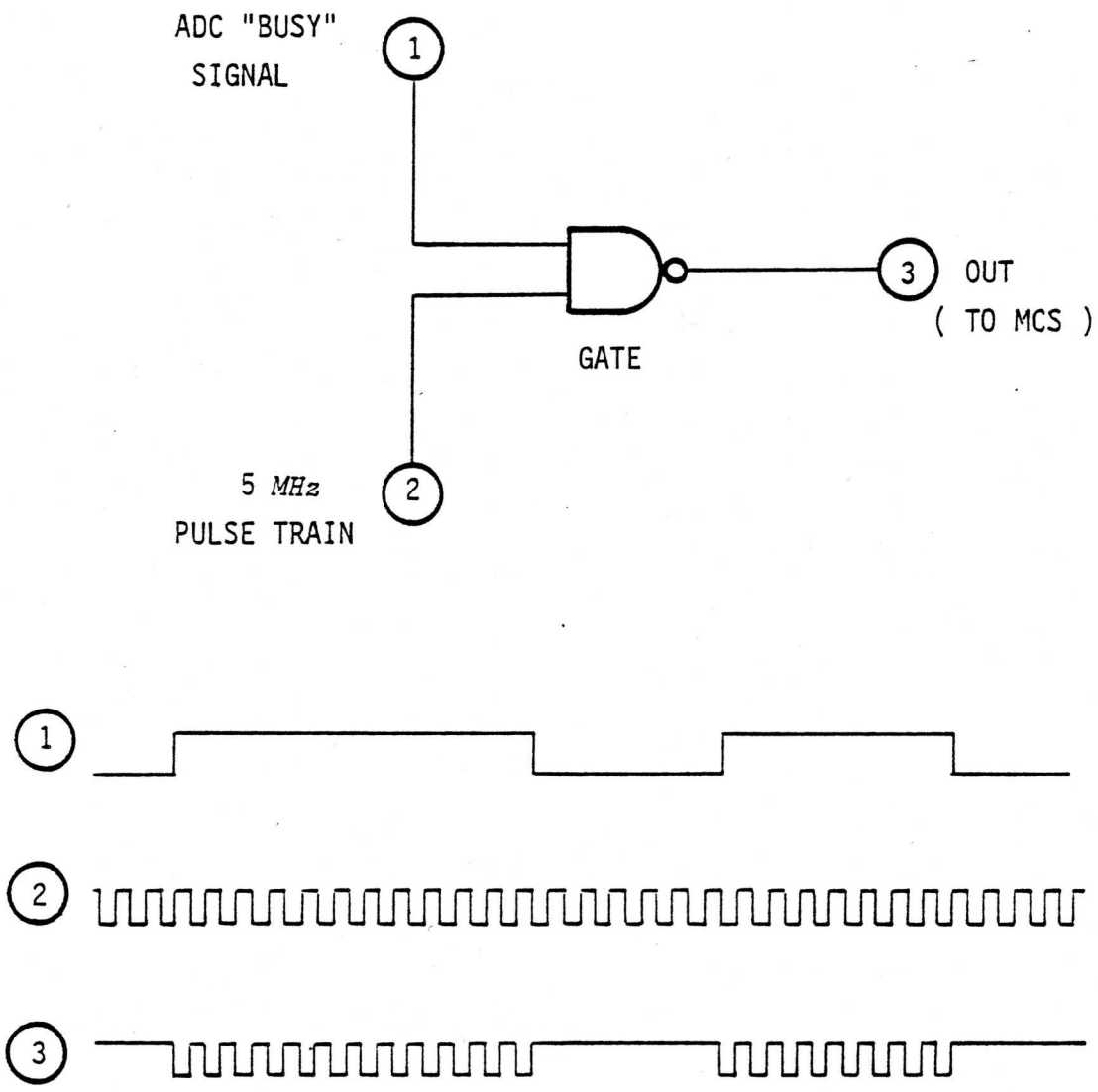

Figure IV-1. The principle of ADC dead-time measurement

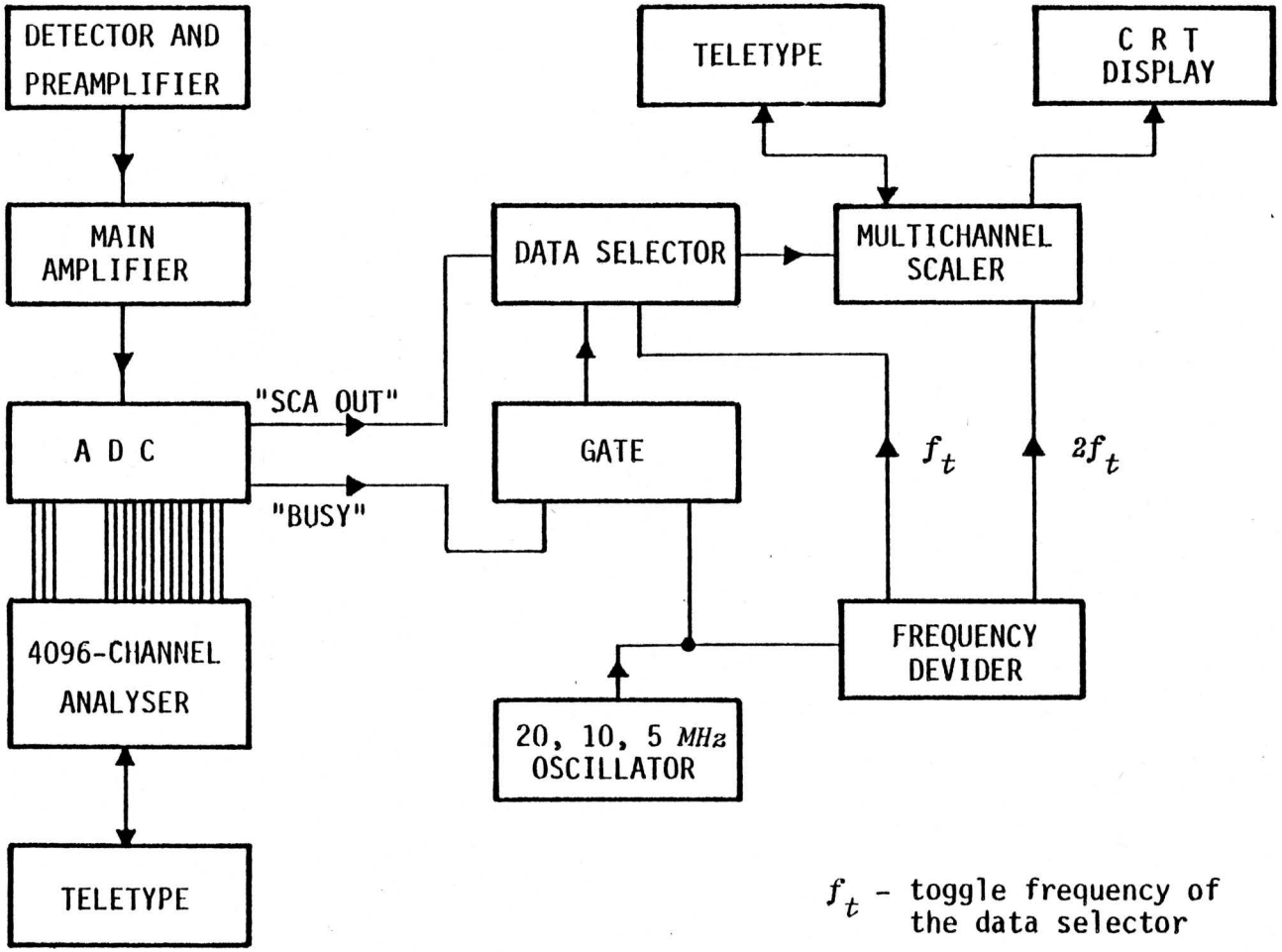

Figure IV-2. A block diagram of complete gamma-ray spectrometry system including the components for dead-time and pile-up correction

$$t_c = t_s + t_{dead} \qquad \text{IV-21}$$

Both t_c and t_s can be directly read from some analysers (such as the TN-1700 used in this work); in others (such as the TN-11, also used in this work), an additional electronic circuit can be used to monitor t_c. However, a separate measurement of t_c can be avoided as follows. The value of t_c can easily be obtained by incorporating the measured time variable DT in the above expression (equation IV-21) as follows:

$$t_c = t_s + \int_0^{t_c} DT\, dt \qquad \text{IV-22}$$

Details of mathematical calculation of equation IV-22 will be given in section IV.B.2

d. *coefficients* C_1, C_2 *and* C_3

Since these parameters are constants for a given arrangement of an analyser, they need to be measured only once for a given pulse shaping time constant of the main amplifier. Moreover, the numerical values of these coefficients will remain the same regardless of a constant count rate (*i.e.* of a mixture of long-lived nuclides only), a variable count rate and a variable composition (*i.e.* mixtures of short- and long-lived nuclides). Therefore, one can easily make use of long-lived nuclides to obtain a simple and an accurate estimate of

these coefficients.

If all the activities of a sample are due to long-lived nuclides and counting is performed in the live-time mode, count losses of a particular photopeak would only be due to pile-up, since losses due to dead-time are completely recovered by extending t_c to compensate for dead-time. This is evident from equation IV-20 which reduces to the following equation IV-23 at constant DT and R_s.

$$K = 1 - C_1\left(\frac{R_s}{1-DT}\right) - C_2\left(\frac{R_s}{1-DT}\right)^2 - C_3\left(\frac{R_s}{1-DT}\right)^3 \qquad \text{IV-23}$$

With the analyser shown in Fig. IV-2, the constant activity of a long-lived radioactive standard can be measured at different total count rates by imparting additional background counts from another long-lived radioactive source. If there are no pile-up losses, the ratio C/C_o should diminish as total count rate - hence R_s - increases. Since both R_s and DT (R_s and DT are constants for long-lived nuclides) can be measured with the arrangement described in Fig. IV-2, C/C_o can be measured for different sets of known R_s and DT. By fitting the data into equation IV-23 using least square method C_1, C_2 and C_3 can thus be estimated. For determining C_1, C_2 and C_3 by this method, one can also use the pulser technique proposed by Anders (69A1) and Strauss (68S1). It should be noted here that the pulser technique cannot be directly applied to short-lived nuclides;

however, once it is used to determine C_1, C_2, C_3 then those terms can be used for short-lived nuclides using equation IV-20.

If one uses the long-lived nuclide-technique for determining coefficients C_1, C_2 and C_3, counting can be continued as long as it is desired in order to improve statistics of the results. When a regular pulser is employed, errors due to non-random nature of the pulser peak can be minimized using a very small pulser count rate compared to the total background count rate. The statistical errors caused by low pulser count rates can be avoided by stretching the counting time as much as required.

2. Mathematical Treatment of Experimental Parameters

It has already been stated that the time variables R_s and DT are sampled for short successive intervals, and are stored alternately in the multichannel scaler. However, these values (which decay with time according to a near-exponential fashion) cannot be directly used for a simple solution of the integration term in equation IV-20 in order to calculate K.

This difficulty can be overcome by fitting the data points obtained for R_s and DT into two polynomials which take the following forms:

$$R_s = a_o + a_1 t + a_2 t^2 + \ldots\ldots + a_n t^n \qquad \text{IV-24}$$

$$DT = b_o + b_1 t + b_2 t^2 + \ldots\ldots + b_n t^n \qquad \text{IV-25}$$

The coefficients a_o, a_1, a_2, . . . and b_o, b_1, b_2, . . . can be calculated by polynomial regression analysis using a computer program.

In addition to simplifying the integration term, the regression analysis will result in the reduction of errors due to statistical fluctuation of the measured data points for R_s and DT. From a computer simulation study with numerous combinations of short- and long-lived activities it was observed that a third or fourth order polynomial is sufficient for fitting the data to the curve with a relative deviation of less than 1% (this is treated in more detail in section VI.D.1). Any further desired accuracy can be obtained by considering other terms with higher orders in the polynomial. However, this will result in a longer computer program for regression analysis.

Even if the time variable polynomial functions DT and R_s are substituted in the integration term of equation IV-20, one can see that the mathematical integration still remains fairly complicated. This difficulty can be considerably overcome by the following procedure.

By defining another time variable function $F(t)$, the expression for the correction factor K (equation IV-20) can be rewritten as

$$K = \frac{\int_0^{t_c} \left[1 - F(t)\right] e^{-\lambda t}\, dt}{(1 - e^{-\lambda t_s})/\lambda} \qquad \text{IV-26}$$

where

$$1-F(t) = \left[1 - C_1\left(\frac{R_s}{1-DT}\right) - C_2\left(\frac{R_s}{1-DT}\right)^2 - C_3\left(\frac{R_s}{1-DT}\right)^3\right] (1 - DT) \qquad \text{IV-27}$$

Since R_s and DT are known for any value of t from equations IV-24 and IV-25 and since the coefficients C_1, C_2 and C_3 are also known for the particular analyser arrangement, $F(t)$ can be calculated for different values of time using equation IV-27. Since $F(t)$ varies with time in a fashion similar to DT and R_s, the calculated values of $F(t)$ also can be fitted to a polynomial which is defined as:

$$F(t) = k_o + k_1 t + k_2 t^2 + \ldots + k_n t^n \qquad \text{IV-28}$$

Then equation IV-26 can be easily solved using the values of k-coefficients obtained by regression analysis of equation IV-28 assuming a fourth order polynomial. After the integration of equation IV-26, the final expression for the correction factor K becomes:

$$K = \frac{1}{(1 - e^{-\lambda t_s})} \left\{ (1 - k_o)(1 - e^{-\lambda t_c}) \right.$$

$$- (1 - e^{-\lambda t_c} - \lambda t_c e^{-\lambda t_c}) \left[\frac{k_1}{\lambda} + \frac{2k_2}{\lambda^2} + \frac{6k_3}{\lambda^3} + \frac{24k_4}{\lambda^4} \right]$$

$$\left. + (t_c^2 e^{-\lambda t_c}) \left[k_2 + k_3 \left(\frac{3}{\lambda} + t_c \right) + k_4 \left(\frac{12}{\lambda^2} + \frac{4t_c}{\lambda} + t_c^2 \right) \right] \right\} \quad \text{IV-29}$$

Since DT is known as a function of time, t_c can be calculated as follows:

$$t_c = t_s + \int_o^{t_c} (b_o + b_1 t + b_2 t^2 + b_3 t^3 + b_4 t^4)\, dt$$

$$t_c = t_s + b_o t_c + \frac{b_1 t_c^2}{2} + \frac{b_2 t_c^3}{3} + \frac{b_3 t_c^4}{4} + \frac{b_4 t_c^5}{5} \quad \text{IV-30}$$

Since t_s and the coefficients, b_o, b_1, . . . are already known, the value of t_c in the equation IV-30 can be obtained by the successive approximation method with the starting value for t_c, on the right hand side taken as t_s. It was observed that calculation of t_c by the above manner with a computer program takes only approximately 5 - 6 loops for a precision of less than 0.01%. However, if counting is performed in the clock-time mode then t_c is same as t_s; consequently, t_c in equation IV-29 should directly be replaced by t_s.

C. Summary of the Proposed Correction Method

Correction factor for dead-time and pile-up losses, K, was derived as (section IV.A):

$$K = \frac{\int_0^{t_c} \left[1 - C_1\left(\frac{R_s}{1-DT}\right) - C_2\left(\frac{R_s}{1-DT}\right)^2 - C_3\left(\frac{R_s}{1-DT}\right)^3 \right] (1-DT) e^{-\lambda t}\, dt}{(1 - e^{-\lambda t_s}) / \lambda} \qquad \text{IV-20}$$

Time variable R_s (from "SCA OUT") and the fractional dead-time DT are electronically monitored using a multichannel scaler. The experimental data points are fitted into two polynomial expressions given as:

$$R_s = a_o + a_1 t + a_2 t^2 + a_3 t^3 + a_4 t^4 \qquad \text{IV-23}$$

$$DT = b_o + b_1 t + b_2 t^2 + b_3 t^3 + b_4 t^4 \qquad \text{IV-24}$$

The above expression for K (equation IV-20) can be written in a simplified form by defining another time variable function $F(t)$:

$$K = \frac{\int_0^{t_c} \left[1-F(t)\right] e^{-\lambda t}\, dt}{(1 - e^{-\lambda t_s}) / \lambda} \qquad \text{IV-26}$$

where,

$$1-F(t) = \left[1 - C_1\left(\frac{R_s}{1-DT}\right) - C_2\left(\frac{R_s}{1-DT}\right)^2 - C_3\left(\frac{R_s}{1-DT}\right)^3\right](1 - DT) \qquad \text{IV-27}$$

Since R_s and DT are known as functions of time, $F(t)$ can be calculated as a function of time. These values are fitted into another polynomial defined as:

$$F(t) = k_o + k_1 t + k_2 t^2 + k_3 t^3 + k_4 t^4 \qquad \text{IV-28}$$

The above procedure simplifies the integration involved in equation IV-20. By substituting the expression for $F(t)$ in equation IV-26 and performing the integration, the final expression for K appears as:

$$K = \frac{1}{(1 - e^{-\lambda t_s})}\left\{(1 - k_o)(1 - e^{-\lambda t_c}) - (1 - e^{-\lambda t_c} - \lambda t_c e^{-\lambda t_c})\left[\frac{k_1}{\lambda} + \frac{2k_2}{\lambda^2} + \frac{6k_3}{\lambda^3} + \frac{24k_4}{\lambda^4}\right] + (t_c^2 e^{-\lambda t_c})\left[k_2 + k_3\left(\frac{3}{\lambda} + t_c\right) + k_4\left(\frac{12}{\lambda^2} + \frac{4t_c}{\lambda} + t_c^2\right)\right]\right\} \qquad \text{IV-29}$$

Calculation of t_c for the above equation is carried out by the successive approximation method using the following equation.

$$t_c = t_s + b_o t_c + \frac{b_1 t_c^2}{2} + \frac{b_2 t_c^3}{3} + \frac{b_3 t_c^4}{4} + \frac{b_4 t_c^5}{5} \qquad \text{IV-30}$$

If counting is performed in the clock-time mode, t_c should be replaced by t_s.

A Fortran IV computer program was written for the above described computation. R_s and DT data were taken to a paper tape and fed to the computer (Cyber 170-720 computer, Dalhousie University). Other parameters which are necessary for computation, such as λ, t_s, standard values *etc.* are fed manually via the terminals. The basic steps in the computer program for calculating K are;

(i) Reading values for R_s and DT from the paper tape

(ii) Calculation of a- and b- coefficients in the corresponding polynomials for R_s and DT by regression analysis

(iii) Calculation of $F(t)$ for each time interval, using the expressions for DT and R_s, according to equation IV-27

(iv) Fitting the above calculated values for $F(t)$ into the polynomial given by equation IV-28 and calculation of k-coefficients

(v) Calculation of t_c using equation IV-30

(vi) Calculation of the correction factor K using equation IV-29.

The results obtained using the above described correction method will be given in Chapter VI.

D. Estimation of Absolute Total Count Rate - R_o

According to the above formulated correction method, in order to calculate the correction factor it is necessary to calculate the absolute total input count rate, R_o. However, for evaluation purposes of the correction method (especially for comparison with several correction methods), at least an approximate value of R_o may be of interest. Therefore, it is necessary to have a method to estimate R_o using the above correction method and derived equations.

Just as when deriving a pulse pile-up correction expression in section IV.A.2, the method of calculating R_o would be different whether or not a pulse pile-up rejector is used. Thus, the aim is to derive separate expressions for R_o for the two cases in terms of empirical parameters, *viz.* R_s and DT.

1. *Case I - when a pile-up rejector is used*

In this situation, ratio of the total count rate measured at the output of the amplifier-pile-up rejector system to the total input count rate, R_a/R_o, would be same as the ratio of output (*i.e.* undistorted) to the input count rate of any photopeak in the spectrum. Therefore, R_a/R_o will be same as the pile-up correction factor K_p, for a given instance of time. Hence,

$$R_o = R_a / K_p \qquad \text{IV-31}$$

By substituting for R_a from equation IV-18 :

$$R_o = R_s / (1 - DT)\, K_p \qquad \text{IV-32}$$

Since K_p can be calculated for measured values of R_s and DT using the previously described correction method, R_o can also be calculated using the above equation IV-32.

2. *Case II - when a pile-up rejector is not used*

Under these circumstances R_a also includes distorted pulses. However, the pile-up correction factor, K_p will still be equal to the fraction of undistorted pulses. Then the relationship between R_o and R_a would not be as straight forward as in equation IV-31. As described previously in section IV.A.2.a, K_p is related to R_o by the following equation.

$$K_p = e^{-R_o \tau} \qquad \text{IV-9}$$

It is evident from the above equation that, in order to calculate R_o, pulse resolving time τ needs to be known. The magnitude of τ can be measured by means of an oscilloscope. However, without additional measurements, a fair estimate of τ can be

mathematically made using the following equation derived in section IV.A.2.b.

$$K_p = (1 - R_a\tau) \qquad \text{IV-14}$$

Then, from the above equation IV-9 and IV-14 the following expression for R_o can be derived:

$$R_o = - \frac{R_a \ln K_p}{1 - K_p} \qquad \text{IV-32}$$

Using equation IV-18, R_a in the above equation IV-32 can be replaced by R_s to obtain the following expression for R_o.

$$R_o = - \frac{R_s \ln K_p}{(1 - DT)(1 - K_p)} \qquad \text{IV-33}$$

Thus, by measuring R_s and DT, and then calculating K_p by the proposed correction method, above equation IV-33 can be solved to obtain the value for R_o.

CHAPTER V

EXPERIMENTAL

A. Neutron Irradiations

All irradiations were carried out in the Dalhousie University SLOWPOKE-2 Reactor (DUSR). SLOWPOKE (an acronym for Safe Low Power Kritical Experiment) is a small swimming-pool type research reactor developed by the Atomic Energy of Canada Limited (AECL). It uses fully enriched ^{235}U fuel with a light water moderator and a beryllium reflector. The reactor is housed in a sealed container which is placed into a sunken pool of water. The maximum power level is 20 *kW* at a flux of 1×10^{12} $n\ cm^{-2}\ s^{-1}$ (in the inner site); the water moderator reaches a temperature of approximately 50 ^{o}C at the maximum power level. All irradiations reported in this work were performed at the normal operating (10 *kW* power level) neutron flux of 5×10^{11} $n\ cm^{-2}\ s^{-1}$ except otherwise mentioned. Dimensions of the polyethylene irradiation capsules used in this facility (supplied by the Durham Aircraft Corporation, New York), and the capsule sealing procedure are given in Fig. V-1. When the normal sealing procedure (Fig. V-1.d) was applied to capsules for use in CINAA, they appeared to open up after a few cycles. This difficulty was considerably overcome by a slight modification of the normal sealing procedure (79T2). In the modified method, the capsule is closed using

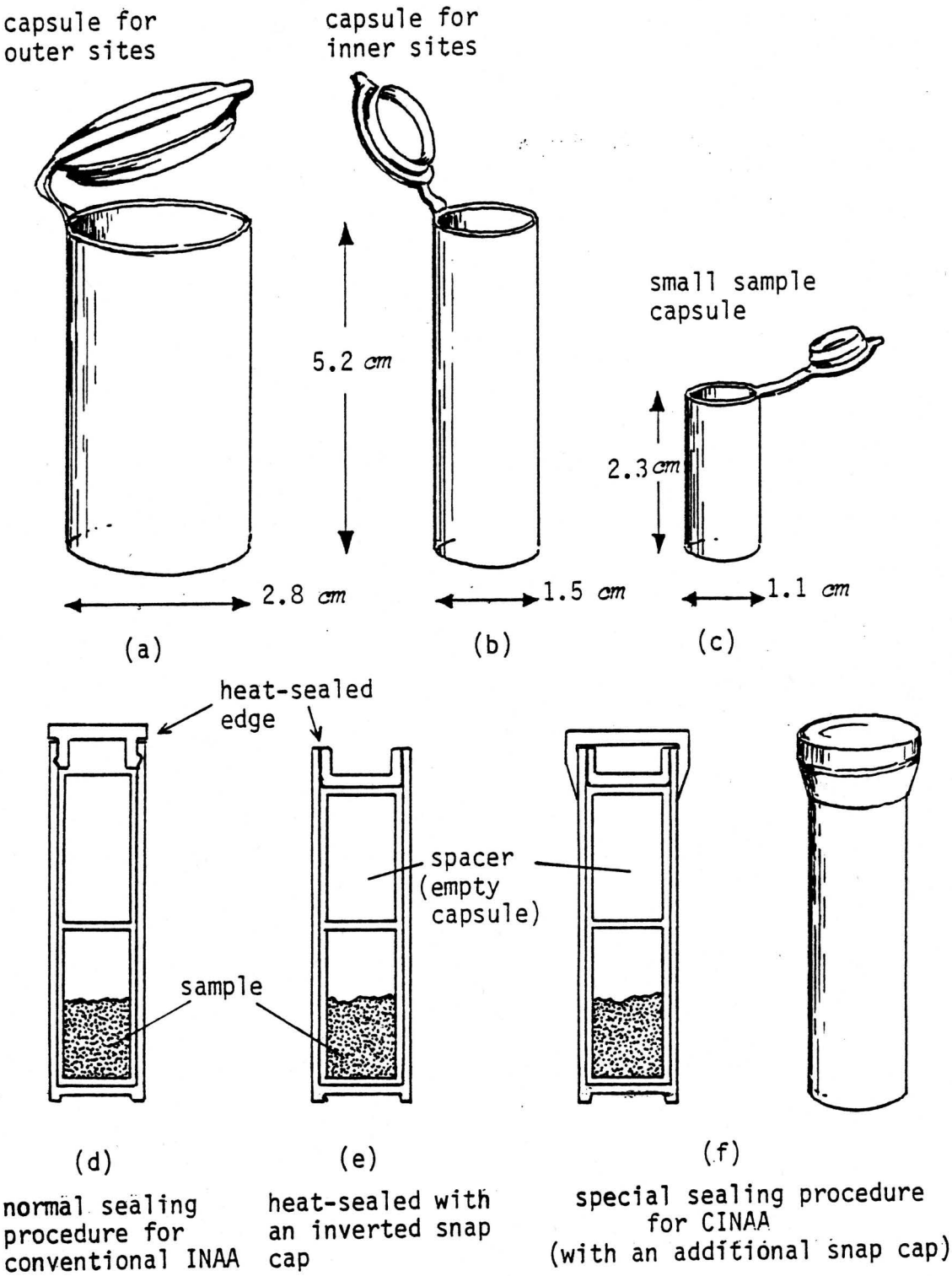

Figure V-1. Dimensions of the polyethylene irradiation capsules (drawn to the actual sizes) and the sealing procedures

an inverted snap cap forced inside the capsule, and then heat-sealed as shown in Fig. V-1.e. Furthermore, an additional polyethylene snap cap was fitted on the top of the capsule in order to improve the fast transfer performance for CINAA work with decay times of less than 2 *s*.

B. Rapid Cyclic Transfer System

1. General Description

A fast transfer system was designed and installed at DUSR in collaboration with AECL Commercial Products. This system has been described by Chatt *et al.* (81C1). In the original system the transfer time was found to be considerably long (600 *ms* at best) and irreproducible. Moreover, the heat-sealed caps of the irradiation capsules sometimes came off after striking the diverters. It was recognized that the transfer times could be further improved by making the system simple. Consequently, it was modified; both systems are shown in Fig. V-2 and V-3. The modified system has two counting positions. The horizontal position being closer to the reactor has a shorter transfer time than the vertical position (Fig. V-3). The CINAA work reported in this thesis was done by counting all samples at the horizontal position.

2. Precision Delay-Timer

For automatic recycling of the sample, a precision timer was designed in this study. This timer was used to actuate the solenoid valve to send the sample back to the reactor from the counting position

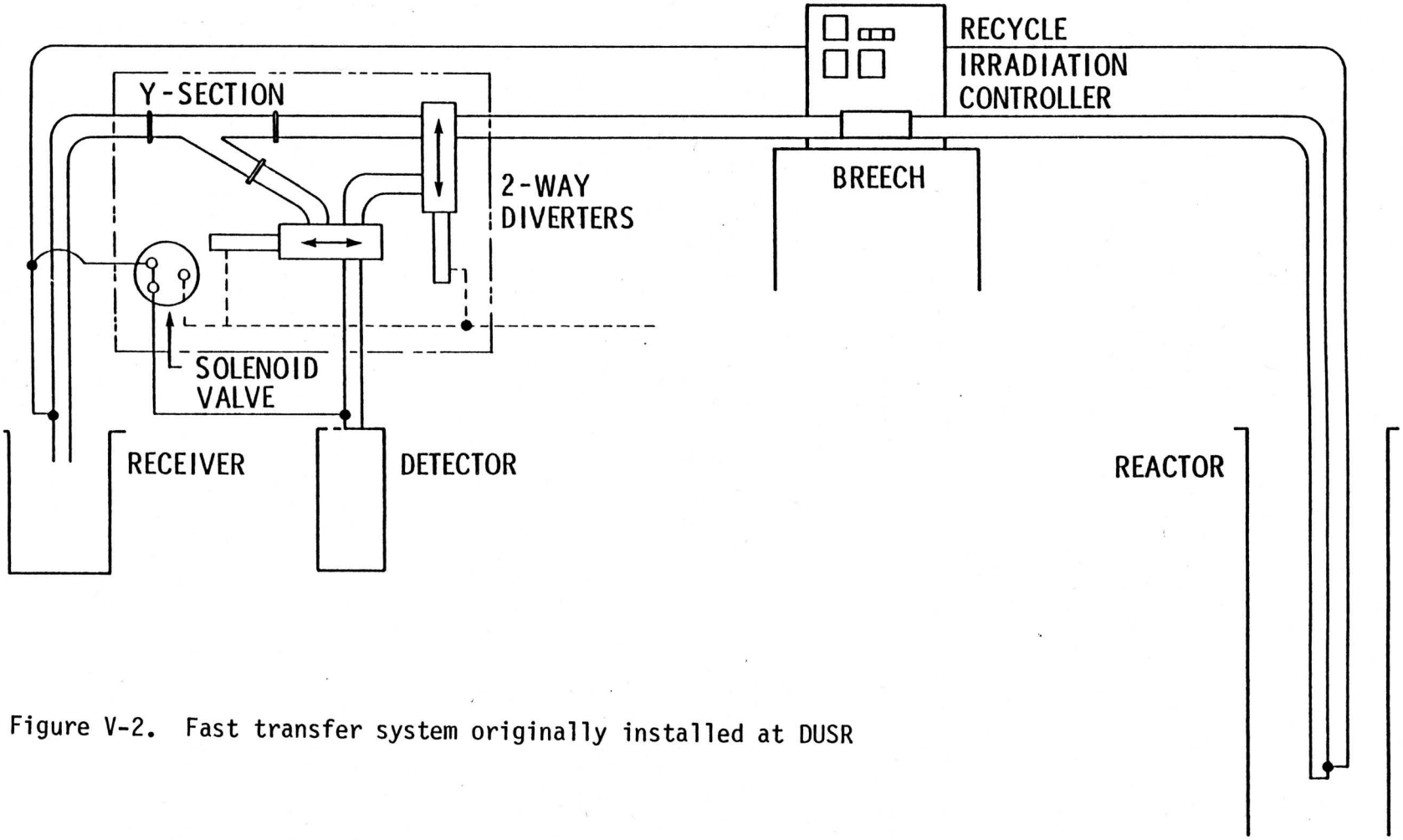

Figure V-2. Fast transfer system originally installed at DUSR

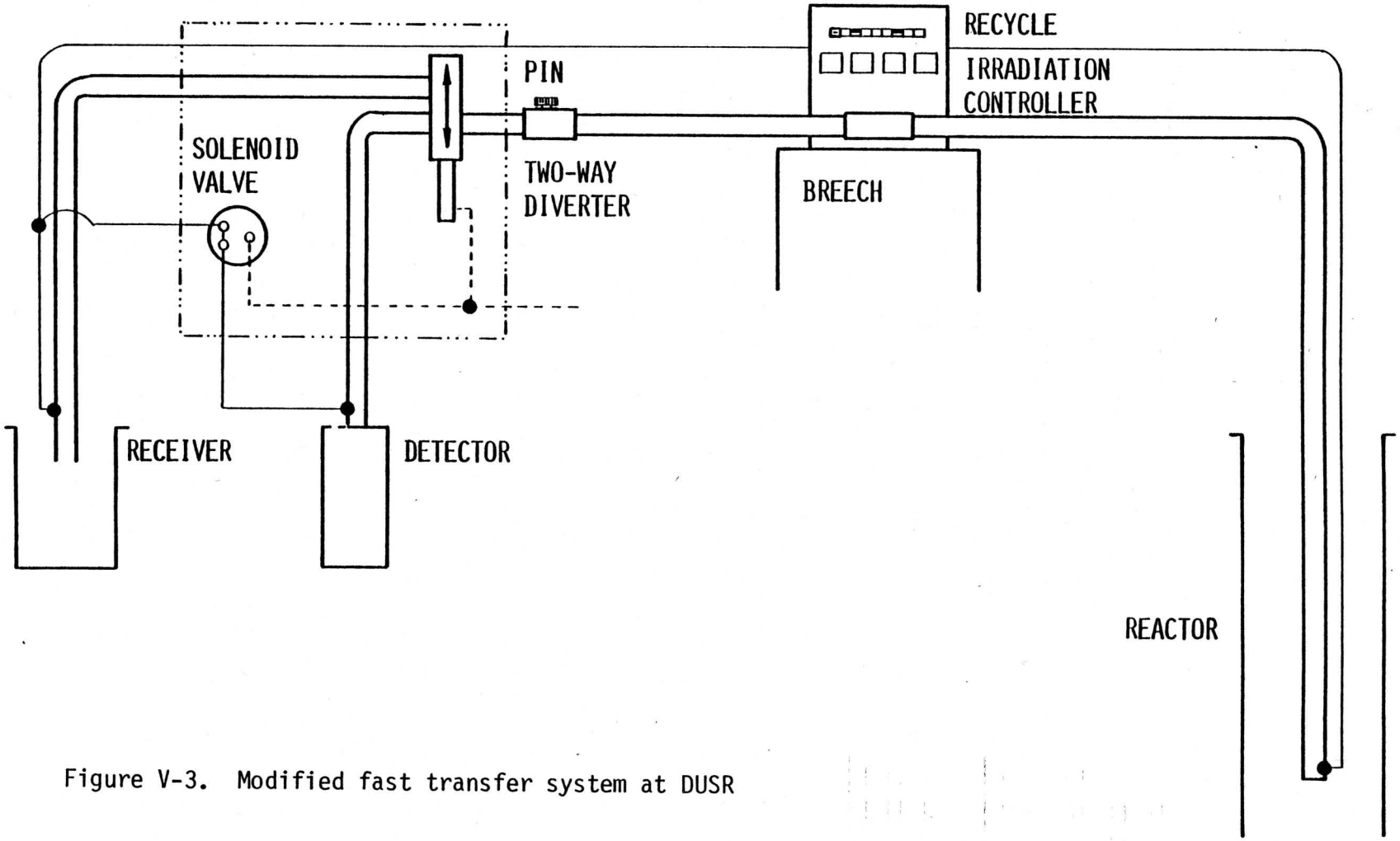

Figure V-3. Modified fast transfer system at DUSR

after a preset time delay. The delay time can be set from 10 *ms* to 999 *s* with a precision and accuracy of less than ±0.05%. The detailed circuit description of the timer is given in Appendix C. The basic operation principles of the timer are outlined below.

The timer is operated by the same crystal oscillator (20.000 *MHz*) which is also used in the dead-time measurement circuit. The above frequency is divided into the appropriate frequency of 100 *Hz* (0.01 *s* range) 10 *Hz* (0.1 *s* range) or 1 *Hz* (1 *s* range), and is used as the *clock* input of three - unit cascaded decade - down - counters (SN 74160). These three down counters are preset to the desired time delay via three other independent decade counters (SN 7490) by connecting the binary outputs of the SN 7490 to the load inputs of SN 74160.

A sample coming out of the reactor core is detected by a photocell. The photodetector actuates the recycle and decay timers which start down counting from the preset times. After the corresponding time is elapsed (when it counts down to zero), the decay timer starts the analyser for counting the sample, afterwards recycle timer actuates the solenoid valve to send the sample back to the reactor. At this moment, irradiation timer starts down counting from the preset irradiation time. Then at the end of irradiation, photo detector again actuates the analyser and the recycle timer. In this manner sample can be irradiated automatically for the required number of cycles. Another down counter, operated in a similar fashion is used to preset the required number of cycles. This counter reaches zero when the number of cycles are

completed and then it disables the signal which sends the sample back to the reactor.

3. Measurement of the Transfer Time

The transfer time of the sample from irradiation position to the counting position (detector) was measured in the following manner. The signal given out by the photodetector at the end of irradiation was used to trigger an analyser operated in the MCS mode with a scaling time normally set to 10 *ms*. The output of the amplifier, connected to a Ge(Li) detector, was taken into the MCS input. With this arrangement (shown in Fig. V-4), from the time the sample left the reactor, the MCS accumulated the detector events for each 10 *ms* time intervals. These events were stored in the MCS memory in successive channels. Samples of approximately 200 *mg* of oil fly-ash (which gets easily activated due to its high V content) were irradiated in the above manner. By scanning through the MCS data, it was possible to measure the transfer time (time difference between the start of the MCS and the detection of sample activity) with an accuracy of ±10 *ms*. Detailed results obtained are given in section VI.C.

C. Gamma-Ray Spectrometry System

1. Pulse Height Analyser (PHA)

For PCINAA and conventional INAA work, gamma-ray spectra were recorded using a Canberra Ge(Li) detector with a resolution 1.9 *keV* at

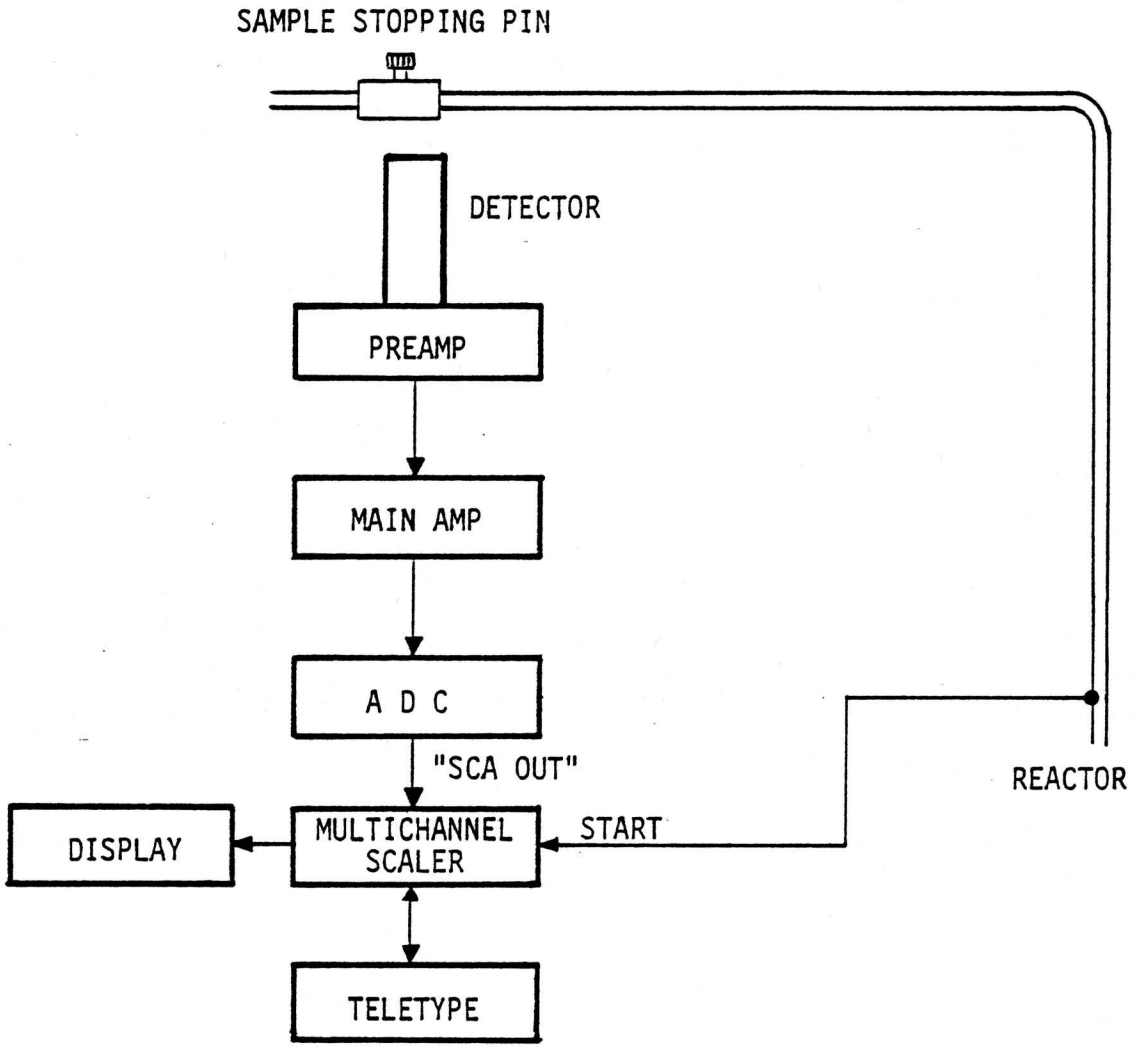

Figure V-4. Analyser arrangement for the measurement of sample transfer time

the 1332 *keV* photopeak of ^{60}Co. The peak to compton ratio at 1332 *keV* was 35:1. The efficiency of the detector relative to the standard NaI(Tl) detector was 9.4%. The detector - preamplifier was attached to an ORTEC 472 spectroscopy amplifier and a Tracor Northern NS 621 ADC operated at 50 *MHz* frequency. These components were connected to a Tracor Northern TN-11 4096 - multichannel pulse height analyser interfaced with a Digital Equipment Corporation PDP-11/05 minicomputer. Bipolar pulses were used throughout this work.

Cyclic INAA work was carried out with a Princeton Gamma-Tech Ge(Li) detector with a resolution of 2.02 *keV* at the 1332 *keV* peak and a peak to compton ratio of 30:1. In comparison to a standard NaI(Tl) detector, the efficiency of this detector was 7.1%. With this detector, a TENELEC TC 203BLR linear amplifier was used. The same ADC and the multichannel analyser described before were used in conjunction with the above detector and amplifier.

2. Analyser Triggering

The above mentioned TN-11 analyser was not provided with a separate trigger input. The input-output device used was a TELETYPE operated in standard ASCII code (American National Standard Code for Information Interchange). The analyser usually was triggered manually by using the appropriate character of the teletype. However, for automated fast cyclic system, an interface, in order to trigger the analyser electronically was found to be essential. Such an interface using simple

electronic components was designed in this work. The circuit description of the interface is given in Appendix D. After receiving the trigger pulse from the delay timer, the interface circuit gave a series of output pulses (equivalent to that given by the teletype) corresponding to the desired character.

3. Multichannel Scaling

Tracor Northern TN-1700, 4096-multichannel analyser operated on MCS mode was used for transfer time measurements and to record the time variables R_s and DT for use in the correction method developed for coincidence losses. This analyser has a maximum MCS operating frequency of 10 *MHz* and the MCS sampling time can be set from 10 μs to 1 s. Similar to the TN-11 analyser, the TN-1700 system also has a CRT display. The other components necessary for dead-time measurements are given in Appendix A.

D. Sample Preparation

1. Comparator Standards

Comparator standards were prepared by adding a known volume of either *Atomic Absorption Standard* solutions (supplied by the Fisher Scientific Company and Alpha Ventron Corporation), or solutions prepared from high-purity grade chemicals onto Nuclepore membrane filters (47 *mm* diameter, 0.4 μm pore size). The filters were dried under an IR lamp at low heat. Dried filters were heat-sealed inside small polyethylene

bags before placing them inside irradiation capsules. Blanks were prepared in a similar manner using the same volumes of deionized water. When larger amounts of standards were desired, the solutions were dried inside small polyethylene sample capsules.

2. Standard Reference Materials

Several standard reference materials (SRM) were analysed in this study. The names, code numbers and suppliers of these SRM are given in the text at appropriate places. These SRM were dried as instructed by the suppliers and weighed into polyethylene sample containers for irradiation.

3. Sample Preparation for EINAA

Samples available as dry powders (such as coal- and oil-fly-ash, UPM SRM) caused considerable difficulties in packing them for the purpose of EINAA. Due to the limited space available for the sample inside a small boron shield developed for the inner irradiation sites, the shape and the sealing method of samples should be a matter of concern. Moreover, due to build-up of static charges in powders, it was virtually impossible to insert the sample into a polyethylene bag, using a spatula alone, without spilling it on the sides. Since this spilling makes the sealing of the bag difficult and the boron shield contaminated, a special packing and sealing method was developed in this work for such samples. This procedure is explained schematically in Fig. V-5. The sample is inserted through a glass tube (with which

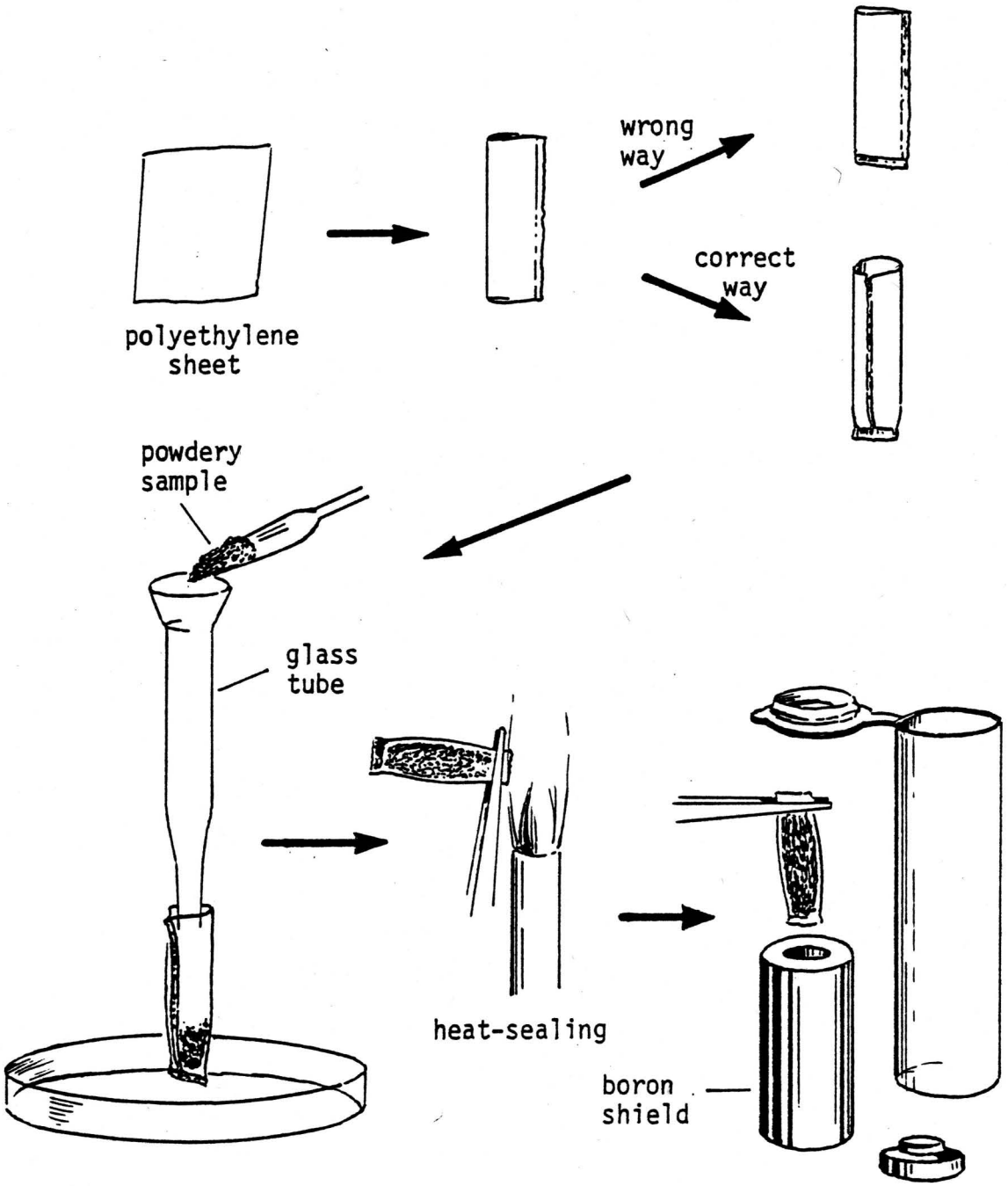

Figure V-5. Sample packing procedure for EINAA

there is no significant static interactions) into a small polyethylene bag, weighed and then it is heat-sealed. Samples weighing up to 250 *mg* could be placed inside the shield in this manner. If larger sample weights are desired, long shields of the same wall thickness can be used.

E. Materials for the Construction of Boron Shields

1. Boron Compounds

Several boron compounds were tested for purity. These included: powders of boron carbide, decaborane, elemental boron (Alfa Ventron Corporation, MA, USA), boron powder enriched with ^{10}B (Oak Ridge National Laboratory, TN, USA) and boron nitride powders (Union Carbide). The relative trace element content of these materials are given in section VI.F.1.

2. Styrene

Styrene is commercially available as a liquid along with a polymerization inhibitor. Before polymerization, styrene has to be distilled to remove this inhibitor. Normal distillation (at the boiling point of 145 ^{o}C) cannot be used due to polymerization of the distilled product at elevated temperatures. Therefore, styrene was distilled at reduced temperature ($\simeq$ 80 ^{o}C) and pressure. Distilled styrene could be kept in the dark without any appreciable polymerization over a period of 2 months. The distillation also served as a purification step.

Liquid styrene was mixed with benzoyl peroxide which served as a free radical initiator for the polymerization reaction. Chemical structures of the styrene monomer and polymer are given in Fig. V-6. Design description of the mould and optimization of experimental parameters is given in Chapter VI.

F. Calculation of Detection Limits

Detection Limits (L_D) and Determination Limits (L_Q) were calculated according to the method prescribed by Currie (68C1). The lower limits for a measurement, as shown by him, requires introduction of three specific levels (i) a *decision limit* (L_C), at which one may decide whether or not the result of an analysis indicates detection; (ii) a *qualitative detection limit* (L_D), at which a given procedure may be relied upon to lead to detection; and (iii) a *quantitative determination limit* (L_Q), at which a given procedure will be sufficient ly precise to yield a satisfactory quantitative estimate. By applying this concept to radioactivity, the three limits were derived by Currie (68C1) as:

$$L_C \text{ (counts)} = 2.33 \sqrt{\mu_B}$$

$$L_D \text{ (counts)} = 2.71 + 4.65 \sqrt{\mu_B}$$

$$L_Q \text{ (counts)} = 50 \left[1 + (1 + \mu_B/12.5)^{\frac{1}{2}}\right]$$

where μ_B is the number of counts in the background under the photopeaks of interest.

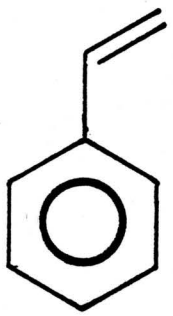

STYRENE MONOMER

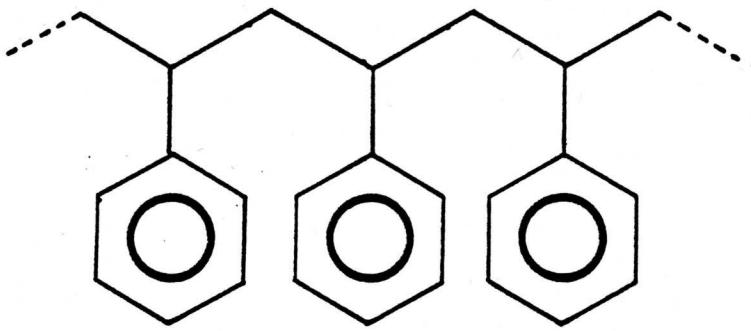

STYRENE POLYMER

Figure V.6. Chemical structures of styrene monomer and the polymer

CHAPTER VI

RESULTS AND DISCUSSION

A. Homogeneity and Stability of Neutron Flux

1. Homogeneity

Both the horizontal and vertical flux variations of the Dalhousie University SLOWPOKE-2 Reactor (DUSR) have been measured (78R1) to be less than 1% cm^{-1} for the inner site, indicating that a slight variation in positioning of the sample in the irradiation capsule would not impart any detectable error. On the other hand, the horizontal flux variation at the outer site is measured to be approximately 5% cm^{-1} and thus care should be taken in positioning smaples and standards to obtain highest possible accuracy. Since all irradiations reported in this thesis were carried out in the inner sites, no corrections for flux variations were necessary.

2. Stability

The stability of neutron flux should also be a matter of concern, especially for studies involving short-lived nuclides, since errors due to any fluctuation in the neutron flux can be expected to be more acute for short irradiations than for long irradiations.

For measuring the neutron flux, Ryan *et al.* (78R1) have reported a maximum standard deviation (as 2σ) of ±2.8% (12 determinations) over a period of two months for the inner sites. The value of ±2.8% includes errors due to counting statistics and possible errors in weighing the flux wires. This excellent stability of neutron flux was observed by employing 10 *min* irradiations. However, the stability of the flux was reinvestigated for short irradiation conditions (of the order of seconds) since emphasis was placed on short-lived nuclides in the present study.

For the above purpose, a series of standards with 200 μ*g* of vanadium (200 μ*l* of 1000 *ppm* solution on Nuclepore membranes) were carefully prepared and each standard was irradiated at the same pneumatic site for 3 *s* with a 10 *min* interval in between two irradiations. Vanadium was selected as the standard for the following reasons. Firstly, half-life of the product nuclide ^{52}V (3.77 *min*) is long enough to allow sufficient time for accurate and manual positioning of the standard above the detector. In addition, to avoid possible errors due to slight variation in placing the standards, they were counted at approximately 15 *cm* from the window of the detector. Secondly, the half-life of ^{52}V is short enough to obtain sufficient activity by irradiating only for a few seconds. In order to investigate any variation that may occur due to sample preparation, the same standard was reanalysed under similar conditions. Then a sufficient cooling time should be allowed in between each irradiation to avoid

interference from the previous irradiation. The half-life of ^{52}V is sufficiently short to carry out the irradiations without such interferences.

Results given in Table VI-1 show an excellent stability of the neutron flux even for 3 *s* irradiation; this is similar to 10 *min* irradiation condition reported earlier (78R1). It can be concluded, therefore, that the flux monitors are not necessary for each irradiation. Consequently, it is necessary to calibrate the experimental conditions only once for a specific element even for very short-lived nuclides. No significant variation in number of counts was observed for the short irradiations using the same standard and also different standards as shown in Table VI-1.

Table VI-1. Stability of the neutron flux for short irradiations

(t_i = 3 s; t_d = 60 s; t_s = 200 s; 200 µg of vanadium)

standard	counts	standard*	counts
V-1	9040**	V-1	9040**
V-2	9328		9414
V-3	9299		9213
V-4	9040		9385
V-5	9068		
V-6	9327		
average	9184 ± 147		9263 ± 173
% standard deviation	1.6		1.9

* standard V-1 was used for 4 independent measurements

** refers to the same measurement

B. Pseudo-Cyclic Instrumental Neutron Activation Analysis

1. General Discussion

During the early stages of this thesis work, using available facilities for conventional INAA, a pseudo-cyclic INAA (PCINAA) method was developed based on the principles of cyclic INAA. The theory of PCINAA has already been described in section II.A. This technique involves short irradiations for tens of seconds, manual transfer of the sample to detector within 10 *s*, counting for tens of seconds, and repeating the entire process for a suitable number of cycles. The applicability of the method was tested by analysing various biological materials for several short-lived nuclides, namely, Ag, F, Rb, Sc and Se with half-lives ranging from 11.2 to 62 *s*.

Relevant nuclear data for both short- and long-lived nuclides of the elements of interest are given in Table VI-2. Fluorine can only be determined through the short-lived nuclide (^{20}F) whereas Ag, Rb and Sc have both short- and long-lived nuclides produced from the same parent isotope. Even though Rb and Sc have lower cross-sections for the production of short-lived nuclides from the same target isotope, measurement via short-lived nuclides may be more sensitive depending on the experimental conditions and the matrix activity, in addition to reduction of total analysis time. This is mainly because the saturation activity is easier attained for short-lived nuclides than for long-lived nuclides. However, a different situation arises in the case

Table VI-2. Comparison of nuclear data of short- and long-lived neutron activation products of interest by PCINAA (78L1)

element	short-lived nuclide				long-lived nuclide			
	target isotope	cross section(b)	nuclide	half-life	target isotope	cross section(b)	nuclide	half-life
Ag	^{109}Ag	89	^{110}Ag	24.0 s	^{109}Ag	3.2	^{110m}Ag	252 d
F	^{19}F	0.0098	^{20}F	11.0 s	-	-	-	-
Rb	^{85}Rb	0.10	^{86m}Rb	61.2 s	^{85}Rb	0.91	^{86}Rb	18.8 d
Sc	^{45}Sc	11	^{45m}Sc	18.7 s	^{45}Sc	23	^{46}Sc	83.8 d
Se	^{76}Se	21	^{77m}Se	17.4 s	^{74}Se	30	^{75}Se	118.5 d

of Se. The short- and long-lived nuclides of Se originate from two different parent isotopes, namely ^{76}Se and ^{74}Se, respectively. Although ^{76}Se has a slightly lower cross-section for the production of the short-lived nuclide, its isotopic abundance is higher than that of the parent isotope (^{74}Se) of the long-lived nuclide (Table VI-2). Therefore, when saturation factor is also taken into consideration, short-lived ^{77m}Se is expected to be much more sensitive than long-lived lived ^{75}Se.

2. Interferences

a. *Total Sample Activity*

A minimum decay time of 10 *s* was employed in PCINAA, and consequently no interference from very short-lived nuclides such as ^{38m}Cl (half-life - 0.72 *s*) was encountered. The major interferences observed here were from ^{28}Al, ^{38}Cl, ^{56}Mn and ^{24}Na depending on the nature of the biological materials analysed. Since these nuclides have relatively long half-lives (longer than several minutes), the total activity (hence the dead-time) did not change appreciably during the counting period used (30 *s*). Under these experimental conditions, an average dead time correction treatment was considered sufficient. However, in order to minimize the errors caused by the above assumption and not accounting for pile-up losses, the distance between the detector and sample was adjusted to maintain a dead-time of less than 10%.

b. *Interfering Nuclear Reactions and Overlapping Gamma-Rays*

Among the nuclides listed in Table VI-2, only the determination of F required any appreciable correction for interfering nuclear reactions. The $^{19}F(n,\gamma)^{20}F$ reaction was observed to be interfered with by $^{23}Na(n,\alpha)^{20}F$; consequently, appropriate correction factor for each cycle was estimated by irradiating a sodium standard under similar experimental conditions, and was used in this work. The contribution from the other possible interfering reaction, namely, $^{20}Ne(n,p)^{20}F$, was found to be negligible.

Depending on the resolution of the particular analyser system and the relative magnitudes of the 1633 and 1642 *keV* photopeaks of ^{20}F and ^{38}Cl respectively, interferences can be encountered due to their overlapping in energy. In such a situation, the sum peak area (due to both the peaks) can be measured, and the contribution from ^{38}Cl can be subtracted by estimating the peak area due to ^{38}Cl through its alternative interference-free gamma-ray of 2167 *keV*. However, for the samples analysed these two peaks were well resolved with the analyser used and hence above mentioned correction was not necessary.

Similar interferences could occur for 658 *keV* peak of ^{110}Ag by 657 *keV* peak of ^{76}As, and for 556 *keV* of ^{86m}Rb by 554 *keV* peak ^{82}Br. As described before, the possibility of these interferences was checked through the detection of other peaks of the interfering nuclides; no such interferences were observed.

3. Applications of PCINAA

The PCINAA method developed was applied to fisheries samples (79C1) for determining concentrations of a number of elements as shown in Table VI-3. Although experimental conditions were optimized for the nuclides listed in Table VI-2, several other medium-lived nuclides could also be detected simultaneously. Precision and accuracy of the method were evaluated by analysing a few standard reference materials (SRM). The results obtained for SRM are discussed below.

Table VI-4 summarises the results obtained for Se in several standard reference materials. Each concentration value is the average of 4 independent determinations. It can be seen that precision, expressed in terms of relative standard deviation (calculated from the determined values) improves significantly from first through fourth cycle in each case, and in some cases by as much as seven times.

Qualitative detection limit, L_D, and quantitative determination limit, L_Q, (see section V.F for definition of L_D and L_Q) have decreased as the number of cycles is increased. The measured Se content agrees fairly well with the reported values for each SRM. Due to relatively large interferences from ^{28}Al and ^{56}Mn (because of high concentrations of Al and Mn), botanical samples show higher detection limits for Se than zoological samples. This interference was so severe that for botanical samples a shorter irradiation time (10 *s/cycle*) had to be employed in comparison to zoological samples

Table VI-3. Range of elemental content in cod muscles and livers determined by PCINAA

element	range[a]	
	Cod Muscle	Cod Liver
Ag	0.020-0.040	0.35-1.03
Al	2.88-8.20	3.4-15.5
Br	5.5-12.3	9.68-24.9
Ca	43-237	74-588
Cl	772-1865	942-1637
Cu	0.33-2.8	2.58-11.1
I	0.36-2.87	2.84-11.2
K(%)	0.280-0.503	0.135-0.213
Mg	113-390	82-174
Mn	0.04-0.35	0.62-1.83
Na(%)	0.050-0.130	0.061-0.108
Rb	0.230-1.24	0.20-0.80
S(%)	n.d.-1.20	n.d.-1.10
Se	0.190-0.335	0.344-0.945
V	n.d.-0.10	n.d.-0.15

[a]Concentrations given in $\mu g\ g^{-1}$ unless otherwise specified; wet weight basis

n.d. - not detected

Table VI-4. Precision, accuracy, and detection limits for Se in biological materials by PCINAA

material	reported value [a]	no. of cycles	this work[a,b]	rel. std. dev.(%)	limits[a] L_D	L_Q
Albacore Tuna	(3.6±0.4)[c]	1	3.43±0.28	8	0.085	0.38
		2	3.19±0.14	5	0.062	0.24
		3	3.06±0.11	4	0.053	0.19
		4	3.33±0.12	4	0.049	0.17
Animal Muscle	(0.275)[d]	1	0.307±0.065	21	0.087	0.382
		2	0.289±0.028	10	0.061	0.240
		3	0.277±0.009	3	0.053	0.184
		4	0.277±0.009	3	0.041	0.162
Bovine Liver	1.1±0.1[e]	1	1.04±0.05	5	0.105	0.46
		2	1.00±0.02	2	0.081	0.29
		3	1.00±0.03	3	0.067	0.22
		4	0.99±0.02	2	0.052	0.18
Fish Meal	...	1	1.52±0.10	7	0.30	1.34
		2	1.36±0.04	3	0.23	0.88
		3	1.32±0.05	4	0.20	0.71
		4	1.37±0.03	2	0.18	0.67
Orchard Leaves	0.08±0.01[f]	1	0.095±0.031	33	0.24	1.02
		2	0.069±0.012	17	0.15	0.57
		3	0.077±0.0006	8	0.12	0.44
		4	0.087±0.0009	10	0.10	0.41
Pepperbush	...	4	n.d.		2.5	8.9
Pine Needles	...	4	n.d.		0.50	1.7

[a] all values are in μg/g dry-weight basis. [b] average of 4 determinations.
[c] NBS most probable value (77N4). [d] IAEA (80I1). [e] NBS certified value (77N1).
[f] NBS certified value (77N2). n.d. - not detected.

which were irradiated for 30 *s/cycle*.

The effect of irradiation time on the detection limits for Se in Orchard Leaves and Bovine Liver can be seen from Fig. VI-1 and VI-2, respectively. The value of L_Q in Orchard Leaves is lower for 10 *s* than for 30 *s* irradiations; also L_Q does not appear to improve beyond 3 cycles with a further increase in the number of cycles. This observation can be explained by the build-up of activity due to ^{28}Al and ^{56}Mn in Orchard Leaves. On the other hand, for Bovine Liver, L_Q has a lower value for irradiation time of 30 *s* than for 10 *s*. In the absence of severe interferences the increased activity of the nuclide of interest due to longer irradiation time would result in improved sensitivity. Even though the measured Se content in Bovine Liver is above L_Q even at the first cycle, it should be noted that there is a significant improvement of L_Q with increasing number of cycles. Same irradiation conditions are compared in Fig. VI-3 for a slightly longer lived nuclide, namely, ^{86m}Rb (62.4 *s*), measured in the same matrix (Bovine Liver). In this case, L_Q goes below the measured value after two cycles of 30 *s* irradiation whereas in 10 *s* irradiations it would be necessary to increase the number of cycles in order to achieve L_Q below the concentration of the sample. Furthermore, by comparing Fig. VI-2 and Fig. VI-3 one can note that the relative difference in L_Q for two irradiation conditions is more pronounced for Rb than that for Se. This is because 30 *s* irradiations are more preferable for Rb than for Se due to the longer half-life of ^{86m}Rb.

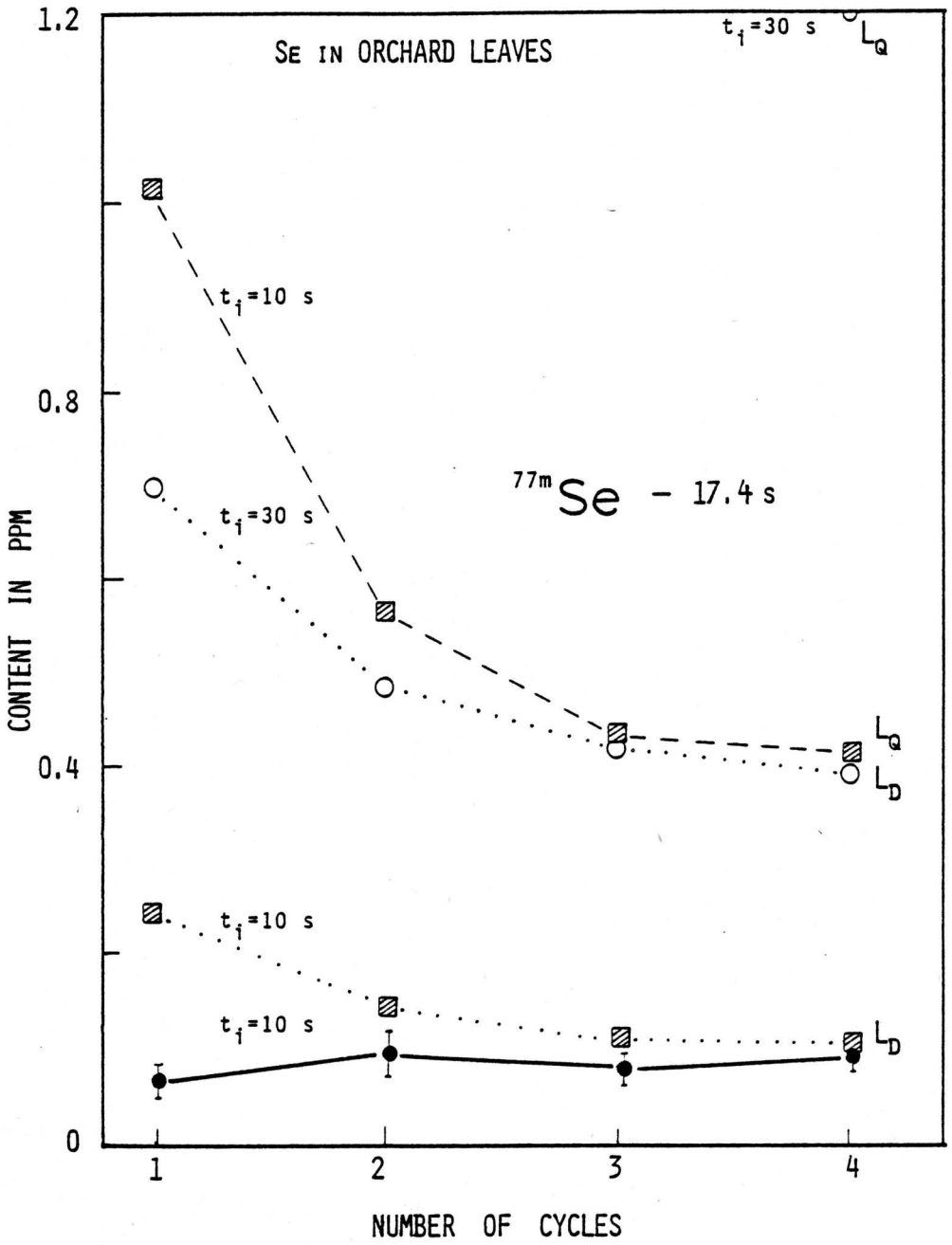

Figure VI-1. Determination of Se in Orchard Leaves by PCINAA

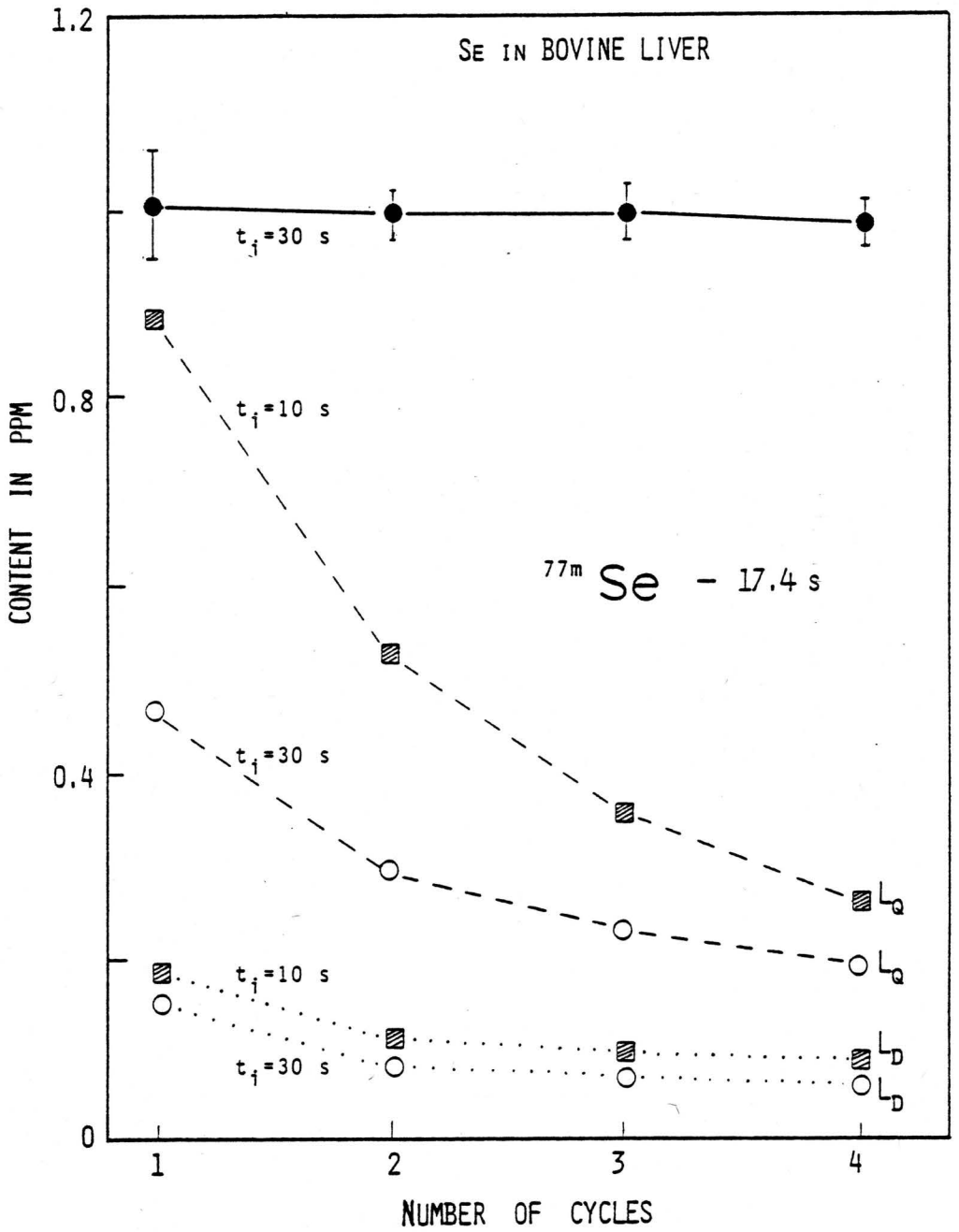

Figure VI-2. Determination of Se in Bovine Liver by PCINAA

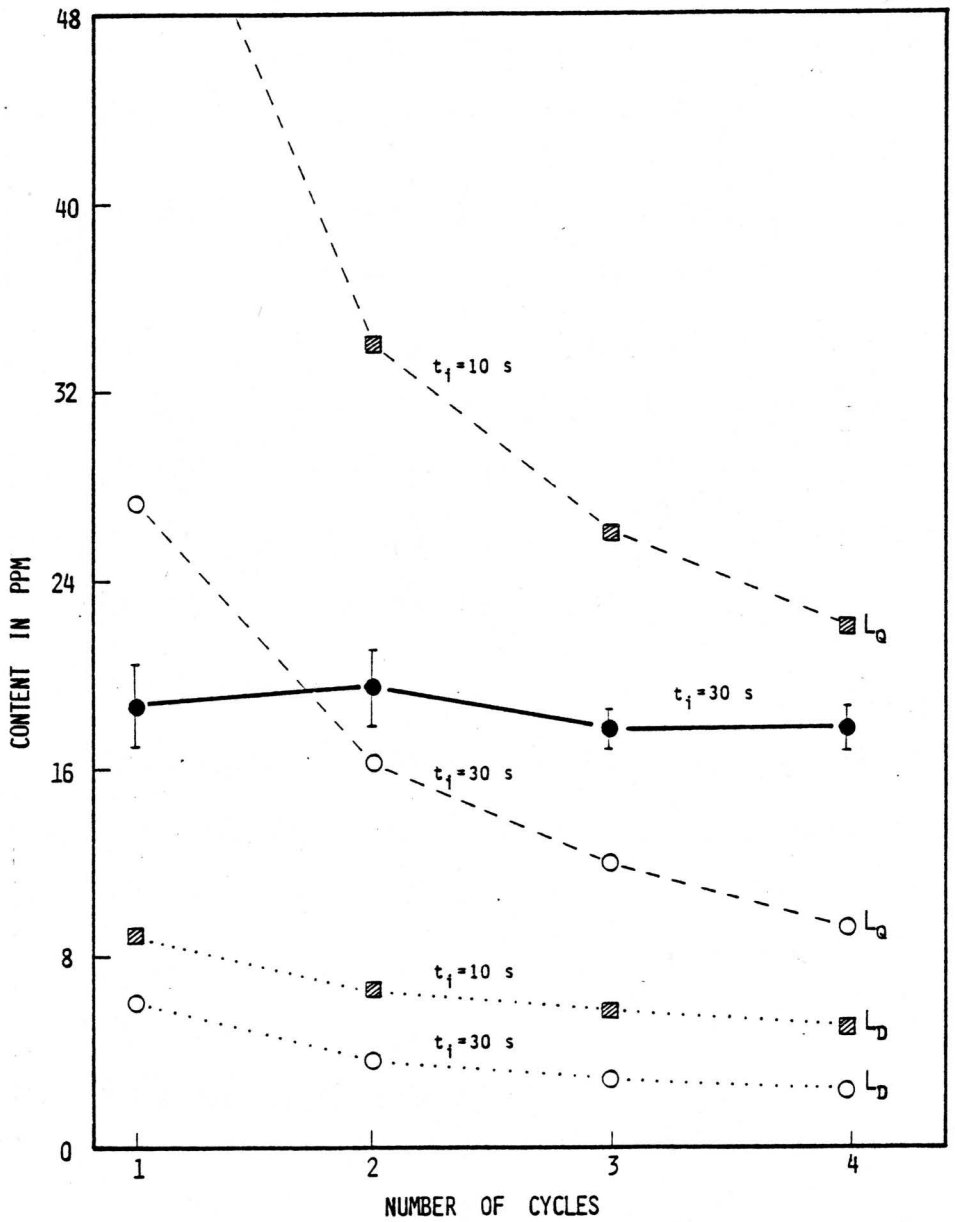

Figure VI-3. Determination of Rb in Bovine Liver by PCINAA

The above discussions point out the need to consider the nature of the matrix and the half-life of the nuclide of interest in selecting time parameters for maximum sensitivity.

The PCINAA method was applied to several SRM for determining Ag, F, Rb and Sc. The results are presented in Tables VI-5 through VI-7. Trends in precision, accuracy and detection limits similar to those observed for Se are evident from these tables. A typical gamma-ray spectrum of PCINAA of Bovine Liver is shown cycle by cycle in Fig. VI-4. As the number of cycles is increased, photopeaks for several medium-lived nuclides can be detected in the spectrum in addition to short-lived nuclides.

Elemental concentrations of Bovine Liver and Orchard Leaves determined by three different INAA methods are given in Table VI-8 along with the values provided by the NBS for comparison purposes. The three INAA methods developed were: (i) PCINAA; (ii) INAA using conventional short irradiations with the same total irradiation times as in PCINAA; and (iii) INAA using long-lived nuclides by 16 h irradiation, 3 weeks decay and counting time of 2000 s. The values obtained by the three INAA methods and NBS-values agree well showing the reliability of the PCINAA method developed here. The detection limits calculated by three methods are summarized in Table VI-9. Although in some cases lower detection limits can be obtained via long-lived nuclides, PCINAA or conventional short irradiations may be preferable due to short experimental time involved.

Table VI-5. Precision, accuracy, and detection limits for Ag and F determined by PCINAA

element (matrix)	reported [a] value	no. of cycles	this work[a,b]	rel. std. dev.(%)	limits [a] L_D	limits [a] L_Q
Ag (Bovine Liver)	(0.06) [c]	1	0.085±0.072	85	0.089	0.48
		2	0.060±0.028	47	0.063	0.28
		3	0.055±0.032	58	0.060	0.22
		4	0.066±0.021	32	0.052	0.19
F (ICES Fish Flour)	...	1	46±28	61	49	268
		2	57±13	23	31	161
		3	62±9	14	24	110
		4	58±8	16	19	85

[a] all values are in μg/g; dry weight basis. [b] average of 4 deteterminations.
[c] value recommended by NBS (77N1)

Table VI-6. Precision, accuracy, and detection limits for Rb in biological materials by PCINAA

material	reported value [a]	no. of cycles	this work[a,b]	rel. std. dev.(%)	limits[a] L_D	limits[a] L_Q
Albacore Tuna	...	4	n.d.	...	1.9	7.5
Animal Muscle	(18.4)[c]	1	24.6±3.7	15	4.6	25.6
		2	20.9±1.9	9	3.0	13.6
		3	21.3±1.2	6	2.4	9.9
		4	19.9±0.9	5	1.9	7.2
Bovine Liver	18.3±1.0[d]	1	18.6±3.2	17	6.0	29.2
		2	19.4±1.6	8	3.6	16.2
		3	17.6±0.9	5	2.9	12.0
		4	17.6±0.9	5	2.4	9.2
Fish Meal	...	4	n.d.	...	6.1	26
Orchard Leaves	12±1[e]	1	6.1±3.8	62	14.2	70
		2	10.5±2.2	21	9.9	42
		3	9.8±2.5	26	8.3	33
		4	10.2±2.0	20	7.2	26
Pepperbush	...	4	n.d.	...	126	466
Pine Needles	11.7±0.1 [f]	1	15±9	60	34	175
		2	12±6	50	26	111
		3	14±3	21	22	90
		4	19±3	16	20	80

[a]all values are in $\mu g/g$, dry weight basis. [b]average of 4 determinations.
[c]IAEA (80I1). [d]NBS certified value (77N1). [e]NBS certified value (77N2).
[f]NBS certified value (76N1). n.d. - not detected.

Table VI-7. Precision, accuracy, and detection limits for Sc in biological materials by PCINAA

material	reported value [a]	no. of cycles	this work[a,b]	rel. std. dev.(%)	limits[a]	
					L_D	L_Q
Albacore Tuna	...	4	n.d.	...	0.0041	0.014
Animal Muscle	(8.24×10^{-4})[c]	4	n.d.	...	0.0040	0.014
Bovine Liver	...	4	n.d.	...	0.0053	0.018
Fish Meal	...	4	n.d.	...	0.016	0.056
Orchard Leaves	(0.04-0.2)[d]	1	0.096±0.018	19	0.028	0.113
	0.054±0.004[e]	2	0.061±0.005	8	0.017	0.073
		3	0.052±0.002	4	0.013	0.047
		4	0.052±0.002	4	0.011	0.031
Pepperbush	...	4	n.d.	...	0.12	0.43
Pine Needles	(0.03)[f]	1	0.013±0.010	77	0.031	0.15
	(0.13)[e]	2	0.018±0.006	33	0.027	0.11
		3	0.021±0.004	19	0.023	0.087
		4	0.019±0.005	26	0.019	0.072

[a] all values are in μg/g, dry weight basis. [b] average of 4 determinations.
[c] IAEA (80I1). [d] ref. (76B1). [e] ref. (80V1). [f] NBS recommended value.

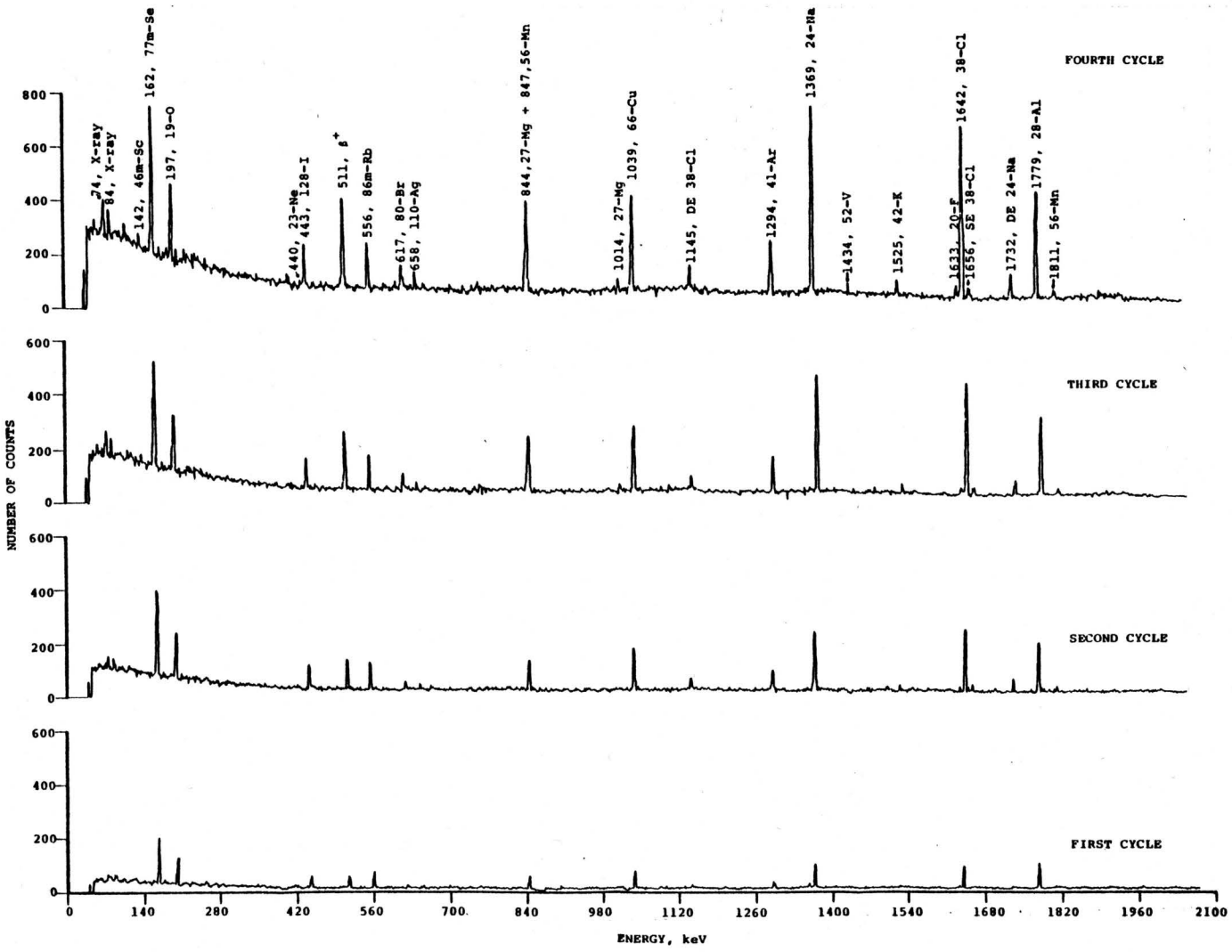

Figure VI-4. A typical gamma-ray spectrum of Bovine Liver observed by PCINAA

Table VI-8. Comparison of elemental content of NBS SRM Bovine Liver and Orchard Leaves by three INAA methods

element	Bovine Liver (NBS SRM-1577)				Orchard Leaves (NBS SRM-1571)			
	pseudo-cyclic	conv. short	conv. long	NBS[a]	pseudo-cyclic	conv. short	conv. long	NBS[b]
Ag	0.006±0.021	n.d.	n.d.	(0.06)	n.d.	n.d.	n.d.	...
Al	29.5±2.5	33.1±1.2	n.a.	...	350±17	299±14	n.a.	...
Br	9.4±0.4	9.2±0.2	8.5±1	...	11.5±2.1	9.8±0.3	10.6±0.2	(10)
Ca	160±40	121±7	n.d.	...	2.09±0.19%	2.02±0.08%	n.d.	2.09±0.03%
Cl	0.270±0.027%	0.249±0.01%	n.a.	(0.27%)	690±27	662±61	n.a.	(690)
Cu	197±13	193±9	n.d.	193±10	n.d.	n.d.	n.d.	12±1
I	0.14±0.07	0.16±0.08	n.a.	(0.18)	n.d.	n.d.	n.a.	(0.17)
K	0.92±0.09%	0.95±0.04%	0.97±0.09%	0.97±0.06%	1.3±0.4%	n.d.	1.49±0.01%	1.47±0.03%
Mg	675±54	550±110	n.a.	604±9	0.64±0.03%	0.64±0.01%	n.a.	0.62±0.02%
Mn	12.4±1.3	11.8±1.0	n.a.	10.3±1.0	88±11	82±13	n.a.	0.62±0.02%
Na	0.236±0.011%	0.236±0.016%	0.243±0.015%	0.243±0.013%	n.d.	n.d.	76±7	82±6
Rb	17.6±0.9	18.0±0.8	18.7±1.5	18.3±1.0	10.2±2.0	9.8±3.1	10.4±0.9	12±1
Sc	n.d.	n.a.	n.d.	...	0.052±0.002	0.041±0.01	0.04±0.02	...
Se	0.99±0.02	1.01±0.12	1.1±0.1	1.1±0.1	0.087±0.009	n.d.	n.d.	0.08±0.01
V	0.17±0.06	0.08	n.a.	...	0.45±0.21	0.44±0.06	n.a.	...

All values are in μg/g unless otherwise indicated. n.a. - not applicable. n.d. - not detected.

[a] NBS value (77N1). [b] NBS value (77N2).

Table VI-9. Comparison of elemental detection limits for Bovine Liver and Orchard Leaves

element	Bovine Liver (NBS SRM-1577)						Orchard Leaves (NBS SRM-1571)					
	pseudo-cyclic		conv. short		conv. long		pseudo-cyclic		conv. short		conv. long	
	L_D	L_Q	L_D	L_Q	L_D	L_Q	L_D	L_Q	L_D	L_Q	L_D	L_Q
Ag	0.052	0.19	0.11	0.38	0.12	0.47	0.11	0.44	0.53	2.1	0.26	0.96
Al	1.0	4.3	0.68	2.7	n.a.	n.a.	1.9	9.3	1.4	7.5	n.a.	n.a.
Ca(%)	0.018	0.18	0.011	0.086	0.102	0.339	0.066	0.59	0.072	0.67	0.264	0.832
Cl(%)	0.007	0.028	0.005	0.019	n.a.	n.a.	0.026	0.096	0.025	0.097	n.a.	n.a.
Cu	12.9	49.3	7.2	26.4	306	983	23	97	26	112	123	428
F	5.6	24	32	119	n.a.	n.a.	15	62	59	210	n.a.	n.a.
I	0.12	0.46	0.12	0.42	n.a.	n.a.	0.32	1.1	0.36	1.4	n.a.	n.a.
K(%)	0.25	0.99	0.234	0.879	0.037	0.120	0.88	3.24	2.6	9.3	0.013	0.047
Mg(%)	0.030	0.12	0.020	0.072	n.a.	n.a.	0.091	0.368	0.114	0.48	n.a.	n.a.
Mn	4.6	19.8	3.6	14	n.a.	n.a.	7.0	32	11.1	61	n.a.	n.a.
Na(%)	0.007	0.026	0.0058	0.0214	0.007	0.0023	170	625	182	710	1.10	3.66
Rb	2.4	9.2	1.4	5.2	0.67	2.8	7.2	26	9.2	36	3.02	12.6
Sc	0.005	0.018	0.006	0.021	0.006	0.011	0.011	0.031	0.091	0.32	0.005	0.020
Se	0.052	0.18	0.17	0.58	0.16	0.52	0.10	0.41	1.1	3.8	0.417	1.450
V	0.25	1.0	0.07	0.27	n.a.	n.a.	0.16	0.61	0.18	0.63	n.a.	n.a.

All values are in $\mu g/g$ unless otherwise indicated. n.a. - not applicable. n.d. - not detected.

The PCINAA method offers several advantages: (i) short experimental time (ii) simultaneous measurement of short- and medium-lived nuclides (iii) significant improvement of precision, accuracy and detection limits (iv) no requirement of expensive instrumentation (v) no interference from ^{24m}Na and ^{38m}Cl. It has three main disadvantages: (i) not suitable for detecting nuclides with half-lives of few seconds due to the necessary 10 *s* manual transfer time (ii) needs some sacrifice of sensitivity to avoid coincidence losses unless elaborate correction methods are employed (iii) errors in timing may occur during manual transfer of a sample and triggering the analyser within a short time. For example, an error of ±0.5 *s* in delay time would cause errors of ±3.4% and ±1.7% for half-lives 10 and 20 *s*, respectively. However, this error will be further reduced due to averaging of the random deviation over a number of cycles.

In order to minimize - if not possible to eliminate - the above disadvantages of PCINAA, an automated rapid pneumatic cyclic transfer system was designed and used in later work. This automated system was used in CINAA work with the developed correction method for coincidence losses for the measurement of activities with half-lives as short as a fraction of a second.

C. Performance of the Cyclic Transfer System

1. General Comments

It has been mentioned earlier that the lower limit of half-lives which can be utilized for INAA depends mainly on the reproducibility and rapidity of sample transfer times. Therefore, it is important to investigate the effects of various factors on transit time of the rapid transfer facility. Since the shortest possible transfer time was of interest in this study, all measurements were carried out at the horizontal counting position which is nearest to the reactor core (see Fig. V-3).

Three main factors which can affect the transfer time, namely, pressure, irradiation time and the weight of the sample, were investigated. Details of the transfer system and the experimental set-up for measuring transfer time by means of a multichannel scaler (MCS) are given in section V.B.3. Multichannel scaling time was set to 10 *ms*. Capsules containing about 200 *mg* of oil fly ash (which gets easily activated due to its high vanadium content) were irradiated several times and the transfer times after each irradiation were recorded. A typical set of data recorded by the MCS for a single measurement is plotted in Fig. VI-5.

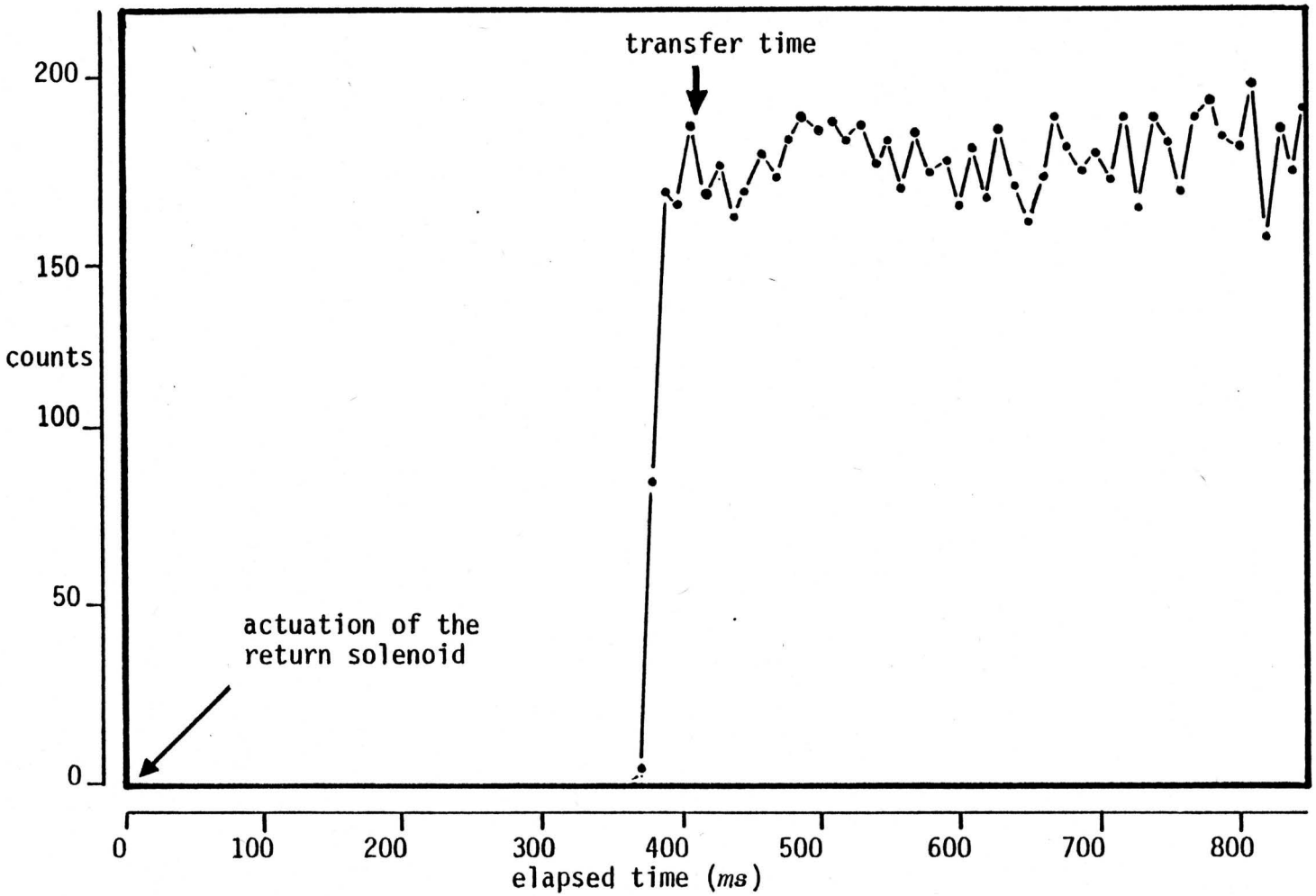

Figure VI-5. Measurement of sample transfer time

2. Effect of Pressure on Transfer Time

Transfer time characteristics observed at four different air pressure settings for a constant sample weight of 200 *mg* are given in Table VI-10. It is clear that there is no significant effect of pressure between 20 and 50 *psi* except for a possible slightly worse reproducibility at 20 *psi*. Therefore, if a value of 600 *ms* is selected as the decay time, then there is less than 1% probability that the sample will not arrive within the set time at normal operating pressure of 38 *psi*. A decay time of 700 *ms*, from the end of irradiation to the beginning of counting, was considered more than sufficient for routine analysis.

3. Effect of Sample Weight on Transfer Time

The weights of the samples were varied between 200 *mg* and 2 *g* by adding paraffin into the irradiation capsules. The transfer times obtained are summarized in Table VI-11. It is apparent that for normal samples (in the range of 200 - 700 *mg*) no significant effect of the sample weight can be seen. However, for sample weights exceeding one gram, the decay time has to be slightly increased in order to achieve a high reproducibility for the decay time.

4. Effect of Length of Irradiation on Transfer Time

Although the effect of pressure and the sample weight may appear to be obvious, any effect of irradiation time t_i, on capsule

Table VI-10. Effect of air pressure on transfer time (t_i = 10 s, 20 determinations for each setting, average weight of the sample ≈0.2 g, average weight of the empty capsule ≈5.8 g)

pressure (psi)	mean tr. time (s)	std. dev. (s)	transfer times at different probabilities[a] (p)		
			p = 90%	p = 95%	p = 99%
20	0.35	0.13	0.52	0.57	0.68
30	0.31	0.10	0.44	0.48	0.56
38	0.35	0.10	0.48	0.52	0.60
50	0.30	0.11	0.45	0.49	0.58

[a] p = probability of sample arrival; *e.g.* when p = 90%, 90 times out of 100 the sample will reach the horizontal counting position within 0.52 s at a pressure of 20 psi.

Table VI-11. Effect of sample weight on transfer time (P = 38 psi, t_i = 10 s, 20 determinations for each setting, average weight of the empty capsule ≃ 5.8 g)

sample weight (g)	mean tr. time (s)	std. dev. (s)	transfer times at different probabilities[a] (p)		
			p = 90%	p = 95%	p = 99%
0.2	0.35	0.10	0.48	0.52	0.60
1.0	0.37	0.12	0.53	0.58	0.67
2.1	0.51	0.13	0.68	0.73	0.84

[a] p - same as in Table VI-10

transfer time may not be so straight forward. For a short t_i, the direction of the air flow has to be reversed within a very short time interval. Depending on the characteristics of the solenoid valves, length of the time interval between two air flows travelling in opposite directions may have an effect on the transfer time.

To investigate this effect, measurements were carried out by varying t_i from 1 s to 10 s for 200 mg samples under a constant pressure of 38 psi. The results summarized in Table VI-12 show that irradiation times exceeding 2 s do not show any significant effect. However, when the irradiation time is 1 s, in order to have a probability of more than 99%, that the sample arrives on time, the set decay time should be more than 1 s. This is contrary to what is desired because the shortest decay times are generally required for shortest irradiation times. Therefore, irradiation times shorter than 1 s are not recommended for the system used in this work except in situations where one needs to minimize background activities and can afford slightly longer decay times.

5. Effect of Sample Settling Time

To partially overcome the problems arising from t_i of less than 1 s (discussed in the above section), it is possible to adjust time settings of the solenoid valves so that the duration of the valve remaining *open* is just enough to transfer the sample. However, in doing so, a more important factor has to be considered. In order to

Table VI-12. Effect of irradiation time on transfer time (P = 38 psi, sample weight ≃ 200 mg, average weight of the empty capsule ≃ 5.8 g)

irradn. time (s)	mean tr. time (s)	std. dev. (s)	transfer times at different probabilities[a] (p)		
			p = 90%	p = 95%	p = 99%
1	0.58	0.17	0.81	0.87	1.0
2	0.31	0.12	0.47	0.52	0.61
3	0.32	0.12	0.48	0.53	0.62
4	0.31	0.10	0.44	0.48	0.56
10	0.35	0.10	0.48	0.52	0.60

[a] p - same as in Table VI-10

maintain the same positioning of the sample near the detector, the capsule should be prevented from bouncing after colliding with the stopping pin. This was done by lengthening the valve opening time for an optimum value so that the air flow acts as a *cushion* for the rebounced capsule. Thus, at this point, one can expect a damping motion before capsule comes to rest. If the settling time, which depends on a number of factors, is relatively long it can cause errors if the counting is initiated within this time. To investigate the magnitude of the settling time, several measurements were performed with MCS scaling time of 1 *ms*. It appears that the settling time is negligibly small as shown in Fig. VI-6.

6. Application of Rapid Transfer System to Cyclic Activation

The various factors studied and optimized for the rapid transfer system can be advantageously used in cyclic activation to improve the sensitivities of very short-lived nuclides (half-lives less than 10 *s*) provided this system can be automated with a high degree of precision. The performance of the cyclic system depends on the proper design and use of a recycle timer. A recycle timer, which can be preset to delay times varying between 10 *ms* and 999 *s* with both precision and accuracy of 0.05%, was designed in this work and described elsewhere (Appendix C). The cyclic activation system with this recycle timer was used to determine concentrations of Br, Cl, In and Pb (via nuclides with half-lives less than 5 *s*) in several standard reference materials using the correction method for coincidence losses - described in Chapter IV.

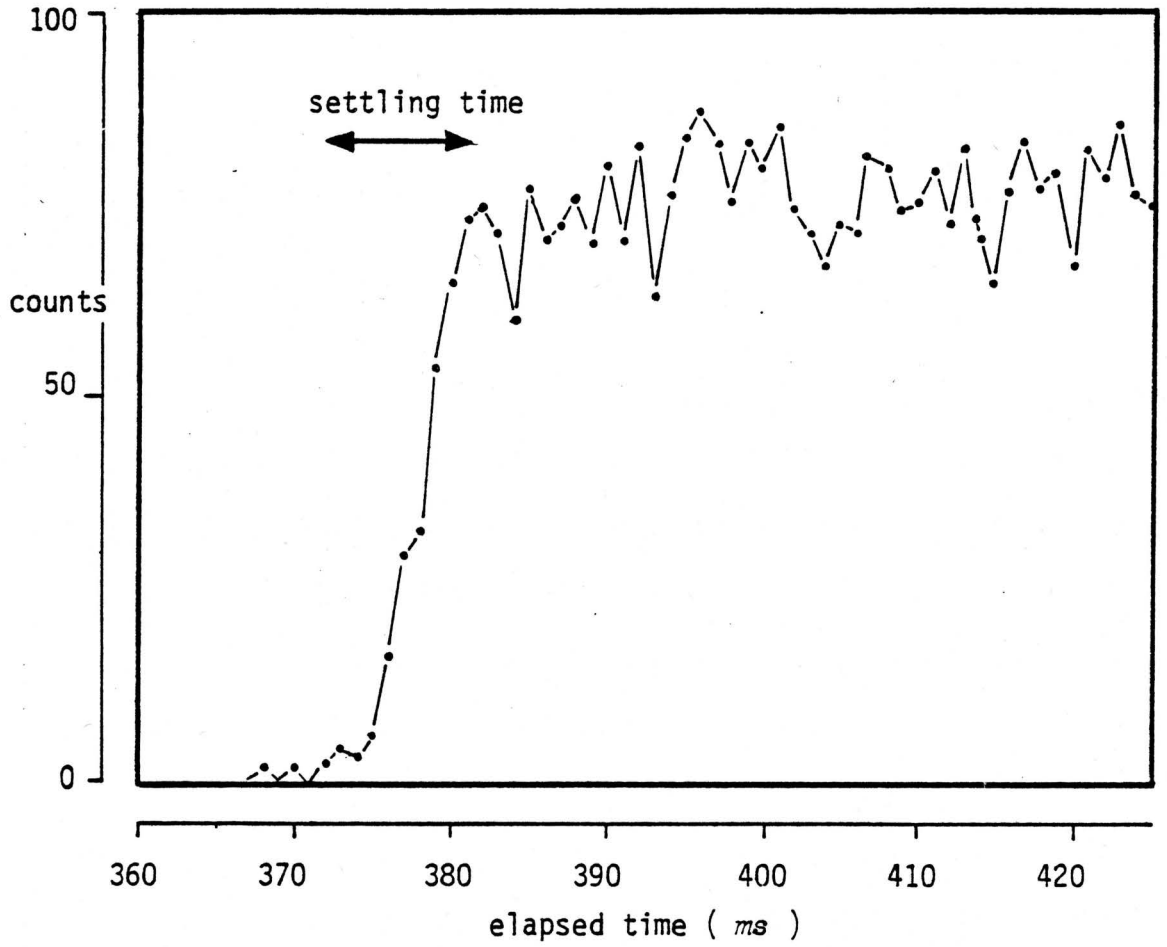

Figure VI-6. Measurement of sample settling time

D. Cyclic Neutron Activation Analysis with the Developed Correction Method

1. Parameters in the Correction Term

In the expression for the correction factor derived in Chapter IV (equation IV-20), the parameters which need to be experimentally determined are the two time variables R_s and DT, and the coefficients C_1, C_2 and C_3.

a. *Determination of C-Coefficients*

The principles of determining the coefficients C_1, C_2 and C_3 in equation IV-20 which appeared due to pile-up losses have been described in section IV.B.1. As mentioned earlier, in order to determine C_1, C_2 and C_3 one has to measure the rate of occurence of undistorted pulses (P) of a particular photopeak which has an actual input pulse rate P_o, at different total activities. Also, the corresponding values for the pulse rate at "SCA OUT" of ADC (R_s) and dead-time (DT) need to be measured. For accurate measurement of the above quantities, non-variable count rates (hence long-lived radioactive sources) can be used.

Measurements were carried out by introducing pulses (at a rate P_o) into the analyser by (i) means of an electronic regular pulser operated at 100 Hz which injects pulses into the preamplifier, and (ii) using a ^{60}Co standard source located at a constant distance from the detector. The total activity was varied to desired levels by

placing an irradiated Sm standard (major activity is due to 103-*keV* peak of ^{153}Sm) at varying distances from the detector. Similar results were obtained with both the regular pulser and ^{60}Co standard except that the reproducibility was somewhat poorer in the latter case. This is probably due to the random variation of the number of photons emitted by the ^{60}Co source. Therefore, the values measured for P using the regular pulser were used to calculate C_1, C_2 and C_3 by regression analysis. Design description of the pulser circuit developed is given in the Appendix E.

The measured values of R_s, DT and P are given in Table VI-13 and VI-14 for time constants 2 μs and 6 μs, respectively. The values for R_a given in these tables represent count rates at the output of the amplifier, which are calculated by the relationship:

$$R_a = R_s / (1 - DT) \qquad \text{IV-18}$$

Values for the pulse pile-up correction factor, K_p, are also tabulated. By using these results as a calibration, it is possible to calculate K_p for known values of R_s without measuring P every time. This can be done by calculating C_1, C_2 and C_3 by a non-linear least square fit of the above results into equation IV-16. Then the necessary corrections due to pulse pile-up as well as dead-time can be performed even for variable count rates (*i.e.* for variable R_s and DT) through the above values of C_1, C_2 and C_3 in equations IV-26 and IV-27. The curves obtained

Table VI-13. Pile-up correction factors at different count rates for 2 μs shaping time constant (set time = 100 *s*, pulser frequency = 100 *Hz*)

% dead-time (DT x 100)	R_s (*cps*)	R_a (*cps*)	C_m (counts)			K_p ($=C_m/C_o$)
			measurement 1	measurement 2	average	
0.5	143	143	10036	10042	10039	1.00
7.6	3260	3530	9926	9953	9925	0.993
11.6	4920	5560	9881	9862	9872	0.987
17.7	7362	8940	9726	9725	9726	0.973
22.4	9118	11740	9640	9654	9647	0.965
24.7	10436	14010	9585	9573	9579	0.958
37.8	15062	24240	9062	9085	9074	0.907
43.9	17558	31288	8799	8724	8762	0.876
51.4	19942	41060	8328	8306	8317	0.832
60.3	22671	57160	7522	7304	7413	0.741
69.6	25684	84653	5610	5484	5512	0.551
74.8	27180	108100	3808	3824	3816	0.382
76.3	27758	119600	3113	3091	3102	0.310

Table VI-14. Pile-up correction factors at different count rates for 6 μs shaping time constant (set time = 100 *s*, pulser frequency = 100 *Hz*)

% dead-time (DT x 100)	R_s (*cps*)	R_a (*cps*)	C_m (counts)			K_p (= C_m/C_o)
			measurement 1	measurement 2	average	
0.8	236	239	10072	10060	10066	1.00
5.9	1846	1960	9826	9959	9892	0.989
9.9	3266	3630	9809	9729	9769	0.977
14.7	5146	6040	9660	9695	9678	0.968
20.4	7146	8980	9331	9374	9353	0.935
24.5	8491	11240	9166	9050	9108	0.911
32.5	10970	16260	8511	8636	8524	0.852
38.2	12910	20910	8055	7935	7995	0.800
44.7	15200	27500	6905	6984	6945	0.695
57.0	18740	43500	4214	4221	4218	0.422
65.0	21010	60500	1299	1322	1311	0.131

by fitting data points of K_p versus R_a for time constants 2 μs and 6 μs are shown in Fig. VI-7. The value of each regression coefficient is very close to unity indicating the reliability of the fits and hence the reproducibility of the coefficients C_1, C_2 and C_3. It is evident from Fig. VI-7 that there is a significant effect on the selection of the shaping time constant for the pulse pile-up correction factor. For example, a value of 50,000 *cps* for R_a corresponds to pile-up correction factors of 0.31 and 0.78 for the time constants 2 μs and 6 μs, respectively. Since all other measurements were carried out using the time constant of 2 μs, the following values for C-coefficients, derived from the corresponding curve, were used for subsequent calculations.

$$C_1 = 0.2615 \times 10^{-5}\ s\ count^{-1}$$
$$C_2 = 0.4383 \times 10^{-10}\ s^2\ count^{-2}$$
$$C_3 = -0.1434 \times 10^{-15}\ s^3\ count^{-3}$$

b. *Measurement of R_s and DT*

As described in section IV.B.1 the variables R_s and *DT* were recorded in alternate channels using a multichannel scaler. The data were fitted into a mathematical model to convert R_s and *DT* into mathematical functions of time, which then can be used to calculate *F(t)* (equation IV-27) and then the integration-term of equation IV-26.

In order to select a suitable mathematical model, three different models were originally considered. A hypothetical equation, which

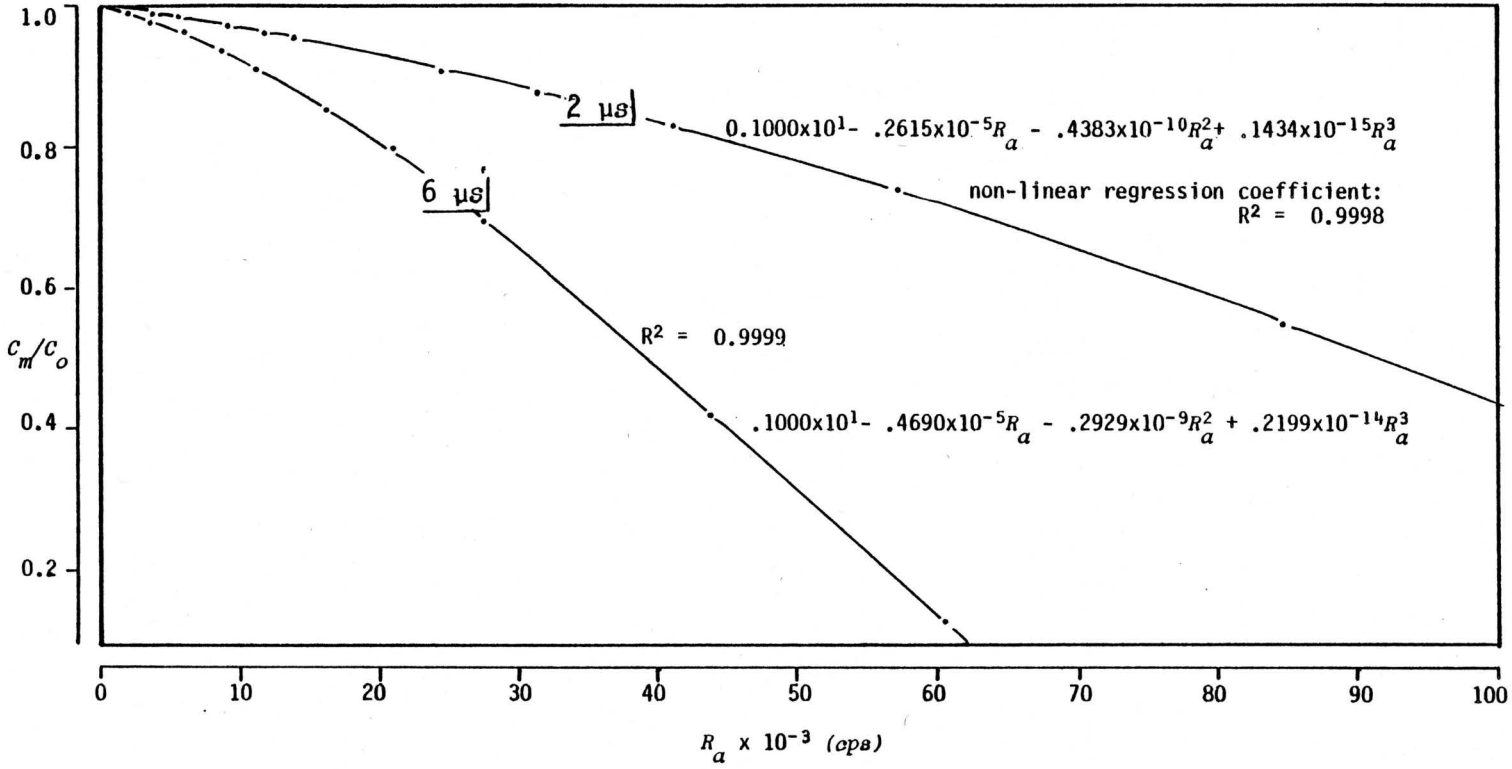

Figure VI-7. Variation of the pile-up correction factor with output count rate, R_a, of the amplifier (at the shaping time constants of 2 μs and 6 μs)

describes the total activity of several nuclides with different half-lives, was applied to examine all three models using a non-linear least square fit. The hypothetical equation assumed was:

$$Y(t) = A\, e^{-\lambda_1 t} + B\, e^{-\lambda_2 t} + C\, e^{-\lambda_3 t} + D\, e^{-\lambda_4 t} \qquad \text{VI-1}$$

The values for λ_1, λ_2, λ_3 and λ_4 were chosen so that they represent a wide spectrum of half-lives of common interfering nuclides ranging from 0.72 *s* (half-life of ^{38m}Cl) to 138 *s* (of ^{28}Al). This range represents a wide spectrum of half-lives compared to an arbitrarily selected counting time of 5.0 *s*.

The three models tested with the above equation assume that the total activity is:

(i) a combination of a constant background and an activity of a single half-life:

$$Y(t) = \alpha + \beta\, e^{-\gamma t} \qquad \text{VI-2}$$

(ii) a third order polynomial of time *t*:

$$Y(t) = a_o + a_1 t + a_2 t^2 + a_3 t^3 \qquad \text{VI-3}$$

(iii) a fourth order polynomial of time *t*:

$$Y(t) = a_o + a_1 t + a_2 t^2 + a_3 t^3 + a_4 t^4 \qquad \text{VI-4}$$

The three mathematical models were tested for various combinations of numerical values of constants A, B, C and D. The typical sets of curves obtained by comparing the three models with the hypothetical equations are shown in Fig. VI-8, VI-9 and VI-10. It is obvious that the exponential model which assumes a combined activity of a single half-life and a constant background is not sufficient due to considerable underestimation of the initial activity. A third order polynomial (Fig. VI-9) represents the assumed function $Y(t)$ reasonably well. An excellent matching (non-linear regression coefficient - 0.99992) between $Y(t)$ and the fourth order polynomial can be seen in Fig. VI-10. The choice of third or fourth order polynomial depends on the desired accuracy and the capacity of the data manipulation system. The least square analysis of a fourth order polynomial can easily be carried out using a computer. In this study, calculations were performed assuming a fourth order polynomial.

A typical set of experimental data obtained for DT and R_s is plotted in Fig. VI-11 along with the fitted curves. These results were obtained for the first cycle in an analysis of an oyster tissue standard reference material. Plotted values of the function $F(t)$ calculated according to equation IV-27 and the fitted polynomial curve are also shown. The regression coefficient (0.999997) obtained for $F(t)$ indicates the reliability of the polynomial assumption for $F(t)$ which was made to simplify the integration.

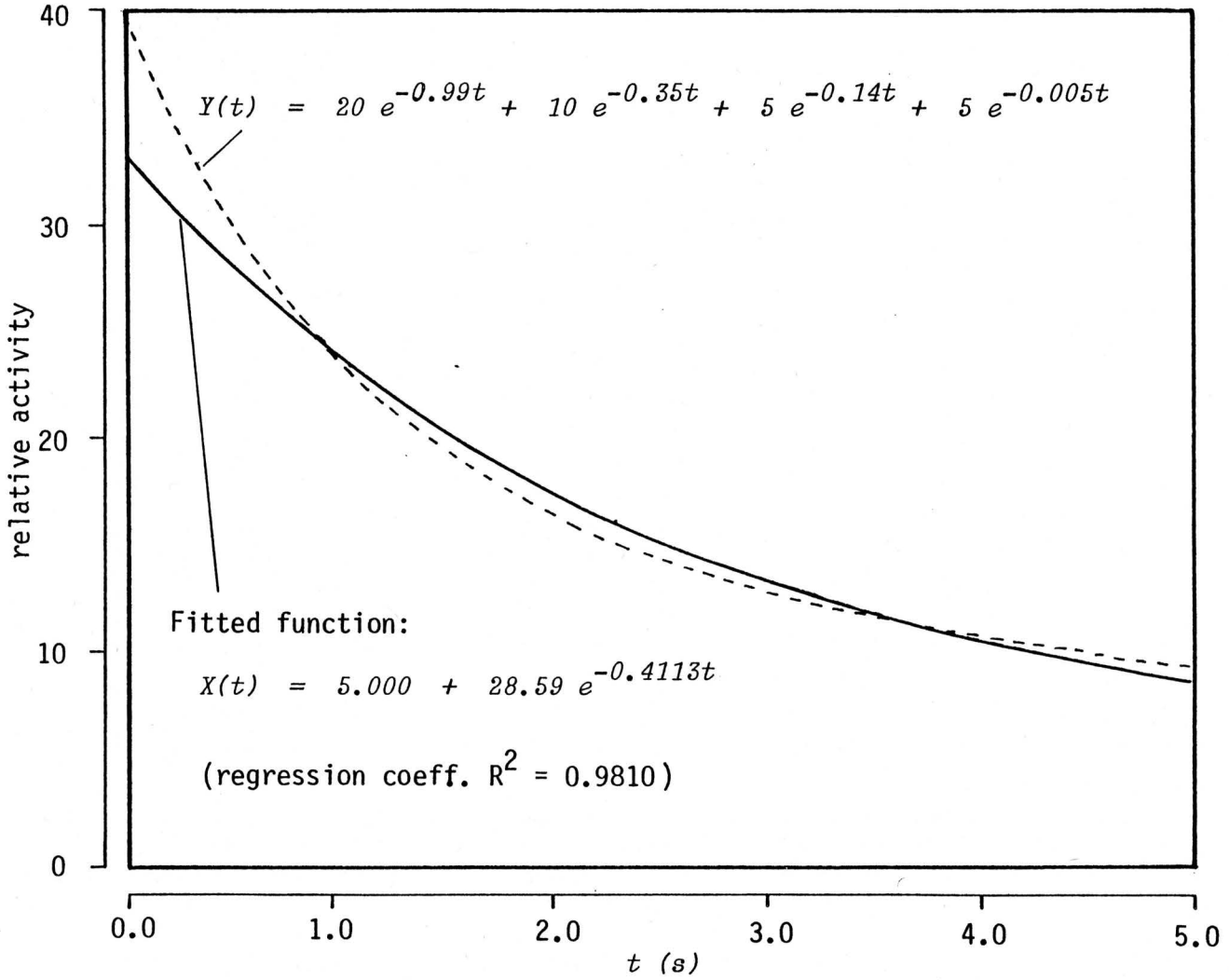

Figure VI-8. Model fitting - a single short-lived nuclide and a constant background

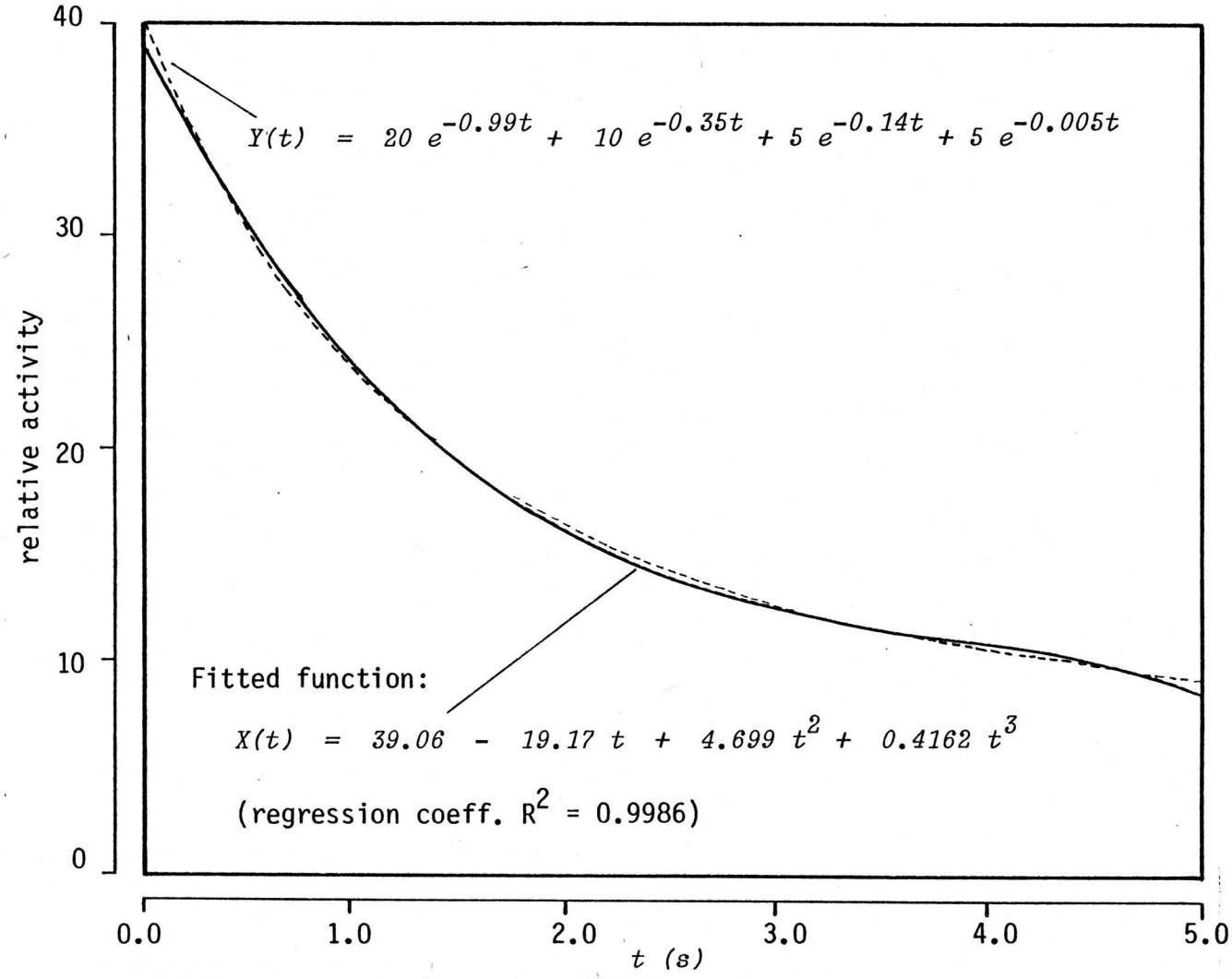

Figure VI-9. Model fitting - a third order polynomial

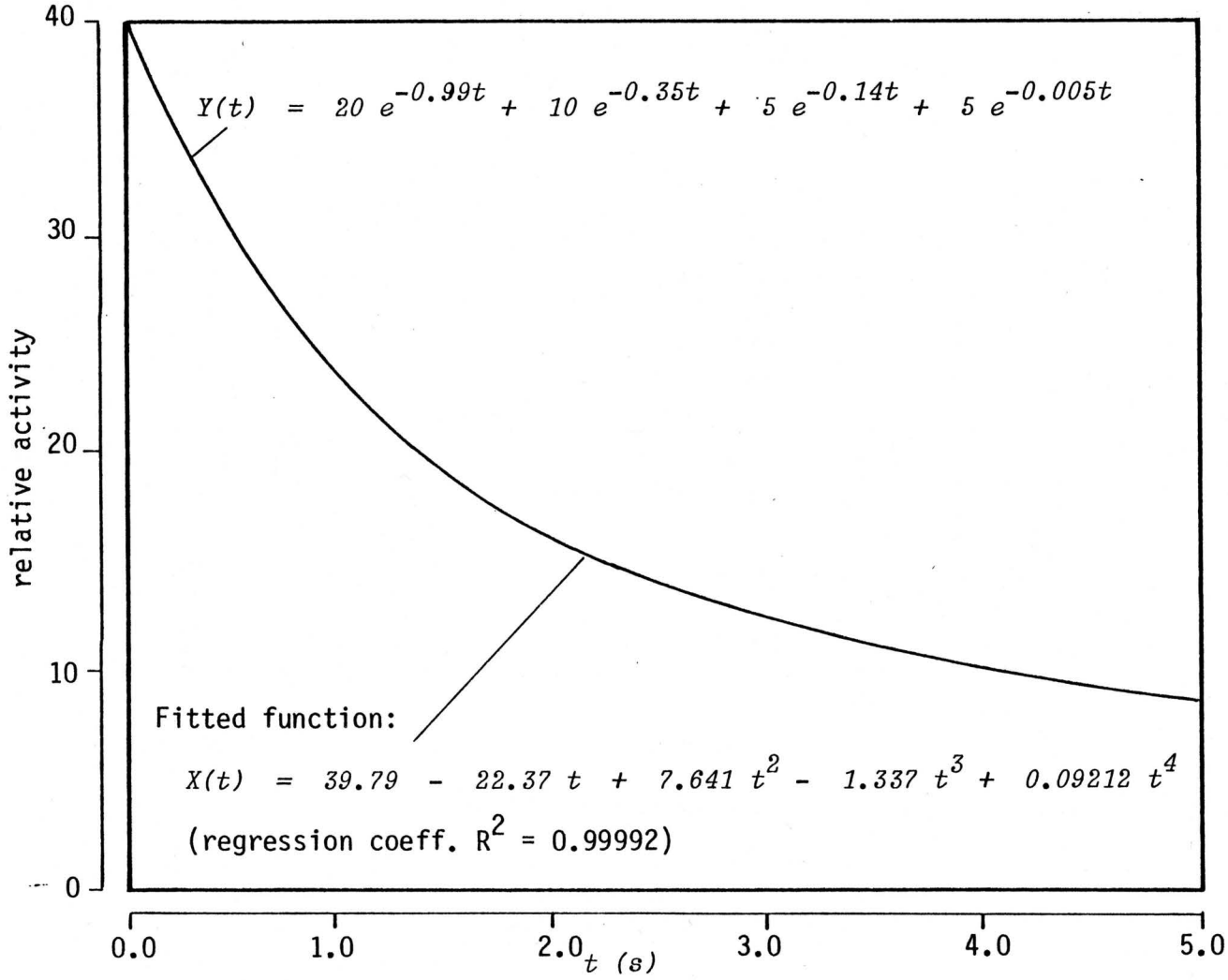

Figure VI-10. Model fitting - a fourth order polynomial

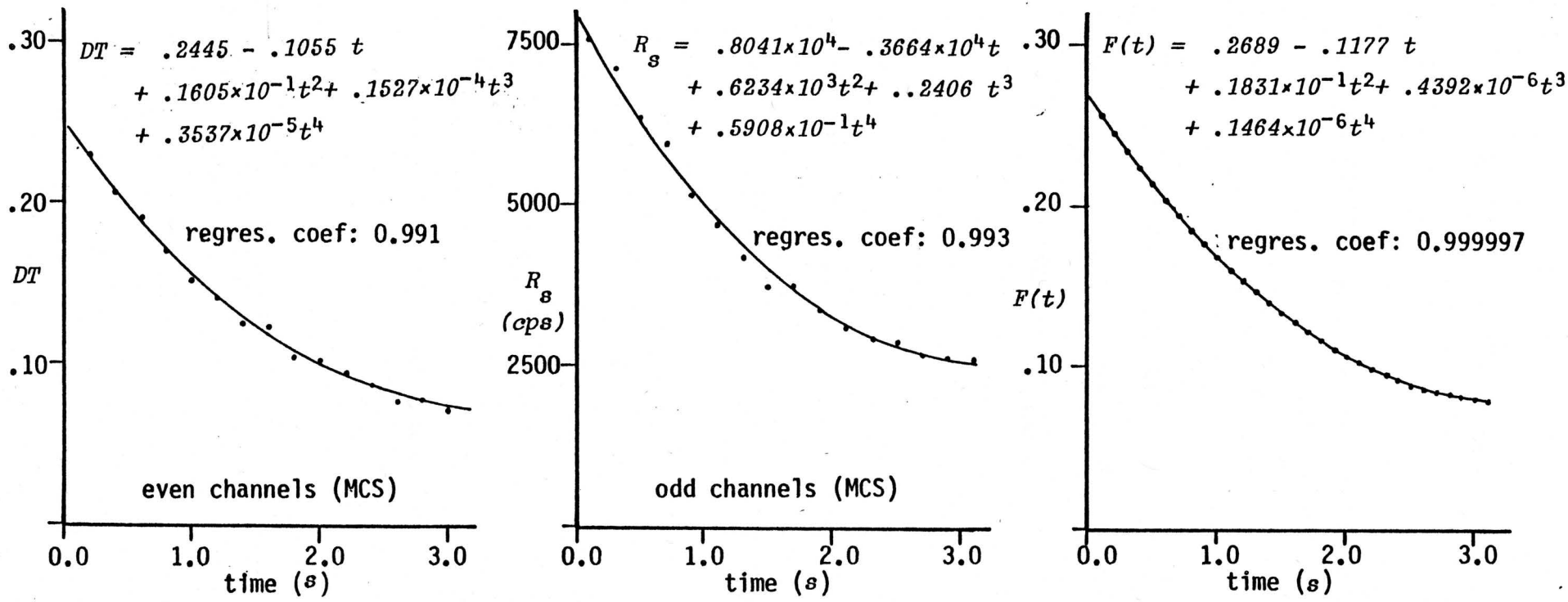

Figure VI-11. A typical set of multichannel scaling data for DT and R_s and the fitted function $F(t)$.

2. Extension of the Correction Method to CINAA

In the case of a single counting procedure the appropriate correction factor for a nuclide of interest can be calculated as described in the previous section. However, in CINAA, since one obtains a cumulative spectrum of several cycles and as each cycle has different values for R_s and DT, the above described correction method needs to be appropriately extended so that correction factors in each cycle can be incorporated in the final correction. One such set of experimental data obtained for R_s and DT over 10 cycles in CINAA of an oyster tissue sample is shown in Fig. VI-12.

In section II.A.2, the cumulative detector response $C_o(c)$ after n cycles, was derived as:

$$C_o(c) = C_o(1)\left\{\frac{1}{1-e^{-\lambda t}}\left[n - e^{-\lambda T}\left(\frac{1-e^{-n\lambda T}}{1-e^{-\lambda T}}\right)\right]\right\} \qquad \text{II-8}$$

where, $C_o(1)$ is the detector response at the first cycle which is given by:

$$C_o(1) = \frac{\varepsilon\,\phi\,\sigma\,m}{\lambda\,M} \times 6.023 \times 10^{23}\ (1-e^{-\lambda t_i})\ (e^{-\lambda t_d})\ (1-e^{-\lambda t_c}) \qquad \text{II-2}$$

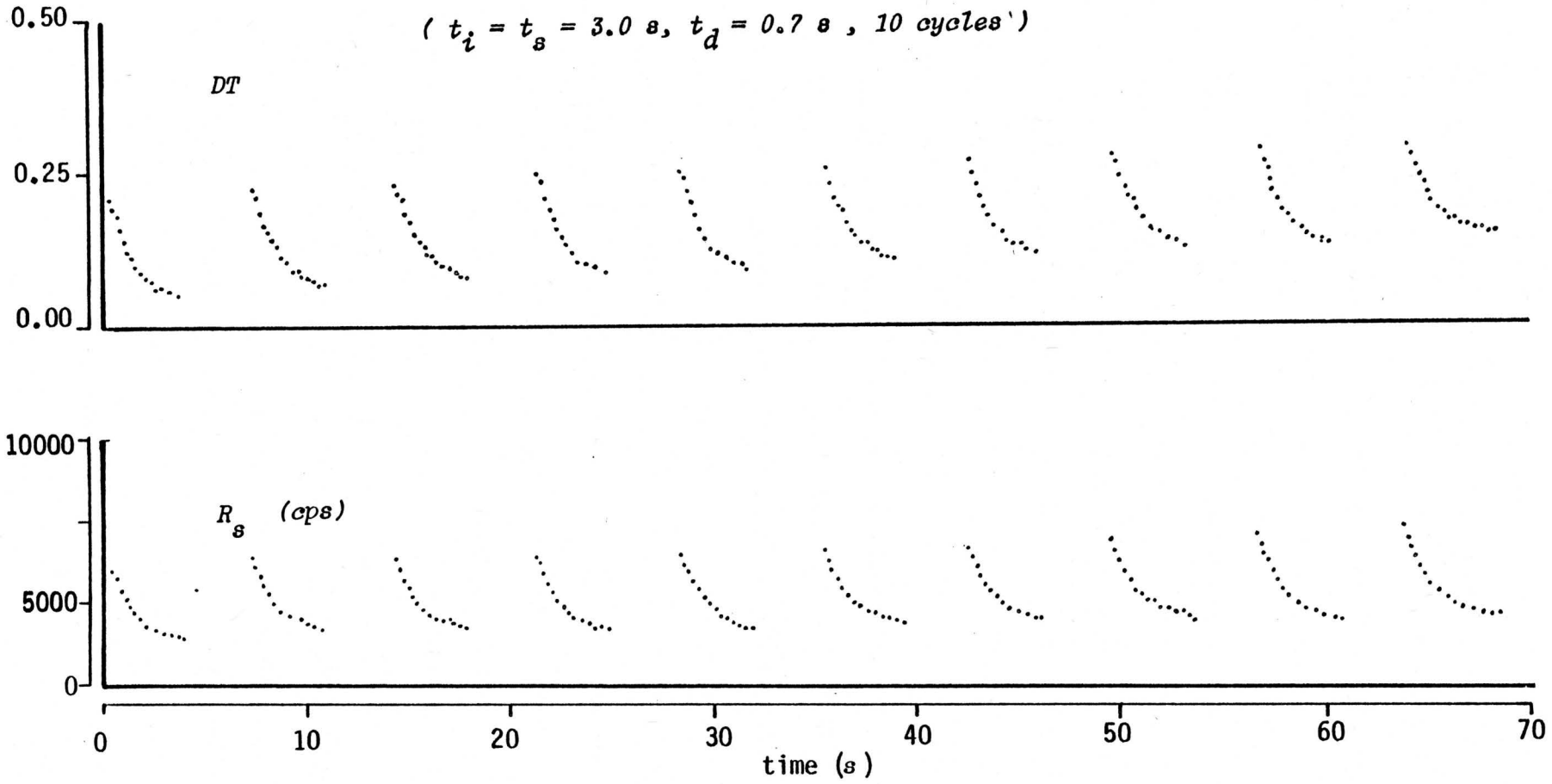

Figure VI-12. A typical set of multichannel scaling data obtained for *DT* and R_s in CINAA of oyster tissue.

The derivations of above equations assumed no dead-time or pulse pile-up losses. Therefore, $C_o(c)$ is the expected cumulative detector response and it would be different from the measured cumulative detector response $C(c)$ due to coincidence losses.

Since dead-time, total activity and activities of interest are different from cycle to cycle, each cycle has a different correction factor and a different accumulated number of counts. Therefore, the number of counts obtained should be corrected individually for each cycle using the corresponding correction factor. With the aid of the circuit designed in this study (section IV.B.1) and the previously described computation method (section IV.B.2) determination of the correction factor for each cycle does not pose much problems. However, the measurement of number of counts in each cycle becomes a difficult task as it requires storage of spectra separately after each cycle or involves data processing and storage of processed data after each cycle. If the cycle time is relatively long, each spectrum can be stored using a suitable storage device. However, if the cycle time is of the order of few seconds, it may not be practically feasible to store each cycle with the currently available analysers. This is one of the main reasons for not having had a simple solution to the correction of coincidence losses in CINAA. An alternative approach has been taken in the present work for a simple and accurate solution through a mathematical treatment.

As in the conventional case (*i.e.* similar to that described in section IV.A.3), correction factor K_c (to correct cumulative response $C(c)$) can be defined as:

$$K_c = C(c) / C_o(c) \qquad \text{VI-5}$$

Although one may define individual K values for each cycle, K_c is not a simple function of these individual K values. As such, up to this point, the problem was the calculation of the correction factor K_c using the known values of correction factors ($K_1, K_2, \ldots K_n$) for each cycle.

If the accumulated number of counts at the nth cycle is $C(n)$ (which is unknown if the spectra are not stored at each cycle) by incorporating the correction factor for the nth cycle K_n, the theoretical equation II-6 for $C_o(n)$ can be modified to the real case as:

$$C(n) / K_n = C_o(1) \left(\frac{1 - e^{-n\lambda T}}{1 - e^{-\lambda T}} \right) \qquad \text{VI-6}$$

Therefore, the expression for the cumulative detector response, $C(c)$ (the quantity which is determined experimentally) can be written as:

$$C(c) = C(1) + C(2) + \ldots + C(n)$$

$$= \sum_{n=1}^{n} C(n) \qquad \text{VI-7}$$

Then, by substituting for $C(n)$ in equation VI-7 using equation VI-6:

$$C(c) = C_o(1) \sum_{n=1}^{n} \left(\frac{1 - e^{-n\lambda T}}{1 - e^{-\lambda T}} \right) K_n \qquad \text{VI-8}$$

(The term $C_o(1)$, which is not known, being independent of n, can be taken out from the summation sign.)

Thus, the expression for the correction factor K_c (which is equal to the ratio $C(c)/C_o(c)$) can be obtained by dividing equation VI-8 by equation II-8:

$$K_c = C(c) \; / \; C_o(c)$$

$$= \frac{C_o(1) \sum_{n=1}^{n} \left(\frac{1 - e^{-n\lambda T}}{1 - e^{-\lambda T}} \right) K_n}{C_o(1) \left\{ \frac{1}{1 - e^{-\lambda T}} \left[n - e^{-\lambda T} \left(\frac{1 - e^{-n\lambda T}}{1 - e^{-\lambda T}} \right) \right] \right\}} \qquad \text{VI-9}$$

This simplifies as:

$$K_c = \sum_{n=1}^{n} (1 - e^{-n\lambda T}) \; K_n \; / \left[n - e^{-\lambda T} \left(\frac{1 - e^{-n\lambda T}}{1 - e^{-\lambda T}} \right) \right] \qquad \text{VI-10}$$

From this expression, with the knowledge of the values for K_1, K_2, ...K_n determined by the method summarized in section IV.C.3, K_c can be

simply calculated for the nuclide(s) of interest.

If the dead-time and pile-up losses are negligible, K_n approaches unity for each cycle. When K_n = 1, denominator and numerator are identical and hence K_c is equal to 1, suggesting that measured cumulative detector response $C(c)$ is the same as the theoretically expected value $C_o(c)$.

The method described above significantly reduces unnecessary data manipulation without any sacrifice of accuracy. In fact, since the correction is done to the final cumulative counts it will provide a better statistical accuracy than that obtained by correcting for individual cycles.

3. Evaluation of the Correction Method Using Elemental Standards

a. *Lead Standards*

The validity of the correction methods proposed in this study was first evaluated by analyzing a series of Pb standards. Lead was of particular interest because it is relatively insensitive to conventional INAA, and the most sensitive way of determining Pb by INAA in conjunction with gamma spectrometry is via ^{207m}Pb nuclide with a half-life of 0.81 seconds which is near the lower limit of half-lives that can be detected with the present rapid transfer facility. Lead standards were prepared by evaporating a known volume of a lead nitrate *Atomic Absorption Standard* solution. Each standard was analysed under

similar conditions by CINAA. Table VI-15 shows the number of counts accumulated over 10 cycles and the corresponding values corrected for dead-time and pile-up losses. It can be seen that,without correction, negative systematic errors of significant magnitudes can occur. This error is more evident from the plot of number of counts versus the amount of Pb shown in Fig. VI-13. For 25 *mg* of Pb, dead-time varied from approximately 22% to 3% during counting. At this low level of radioactivity, it is apparent from Fig. VI-13 that pile-up effect is not very significant so that the correction for dead-time alone may be sufficient.

b. Se *and* In *Standards with Additional Background*

Although at low pulse rates total coincidence losses are mainly due to the analyser dead-time, it was shown in section III.B that the pile-up losses increase more rapidly than the dead-time losses as the total pulse rate increased. In order to investigate the reliability of the correction method at pulse rates where pile-up losses are appreciable, a series of standards containing the same amount of In (1 μg) and Se (20 μg) were spotted separately on Nuclepore membranes and irradiated along with different amounts of sodium chloride and Aluminum to simulate varying background activities. All standards were analysed under similar conditions and accumulated counts at the 164-*keV* photopeak of ^{116m_2}In (half-life 2.16 *s*) and at the 162-*keV* photopeak of ^{77m}Se (half-life 17.4 *s*) were measured along with the simultaneous measurements of R_s and *DT*. The plots of number of counts

Table VI-15. Effect of dead-time and pulse pile-up correction for a series of Pb standards ($t_i = t_s = 3\ s$, $t_d = 0.7\ s$, 10 cycles, $T = 10\ s$, $\phi = 1 \times 10^{12}\ n\ cm^{-2}\ s^{-1}$)

sample number	weight of Pb (*mg*)	observed counts[a]		counts / *mg* [a]					
				uncorrected for losses		corrected for dead-time		corrected for dead-time and pile-up	
		570 *keV*	1064 *keV*	570 *keV*	1064 *keV*	570 *keV*	1064 *keV*	570 *keV*	1064 *keV*
Pb2.5C	2.50	962	463						
Pb2.5D		961	454						
Pb2.5E		898	456						
average		940±65	458±26	376±45	183±18	382±46	186±18	383±46	186±18
Pb5C	5.00	1798	782						
Pb5D		1789	811						
Pb5E		1860	877						
average		1816±90	823±61	363±18	165±12	375±19	170±12	377±19	171±12
Pb15C	15.0	5378	2455						
Pb15D		5271	2492						
Pb15E		5112	2338						
average		5254±153	2428±104	350±10	161±7	381±11	175±11	385±11	177±11
Pb25C	25.0	8643	3711						
Pb25D		8497	3789						
Pb25E		8211	3826						
average		8450±194	3775±121	338±8	151±5	382±9	171±5	390±9	174±5

[a] ± values indicates the standard deviation calculated from counting statistics, for three identical measurements

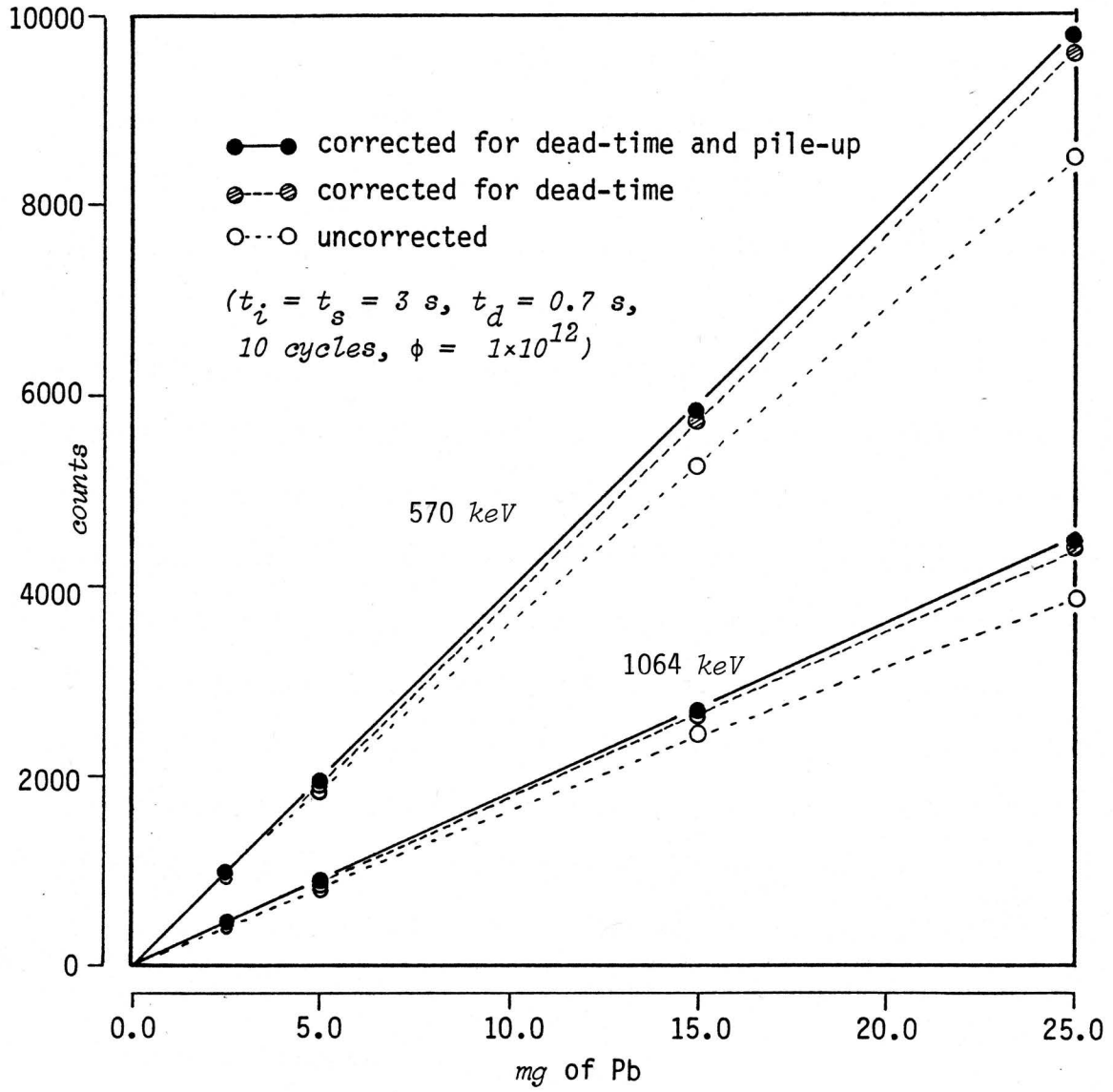

Figure VI-13. Effect of dead-time and pile-up correction for a series of Pb standards

versus the estimated total absolute count rate R_o (see section IV.D for details of calculating R_o) are shown in Fig. VI-14.

It is clear that at high count rates negative errors of as much as 70% and 60% for In and Se, respectively, can occur when no correction is done. As one would expect in the case of In, having the shorter half-life of the two, the dead-time correction is more significant than that for Se since the measurements were done in the live-time mode. By correcting for both dead-time and pulse pile-up, satisfactory results were obtained for absolute total pulse rates of as high as 60,000 pulses per second (corresponding dead-time was over 65%). However, at these levels of high activity, due to the considerably high population of distorted pulses (since no pile-up rejector was used), the gamma-ray spectrum also becomes distorted, consequently, some uncertainity is involved in defining the peak and background areas. One reason for the slight downward trend of the corrected data at excessively high pulse rates may be attributed to such uncertainities. Nevertheless it is encouraging to observe that the above difference is negligible compared to the magnitudes of corrections involved with both dead-time and pile-up effects. Furthermore, the above mentioned severe spectrum distortion can be significantly reduced by using a pulse pile-up rejector.

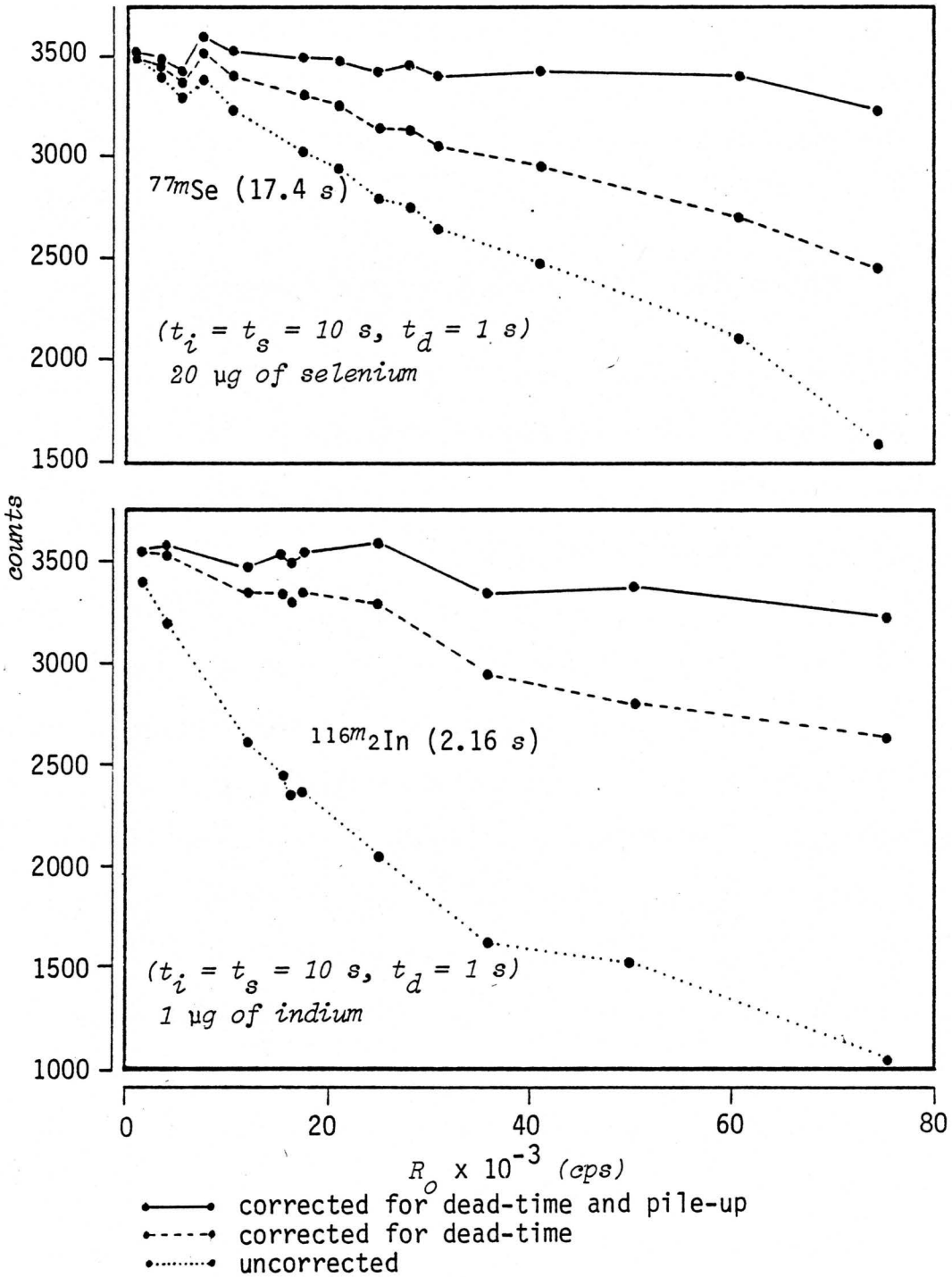

Figure VI-14. Effect of dead-time and pile-up correction on measurement of ^{77m}Se and ^{116m2}In activities

4. Applications

Precision and accuracy of the proposed correction method for coincidence losses were examined by analysing several standard reference materials (SRM) using CINAA. Results obtained for few elements are discussed in the following sections.

a. *Determination of chlorine using ^{38m}Cl in NBS SRM Bovine Liver and Oyster Tissue*

Bovine Liver and Oyster Tissue samples were analysed for chlorine via its ^{38m}Cl nuclide which has a half-life of 0.72 seconds. In order to obtain different total activities, different sample weights of the two SRM were analysed under similar conditions ($t_i = t_s = 3\ s$ $t_d = 0.7\ s$). Triplicate samples of four different weights of Bovine Liver were prepared. The maximum weight of sample that could be placed inside one single small irradiation capsule was approximately 0.5 and 0.7 g for Bovine Liver and Oyster Tissue, respectively. In order to eliminate any errors due to possible variations in the counting geometry, further increase of the sample size was not attempted. However, even with the maximum possible sample weights, initial dead-times were measured as 28% for Oyster Tissue and 7.5% for Bovine Liver. In an attempt to extend the range of dead-times covered by these experiments, SRM samples with maximum weights were reanalysed under similar conditions, except that counting was done in the presence of additional background introduced via long-lived ^{60}Co and ^{22}Na standard sources placed near the detector. The average number of counts and the

calculated values of concentrations of Cl in these two matrices are given Table VI-16 and Table VI-17.

Except in the presence of the additional background, coincidence losses for the Bovine Liver samples analyzed do not appear to be appreciable. On the other hand, in the case of Oyster Tissue where the activity is mainly due to ^{38m}Cl itself, in the absence of any additional background, errors of as much as 22% can occur for the largest sample size if the correction is not done. When the same Oyster Tissue samples are analyzed with additional background, the correction method developed in this work satisfactorily eliminates errors of the order of 30%. A good agreement between the values themselves and that with the NBS value can be seen. Graphical representations of these results in Fig. VI-15 and Fig. VI-16 show the extent of deviations of the corrected values from the uncorrected ones as the sample size is increased. A quite satisfactory linearity is observed for corrected values in contrast to the negative deviation of the uncorrected values.

Chlorine content of blanks was estimated by irradiating several empty polyethylene irradiation capsules under similar conditions to be 25±12 μg. Thus, in the worst case - with the lowest weight of Bovine Liver ($\simeq$ 0.11 g) - blank correction was about 8%. Furthermore, one can expect possible errors due to self-shielding effects with increased sample sizes. Self-shielding effects would result in effectively lower neutron fluxes. Consequently, specific activities in

Table VI-16. Precision and accuracy for the determination of Cl via ^{38m}Cl in Bovine Liver using different sample weights (t_i = t_s = 3 s, t_d = 0.7 s, T = 10 s, n = 10 cycles)

average weight (g)	maximum dead-time (%)	counts/g [a,b]	chlorine content ($\mu g/g$)[b]			limits[c]	
			uncorrected for losses	corrected for losses	NBS certified value	L_D ($\mu g/g$)	L_Q ($\mu g/g$)
0.110	2	4810±640	2620±350	2640±350	2700	120	650
0.248	4	4750±420	2580±230	2630±230		70	330
0.498	7	4649±293	2530±160	2690±180		44	190
0.498 with additional background	22	3801±280	2070±150	2640±190		130	460

[a] corrected for blank

[b] average of three determinations

[c] see section V.F for definitions

Table VI-17. Precision and accuracy for the determination of Cl via ^{38m}Cl in Oyster Tissue using different sample weights (t_i = t_s = 3 s, t_d = 0.7 s, T = 10 s, n = 10 cycles)

average weight (g)	maximum dead-time (%)	counts/g [a,b]	chlorine content[b] ($\mu g/g$)			limits[c]	
			uncorrected for losses	corrected for losses	NBS certified value	L_D ($\mu g/g$)	L_Q ($\mu g/g$)
0.106	5	16660±1230	9060±670	9230±670	10000	190	850
0.270	15	15830±750	8600±410	9150±440		110	430
0.478	21	14480±540	7840±290	9170±340		82	320
0.704	28	13050±420	7090±230	9130±300		70	240
0.704 with additional background	38	10980±390	5970±212	9050±320		120	390

[a] corrected for the blank

[b] average of three determinations

[c] see section V.F for definitions

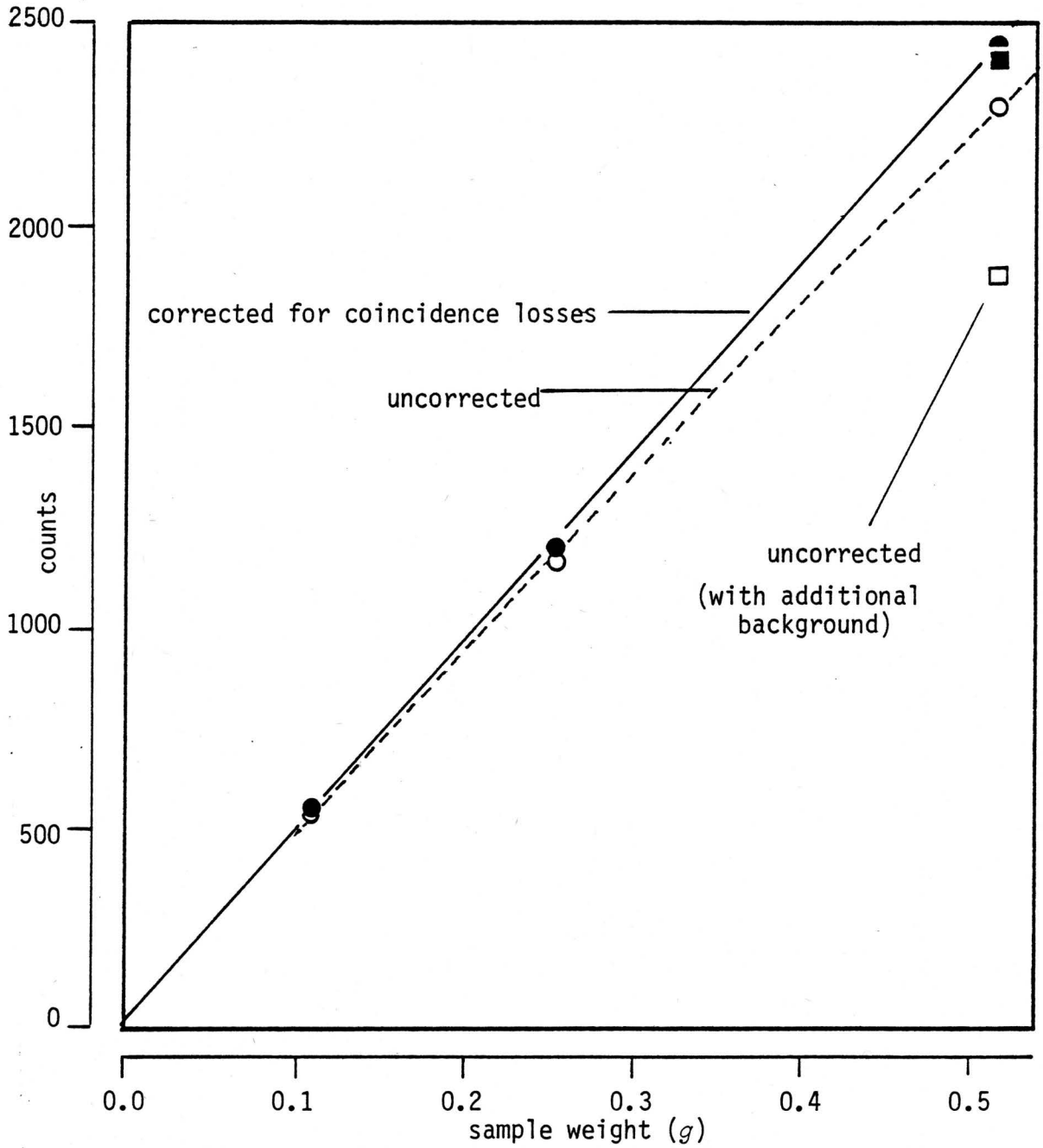

Figure VI-15.. Effect of correction for coincidence losses for the determination of chlorine via ^{38m}Cl in Bovine Liver using different sample weights

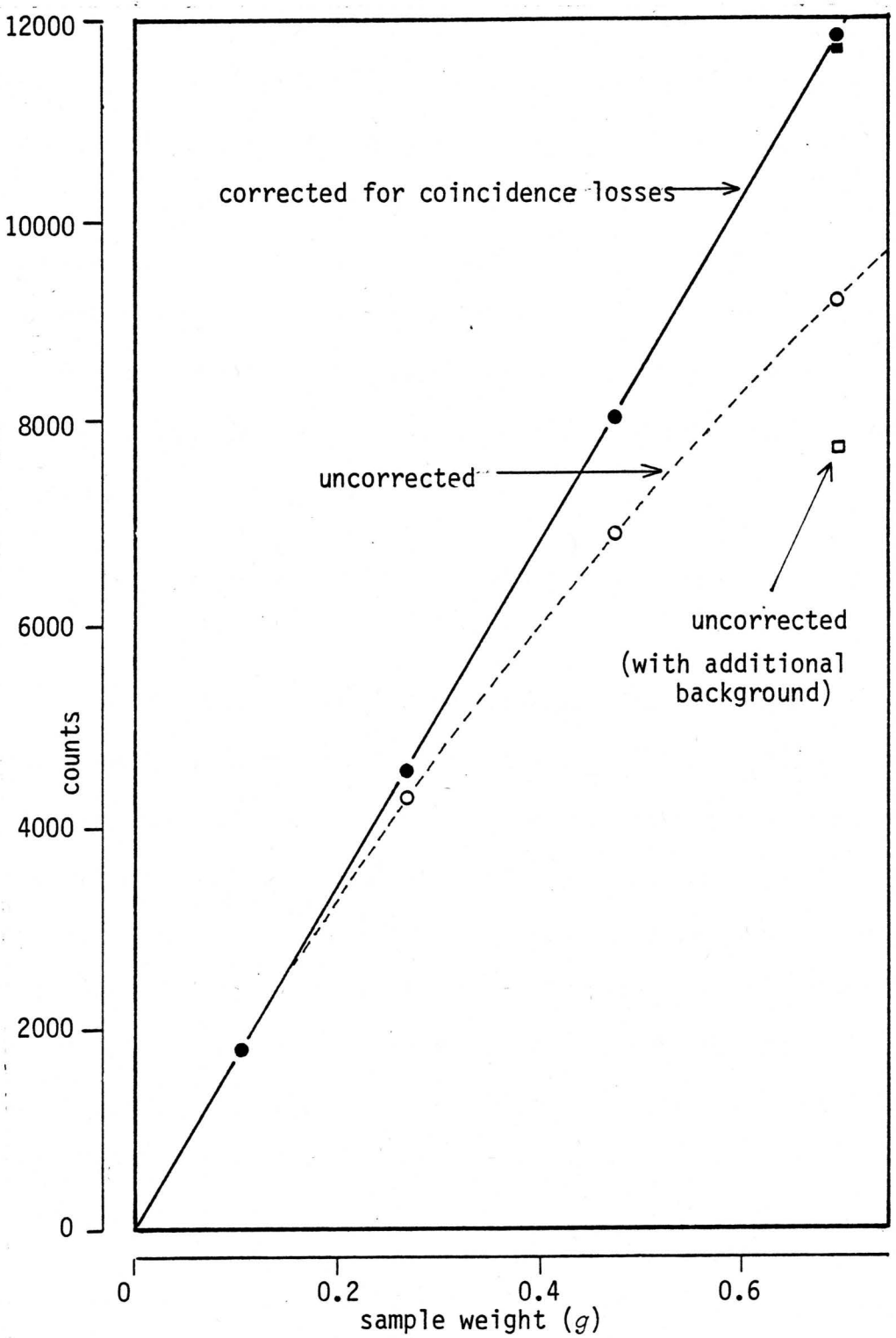

Figure VI-16. Effect of correction for coincidence losses for the determination of chlorine via ^{38m}Cl in Oyster Tissue using different sample weights

larger samples will be lower than those in smaller samples. Possible errors due to this effect were checked by counting the samples again after several minutes of decay for longer-lived nuclides such as ^{38}Cl and ^{24}Na. Since the counting time can be extended to obtain a satisfactory number of counts, the counting geometry could be selected so that coincidence losses are negligible. No significant variation was observed for specific activities of the above long-lived nuclides for different sample weights. Hence errors due to self-shielding effects were considered negligible.

b. *Determination of* Se *in SRM Bovine Liver and Oyster Tissue Using* ^{77m}Se

Although Se could also be detected using the same experimental conditions as used for Cl, in order to improve the sensitivity of ^{77m}Se nuclide (half-life 17.4 *s*) and to deal with a higher matrix background for a better evaluation of the coincidence losses, it was decided to employ 10 *s* irradiation and counting periods. Several days after the chlorine analysis, the same SRM samples were analysed for Se with the above mentioned experimental conditions. Results are summarized in Table VI-18. It is evident that the measured values after correction for coincidence losses agree well with the values certified by the NBS.

A typical gamma-ray spectrum obtained at the tenth cycle for a sample of Oyster Tissue is shown in Fig. VI-17. Even though

Table VI-18. Precision and accuracy for the determination of Se via ^{77m}Se in Bovine Liver and Oyster Tissue using different sample weights ($t_i = t = 10\ s$, $t_d = 2\ s$, $T = 30\ s$; 10 cycles)

Material	average weight (g)	maximum dead-time (%)	counts/g [a]	selenium content[a] ($\mu g/g$)			limits[b]	
				uncorrected for losses	corrected for losses	NBS certified value	L_D ($\mu g/g$)	L_Q ($\mu g/g$)
Bovine Liver	0.1099	3	2900±170	1.05±0.06	1.05±0.07	1.1±0.1	0.32	1.1
	0.2478	7	2710±220	0.98±0.08	1.00±0.08		0.18	0.63
	0.4975	11	2720±160	0.99±0.06	1.02±0.07		0.10	0.36
Oyster Tissue	0.1058	7	5290±320	1.91±0.12	1.94±0.12	2.1±0.5	0.45	1.5
	0.2704	15	5040±190	1.82±0.07	1.92±0.07		0.26	0.86
	0.4782	26	4762±263	1.72±0.09	1.93±0.11		0.19	0.61
	0.7041	32	4379±186	1.59±0.07	1.90±0.08		0.14	0.47

[a] average of three determinations

[b] see section V.F for definitions

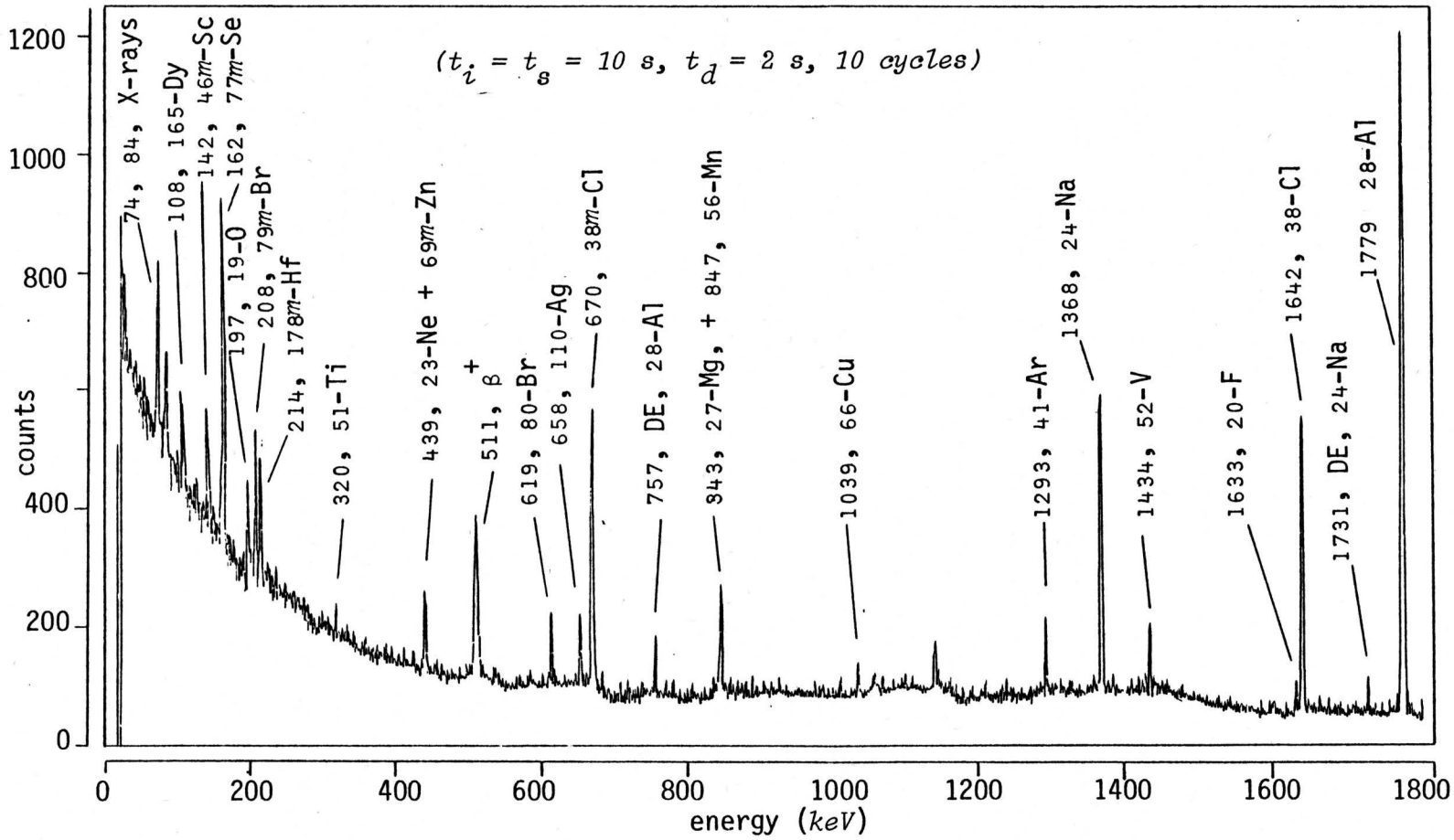

Figure VI-17. CINAA of Oyster Tissue - a typical gamma-ray spectrum

quantitative measurements were done only for chlorine and selenium it is clear from the spectrum that several other nuclides can also be determined simultaneously.

c. *Determination of* Sc *in SRM Orchard Leaves Using* ^{46m}Sc

Due to higher ^{28}Al activity induced after short irradiations, botanical samples are generally more difficult to analyse than zoological samples by CINAA. Therefore, the effect of background activity on the detection limits for short-lived nuclides is more severe for botanical samples. The variation of detection limits and precision with increasing number of cycles were investigated by analysing NBS Orchard Leaves for Sc via ^{46m}Sc ($t_{1/2}$ = 18.7 *s*) using the timing parameters of $t_i = t_s$ = 10 *s*, t_d = 2 *s*, T = 25 *s*. Approximately a four fold enhancement in precision was observed by increasing the number of cycles as shown in Fig. VI-18. The standard deviations were calculated for 4 independent determinations at each cycle. It is apparent that significant improvement in detection limits can also be obtained by increasing the number of cycles although there are no significant changes in both precision and the detection limits beyond the eighth cycle. This observation can be accounted for by the build-up of high activity of ^{28}Al with increased number of cycles. Gamma-ray spectra of a sample of Orchard Leaves obtained using the above timing parameters and recorded after 1st, 6th, and 12th cycle are shown in Fig. VI-19. Although the major interfering activity of

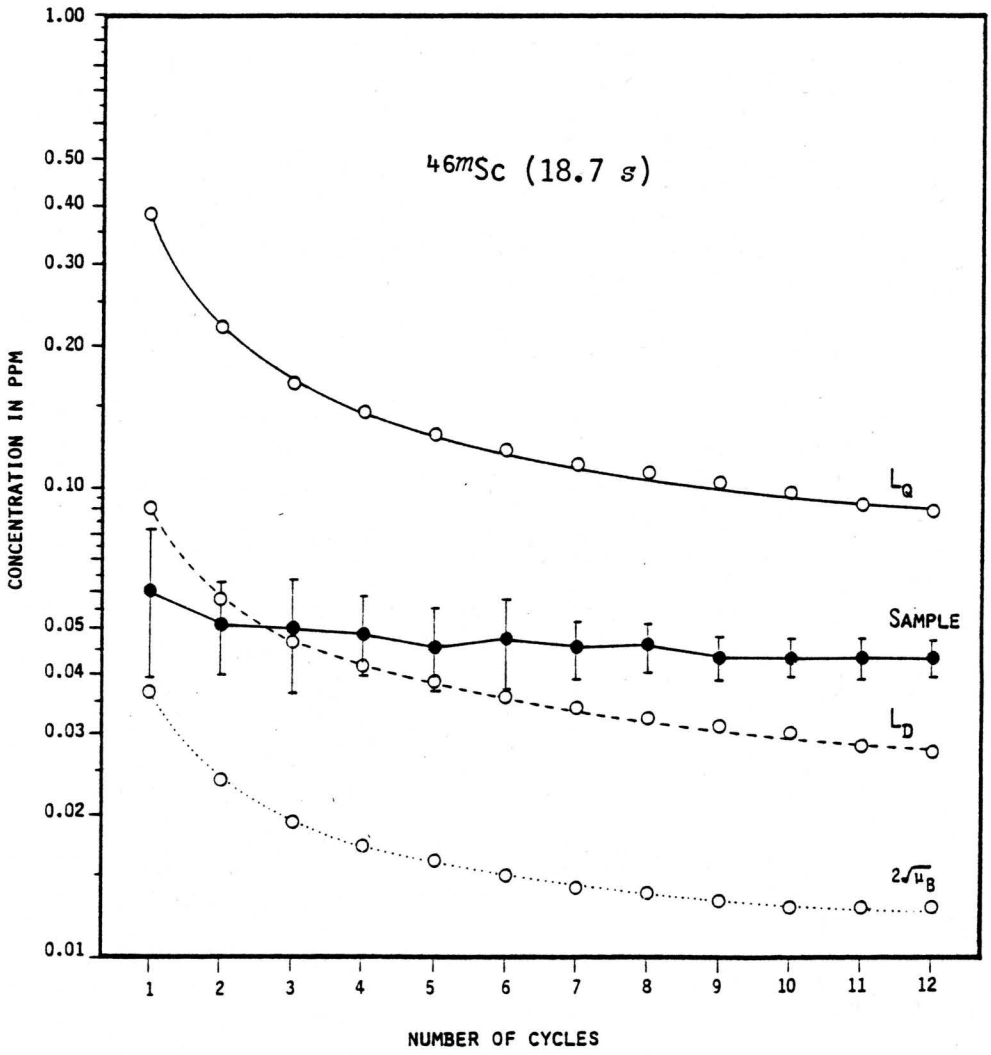

Figure VI-18. Determination of Sc in Orchard Leaves

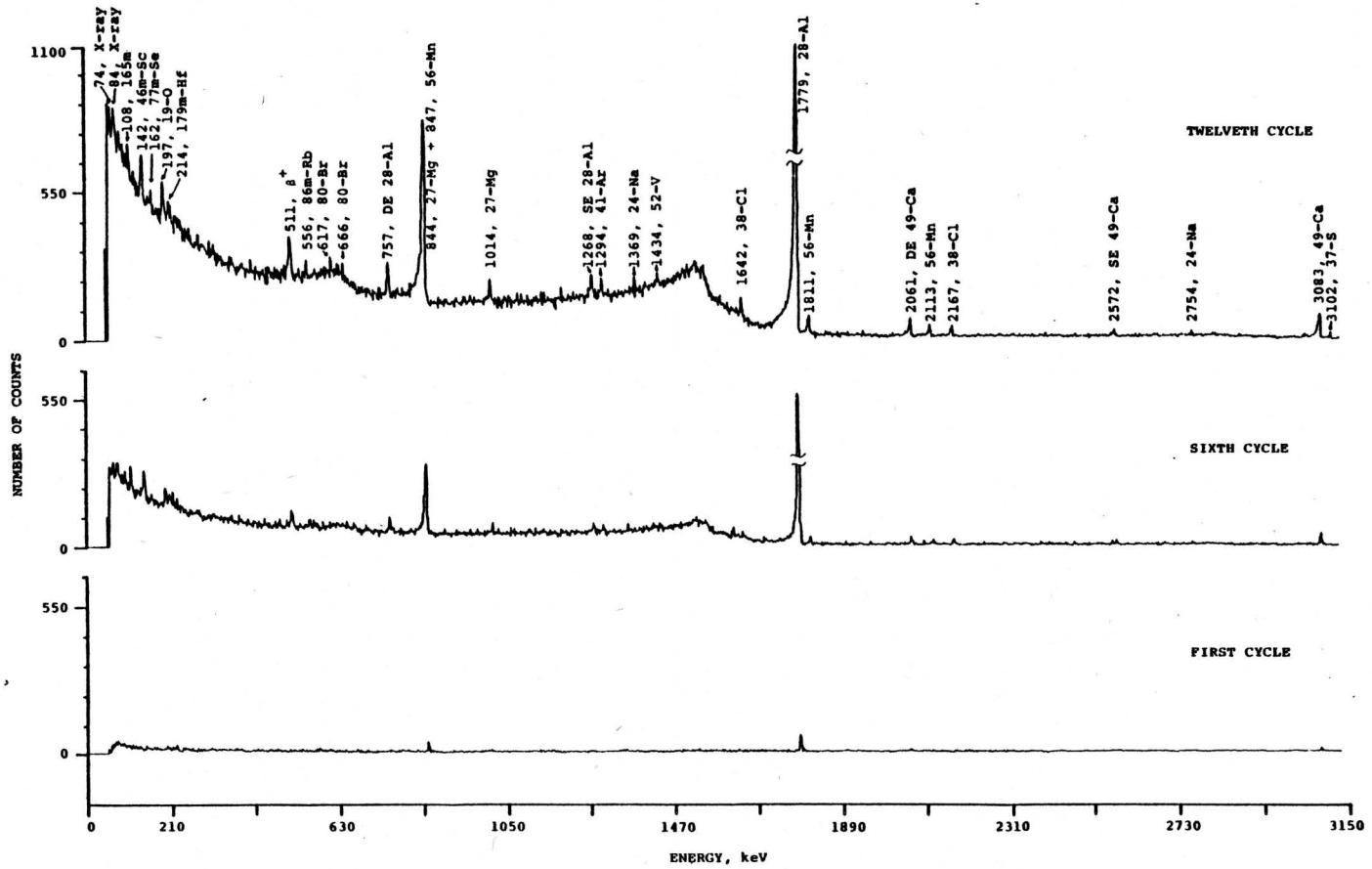

Figure VI-19. CINAA of Orchard Leaves - Gamma-ray spectrum observed at 1st, 6th and 12th cycle

^{28}Al has increased, the number of counts under the photopeaks of short- to medium-lived nuclides of interest has also increased significantly from 1st through 12th cycle leading to reliable determinations of several elements.

d. *Determination of* Pb *in SRM Urban Particulate Matter Using* ^{207m}Pb

From the results presented in section VI.D.3 for Pb by CINAA, it is clear that the sensitivity of ^{207m}Pb is not sufficient for the determination of Pb at very low concentrations in complex matrices without using a higher flux, more efficient geometry, a faster transfer system and/or increased number of cycles than that used in this work. Concentrations of Pb could not be satisfactorily determined in most SRM studied except in the Urban Particulate Matter (UPM). In spite of the severe interference from ^{28}Al activity, a satisfactory quantitative determination of Pb in UPM was made by employing $t_i = t_s = 2\ s$, $t_d = 0.7\ s$, $n = 10$ cycles.

Concentrations of Pb and Sc in UPM and Orchard Leaves, respectively, determined by CINAA are given in Table VI-19. The detection limits, L_D and L_Q, are also given for each case. The relatively high L_D and L_Q values for Pb in UPM are mainly due to small sample sizes which had to be limited to about 30-50 *mg* in order to avoid severe interference from ^{28}Al. For matrices with lower background activities, L_D and L_Q for Pb could be lowered by an order of magnitude using larger sample sizes and increasing the number of cycles.

Table VI-19. Concentrations of Pb and Sc in standard reference materials determined by CINAA

material	element	nuclide (half-life/s)	conditions $t_i/t_d/t_c$, T, n	reported value (μg/g)	this work (μg/g)	limits[c] (μg/g)	
						L_D	L_Q
Urban Particulate Matter	Pb	^{207m}Pb (0.81)	2 s/0.7 s/2 s 22 s, 10 cycles	6550±80[a]	7500±1500	7200	31000
Orchard Leaves	Sc	^{46m}Sc (18.7 s)	10 s/2 s/10 s 30 s, 12 cycles	(0.054±0.004)[b]	0.043±0.004	0.028	0.092

[a] Ref. (77N3)

[b] Ref. (80V1)

[c] see section V.F for definitions

e. *Resolution of Overlapping Gamma-Rays by CINAA*

In some instances, advantage can be taken of the rapidly decaying nature of short-lived nuclides to resolve problems encountered with interfering gamma-rays. One such example was discussed in section I.B.1 where interference caused by 657-*keV* peak of long-lived ^{76}As to the determination of Ag through 658-*keV* of short-lived ^{110}Ag is eliminated by counting the same sample at two different decay times. On the other hand, two nuclides which are mutually interfering may both have short half-lives. Under these circumstances, precise timing and proper correction methods for coincidence losses should be available in order to minimize errors in results. The automated recycle system and the correction method developed in this study were employed to solve such a problem during analysis of Urban Particulate Matter (UPM) SRM for Se and In. The 162-*keV* photopeak of ^{77m}Se ($t_{1/2}$ = 17.4 *s*) overlaps with the 164-*keV* photopeak of $^{116m2}In$ ($t_{1/2}$ = 2.16 *s*). Three samples of UPM were analysed by CINAA first using t_i = 2 *s*, t_d = 0.7 *s*, t_s = 2 *s*, and n = 10 cycles; the same set was then reanalysed using identical conditions except t_d = 10 *s*. In both cases, the cycle period was kept constant at 20 *s*. The sum-peak (162 + 164-*keV*) due to ^{77m}Se and $^{116m2}In$ nuclides was measured in all cases; the contribution from each nuclide was calculated using two simultaneous equations which incorporated appropriate correction factors for coincidence losses as given below.

The objective here is to obtain separately the number of counts corresponding to each nuclide (^{77m}Se and ^{116m2}In) from the two sum-peak areas measured at the two decay periods. If the number of counts obtained for the sum-peak at the first and the second measurement are $C(1)$ and $C(2)$, respectively, then

$$C(1) = K_i(1)\ I_o(1) + K_s(1)\ S_o(1) \qquad \text{VI-11}$$

$$C(2) = K_i(2)\ I_o(1)\ e^{-\lambda_i t} + K_s(2)\ S_o(1)\ e^{-\lambda_s t} \qquad \text{VI-12}$$

where, for In,

$I_o(1)$ = expected counts (free of losses) for the first measurement;
$K_i(1)$ = correction factor for the first measurement;
$K_i(2)$ = correction factor for the second measurement;
λ_i = decay constant

and for Se,

$S_o(1)$ = expected counts (free of losses) for the first measurement;
$K_s(1)$ = correction factor for the first measurement;
$K_s(2)$ = correction factor for the second measurement;
λ_s = decay constant.

From the above equations VI-11 and VI-12, the following expressions for $I_o(1)$ and $S_o(1)$ can be derived.

$$I_o(1) = \frac{C(1)\ K_s(2)\ e^{-\lambda_s t} - C(2)\ K_s(1)}{K_i(1)\ K_s(2)\ e^{-\lambda_s t} - K_i(2)\ K_s(1)\ e^{-\lambda_i t}} \qquad \text{VI-13}$$

$$S_o(1) = \frac{C(2)\ K_i(1) - C(1)\ K_i(2)\ e^{-\lambda_i t}}{K_i(1)\ K_s(2)\ e^{-\lambda_s t} - K_i(2)\ K_s(1)\ e^{-\lambda_i t}} \qquad \text{VI-14}$$

The values of $I_o(1)$, $S_o(1)$ and the corresponding comparator standards were used to calculate the concentrations.

The variation of the relative activities of the two nuclides calculated from the observed difference in intensity for the first two cycles are shown in Fig. IV-20. It is evident from the figure that at a decay time of 0.7 *s*, the major activity is due to ^{116m_2}In whereas the activity of ^{77m}Se becomes predominant after a 10 *s* decay. It should be noted here that the 2 *s* irradiation and counting times used were originally selected for determination of Pb in the same analysis. It is apparent (Fig. VI-20) that better timing parameters for Se and In can be selected for improved results. The measured concentration of the two elements are given in Table VI-20. Although concentrations were calculated using two simultaneous equations, precision obtained for the two values is quite good. The agreement of the measured values with the (noncertified) values supplied by the NBS is also generally good. The gamma-ray spectra recorded after two decay times are shown in Fig. VI-21.

This method can be satisfactorily applied to resolve several

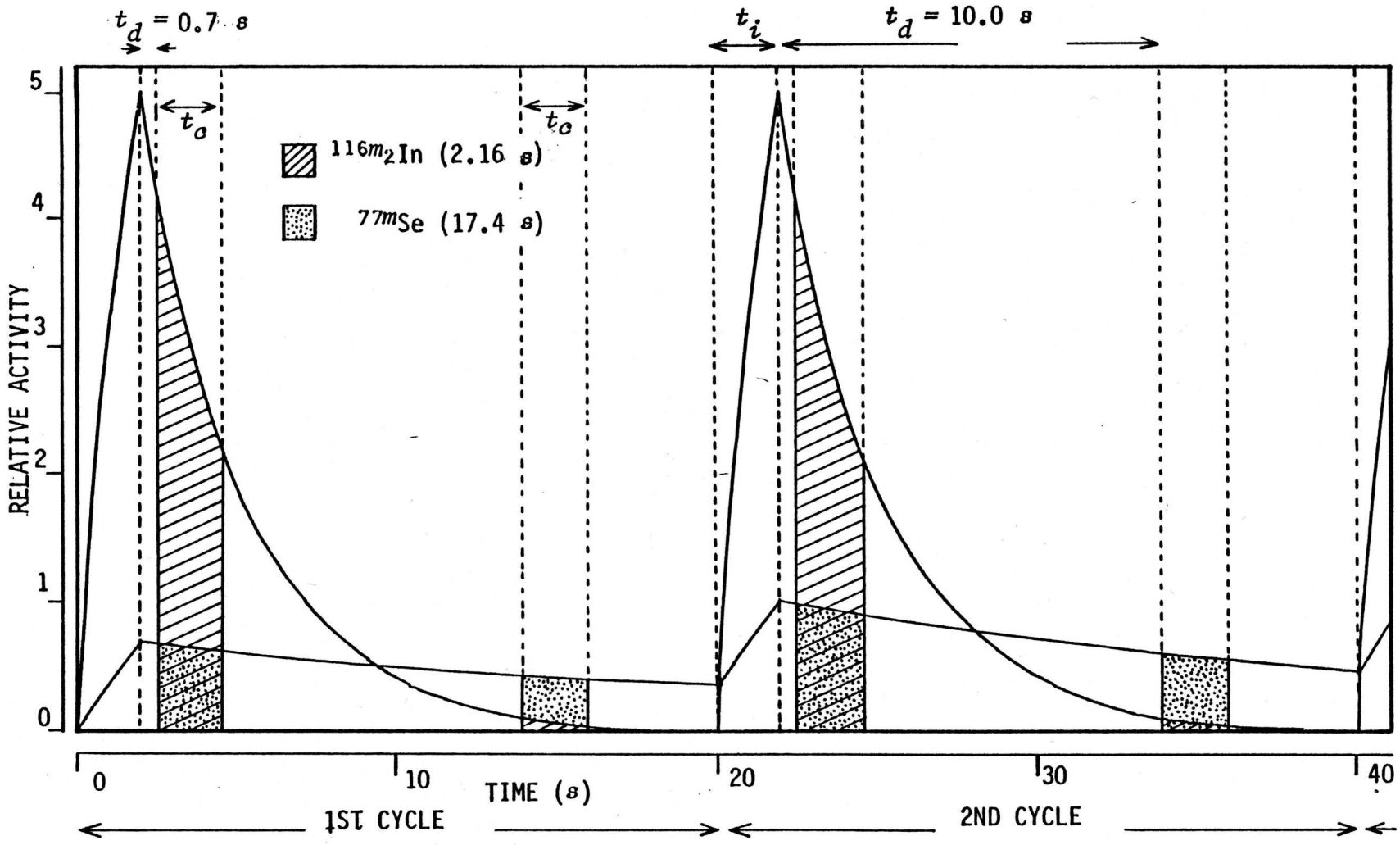

Figure VI-20. Variation of the relative activities of ^{116m_2}In and ^{77m}Se during CINAA of Urban Particulate Matter Standard Reference Material

Table VI-20. Indium and selenium content of Urban Particulate Matter determined in CINAA by discrimination of half-lives (t_i = t_s = 2 s, t_d = 0.7 s and 10.0 s, T = 20 s, 10 cycles)

element	nuclide	half-life (s)	elemental content[a] ($\mu g/g$)	
			measured	non-certified[b]
In	^{116m_2}In	2.16	1.05±0.08	(1.0)
Se	^{77m}Se	17.4	28±1	(24)

[a] average of three determinations

[b] Ref. (77N3)

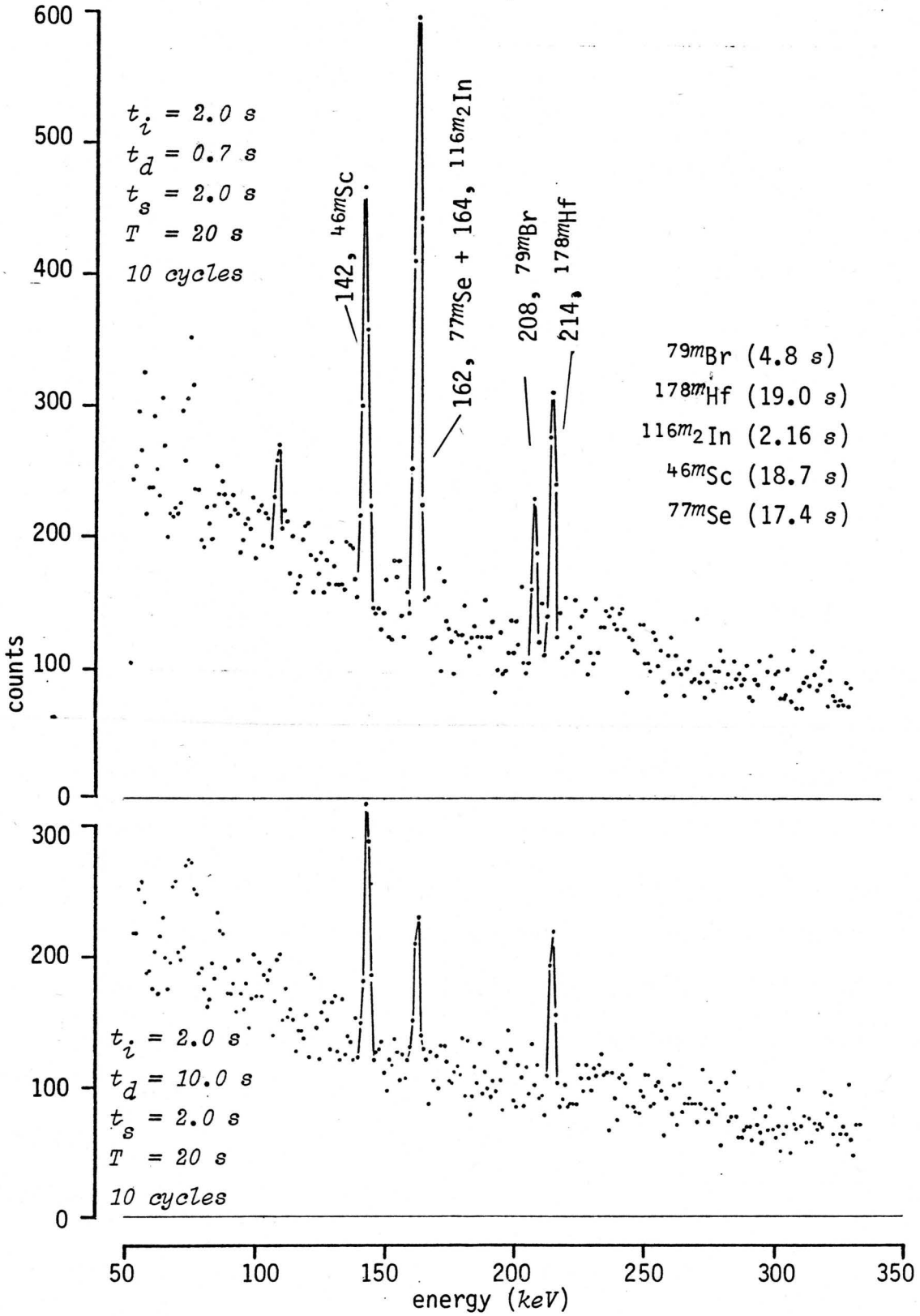

Figure VI-21. CINAA of Urban Particulate Matter - Gamma-ray spectra recorded after two different decay times

other short-lived nuclides with overlapping gamma-ray energies. Other examples of this type include the overlap of 108 *keV* gamma-ray of ^{183m}W ($t_{1/2}$ = 5.3 *s*) with ^{165m}Dy (78 *s*) and that of 208 *keV* gamma-ray of ^{167m}Er (2.3 *s*) with ^{79m}Br (4.8 *s*). The success of this method of activity discrimination depends, on the one hand upon the relative magnitudes of the half-lives (larger the difference in half-lives better is the result) and on the other, upon the difference in intensities of gamma-rays (better results are obtained with comparable intensities).

f. *Detection Sensitivities for Several Short-Lived Nuclides by CINAA*

Recently, a few tabulations (75G1, 71N1) of the nuclear data for over 100 gamma emitting nuclides with half-lives ranging from milliseconds to one minute have been made available. The sensitivities for several of these nuclides were measured in this study and are given in Table VI-21 for information purposes. Depending on the half-life of the nuclide of interest and the matrix, detection sensitivities can be further improved by optimizing timing parameters and the number of cycles.

Table VI-21. Detection sensitivities for selected short-lived nuclides (ϕ = 1x10^{12} *n cm*$^{-2}$ *s*$^{-1}$, $t_i = t_s$ = 3 *s*, T = 10 *s*; = 10 cycles)

element	product nuclide	half-life (*s*)	gamma-energy (*keV*)	sensitivity (counts/μg)
Au	^{197m}Au	7.2	279	1.59x10^{0}
Br	^{79m}Br	4.8	208	3.88x10^{1}
Cl	^{38m}Cl	0.72	671	3.68x10^{1}
Dy	^{165m}Dy	78	108	4.70x10^{3}
Er	^{167m}Er	2.3	208	1.64x10^{5}
F	^{20}F	11.2	1633	4.80x10^{0}
	^{19}O	29.1	197	9.30x10^{-1}
Ge	^{75m}Ge	47.7	160	2.16x10^{1}
In	^{116m_2}In	2.16	164	5.76x10^{4}
Pb	^{207m}Pb	0.81	570	4.56x10^{-1}
Pd	^{107m}Pd	21.3	188	7.90x10^{1}
Sc	^{46m}Sc	18.7	142	1.12x10^{4}
Se	^{77m}Se	17.4	162	1.08x10^{3}
W	^{183m}W	5.3	59	7.54x10^{1}
			108	2.88x10^{1}
Y	^{89m}Y	16.1	909	6.40x10^{0}

E. Extension of the Correction Method to Medium-Lived Nuclides

It has been pointed out in section III.C.1. that as long as the half-life of the nuclide of interest is small in comparison to the counting time (irrespective of the absolute magnitude of the half-life), significant errors can occur due to inadequate correction for the dead-time even when counting is performed in the live-time mode. In multielement INAA using medium-lived nuclides, it may sometimes be necessary to count a sample for periods several times longer than the half-lives of some medium-lived nuclides. This situation arises when statistically significant number of counts are needed for the relatively long-lived nuclides. Furthermore, total activity of the sample can vary during the counting period. If the sample activity is high pile-up losses also become significant. Since the problem is similar to the case of short-lived nuclides, except for the fact that duration of the measurement is longer, the correction method developed here can be applied to medium-lived nuclides as well. However, a slight modification of the electronics would be necessary depending on the capability of the analyser used for multichannel scaling of R_s and DT.

Since the counting time for medium-lived nuclides can extend up to several minutes, multichannel scaling (MCS) procedure used for short-lived nuclides to record R_s and DT will encounter the following difficulties. If the scaling time is set in the order of milliseconds, as done in the case of short-lived nuclides, the number of channels

needed for MCS will be excessively large. For example, for a set scaling time of 0.1 *s* (as used before) and a counting period of 10 *min*, the MCS will require 6000 channels. Then one analysis would require mathematical treatment of 6000 data points. The use of a larger scaling time may appear as a solution to this problem. For example, the use of a 10 *s* scaling time would reduce the required number of channels to 60. However, this reduction would result in a memory overflow of the MCS because the analyser now has to store a 100 times larger number (than that obtained using 0.1 *s* scaling time) in one memory channel. In order to solve this problem, if one uses an oscillator frequency much lower than 5 *MHz* (used for short-lived nuclides) then the measured dead-time will be underestimated due to considerably large width of the low-frequency pulses (see Fig. III-7 for an explanation of a similar problem). Two approaches are proposed below to eliminate the above discussed problem.

1. Use of a Frequency Divider

Oscillator pulses coming out of the gate enabled by the dead-time signal (as previously described in Fig. IV-1) can be divided by a desired factor using a suitable frequency divider before feeding into the MCS. Then one can use considerably large scaling times without having a memory overflow. This procedure is described in Fig. VI-22. However, depending on the particular multichannel scaler, even this procedure may be insufficient to reduce the number of data points if the maximum available scaling time is small. To circumvent such a

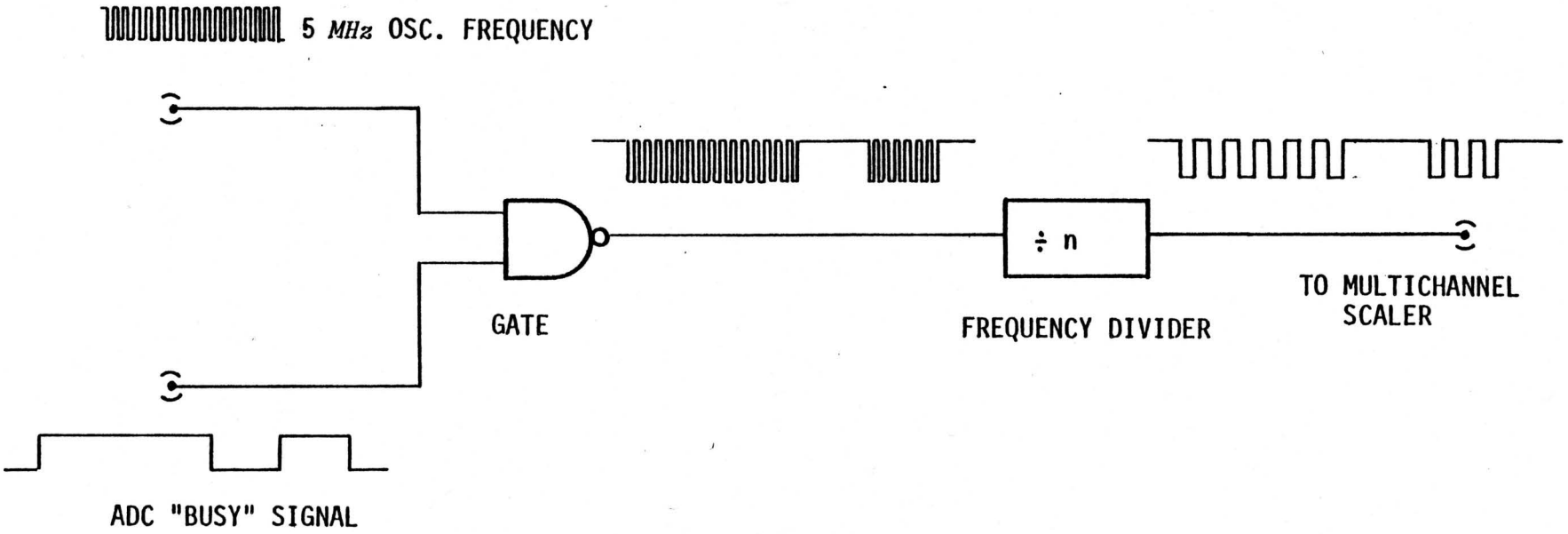

Figure VI-22. Use of a frequency divider to avoid memory overflow of the multichannel scaler

situation, an alternative approach is described below.

2. Periodically Interrupted Sampling

In this approach without carrying out the MCS sampling procedure continuously, it is electronically interrupted at a regular frequency so that MCS data are recorded only for selected sampling times at suitable intervals. The principle of the operation can be clearly seen from Fig. VI-23. A simple electronic circuit used for the above procedure is similar in principle to that is given in Appendix E.

Choice between the two methods depends on the nature of the particular problem, the range of scaling time and the number of channels available in the multichannel scaler. In some cases use of both methods may be desirable. The above procedures were used to make correction for coincidence losses during analysis of fly-ash and air particulates where dead-time varied from 25% to 8% during counting intervals of 10 *min* due to the activities of mainly ^{28}Al and ^{52}V.

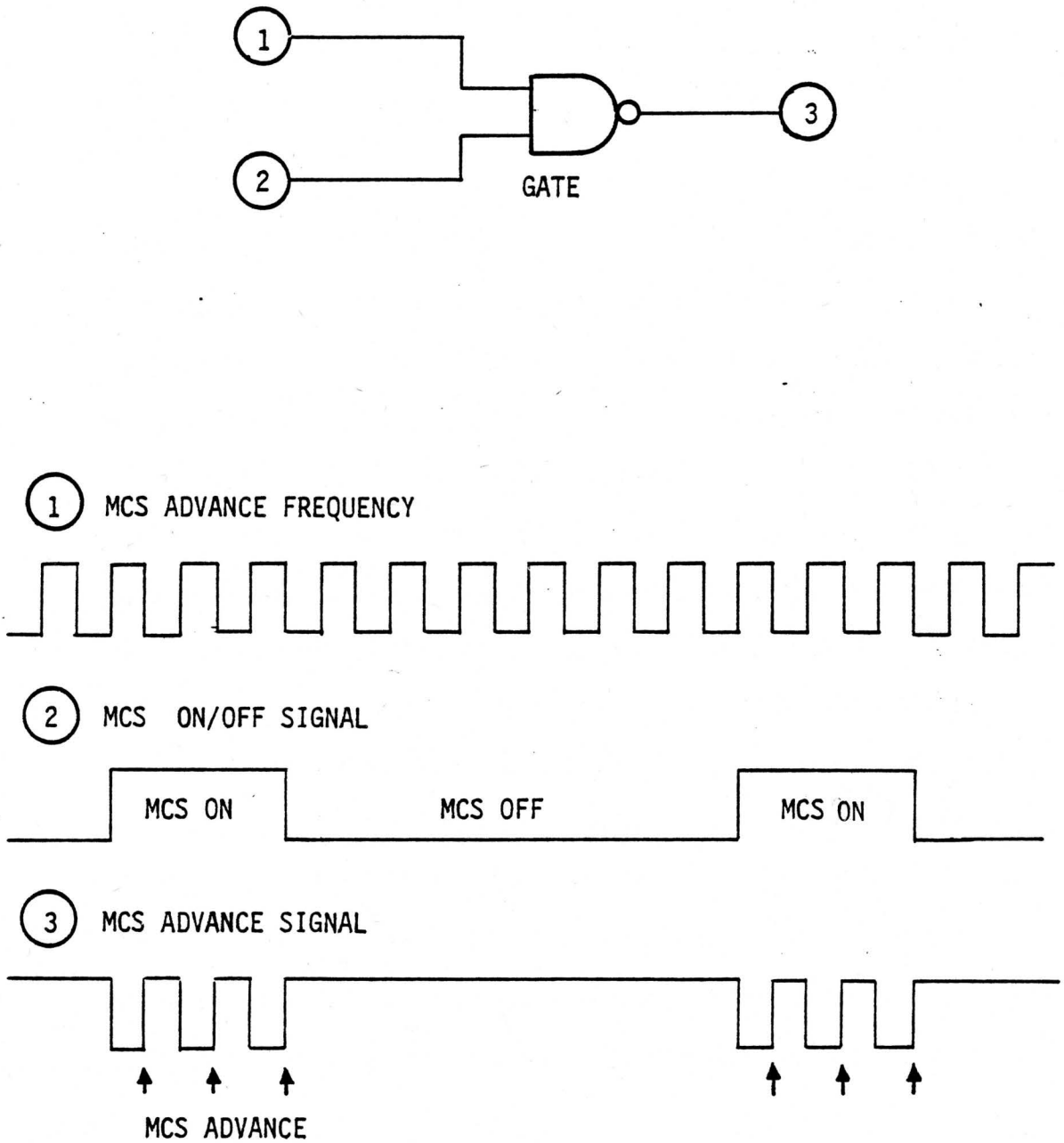

Figure VI-23. Multichannel scaling procedure with interrupted sampling

F. Epithermal Instrumental Neutron Activation Analysis

1. Development of a Thermal Neutron Shield

a. *Selection of a Suitable Boron Material*

Since short decay times are involved in detecting short-lived nuclides, the sample has to be counted along with the shield and hence the shield material has to be considerably pure to minimize corrections for blanks. The purity of several boron compounds, which are available as crystalline or amorphous powders, was examined by irradiating approximately 0.8 *g* of each material under several irradiation and counting times ranging from 10 *s* to 10 *min*. In most cases, no detectable peaks for short-lived nuclides were observed. However, small peaks of several medium-lived nuclides were detected. In order to determine the absolute concentration of each contaminant, conventional procedures cannot be used due to unknown composition and magnitude of the effective flux arising from the thermal neutron absorption by the sample itself. For comparison purposes, results were calculated in arbitrary concentration units and are summarized in Table VI-22. Both boron nitride and boron carbide were observed to be pure enough for fabricating shields to be used in the studies of short-lived nuclides.

b. *Selection of a Binder*

Most high purity boron compounds are generally available in powder form; it is difficult to fabricate rigid and reproducible

Table VI-22. Relative purity of boron compounds

compound	content, in arbitrary units						
	Br	Co	Mn	Ta	Ti	V	W
Boron Carbide	n.d.	20	2.8	n.d.	1.2	130	3.9
Boron Nitride #1	n.d.	175	3.8	n.d.	1.5	6.5	4.6
Boron Nitride #2	1	250	1.7	n.d.	3.5	35	55
Boron Nitride #3	n.d.	1	n.d.	n.d.	2.6	16	1
Boron Nitride #4	n.d.	15	13	1.5	1	1	1
Boron Nitride #5	1.1	5	1	n.d.	n.d.	1.9	n.d.
Borno Nitride #6	n.d.	1.5	n.d.	1	n.d.	3.5	n.d.
Enriched Boron	1.7	3060	22	1790	160	6.7	205

shields from such materials. First an attempt was made by pouring a mixture of boron compounds and melted paraffin into an irradiation vial while keeping a polythene or a glass rod in the middle of the vial to make a hole in the centre for the sample. After solidification, the rod placed at the centre was carefully taken out. This design had to be later discarded due to several drawbacks. The shields were not reusable as they could not be transferred from one irradiation vial to another. Therefore, standards and the sample could not be irradiated using the same shield (if this was possible, problems due to irreproducibility of making the shield with similar characteristics could be partially avoided). On several occasions the shield was broken during cyclic irradiation. Furthermore, the boron-to-paraffin ratio had to be restricted in order to avoid excessive fragility.

Another attempt was made by placing boron powder in between two polythene tubes. However, due to small inner diameter ($\simeq$1.3 *cm*) of the irradiaton vials used in the inner sites (irradiations at the inner sites were of prime interest due to considerably higher epithermal flux than that in the outer sites), this attempt was not particularly suitable. Impregnation of boron powder into melted polythene and then fabrication of the shield by machining the solidified material was also not successful due to low obtainable boron density, non-uniformity and contamination of the material during machining by tungsten carbide tools.

Polymerization of a hydrocarbon in the presence of boron compounds was considered to produce a rigid and suitable shield. One can use unsaturated hydrocarbon monomers such as isoprene and styrene. Considering the physical properties, styrene was selected for polymerization and this attempt was found to be successful.

c. *Polymerization*

Benzoyl peroxide was used as the free radical initiator for polymerization of styrene. However, normal polymerization procedures available in the literature (69R1) involves heating freshly distilled styrene-initiator mixture in a water bath to initiate the reaction, and subsequently allowing the mixture to polymerize at room temperature. Preliminary work carried out in test tubes, using a prescribed procedure indicated that without heating, the mixture (styrene, initiator and boron) did not solidify even after several days (generally, polymerization was observed to be much slower in the presence of boron compared to liquid styrene alone). Heating until the mixture became fairly thick resulted in the formation of cavities in the solid. Furthermore, when the polymerization is carried out inside a mould, heating on a water bath is not readily feasible.

In order to circumvent the above mentioned inconveniences, it was decided to carry out the reaction inside a thermostatted oven. After numerous experiments done at various temperatures, it was observed that an optimum temperature range of 60-70 ^{o}C was best suited for

the reaction to proceed at a reasonable rate without the formation of cavities. Generally, solidification of the mixture was achieved in 1 - 2 days.

d. *Design of a Mould*

A number of moulds was designed, fabricated, and tested in this work using different parts made of either glass, combination of glass and Teflon, or Teflon alone. Three designs, among several tested are shown in Fig. VI-24. Some problems were encountered with designs A and B (Fig. VI-24). The design of the mould A was such that the lid with the central rod (for making space for the sample) had to be tightly closed while the mixture (of styrene and boron) was still fairly thin, and then heated until the polymer solidified. With this approach it was difficult to avoid formation of cavities in the shield, perhaps due to gradual evaporation and change in specific volume of the medium during polymerization. Therefore, for the elimination of cavities, it was expected that closing the mould after polymerization is nearly complete, would provide a solution. Hence, another design was attempted by making the central rod a part of the base (mould B). The mixture was heated until it became fairly thick and then the top cap was placed tightly on the mould. Although no cavities were formed with this design, it was not possible to take out the polymerized shield from the mould without breaking either the glass mould or the shield due to the inelasticity of glass. To eliminate this problem with glass, the mould B was superseded by the mould C

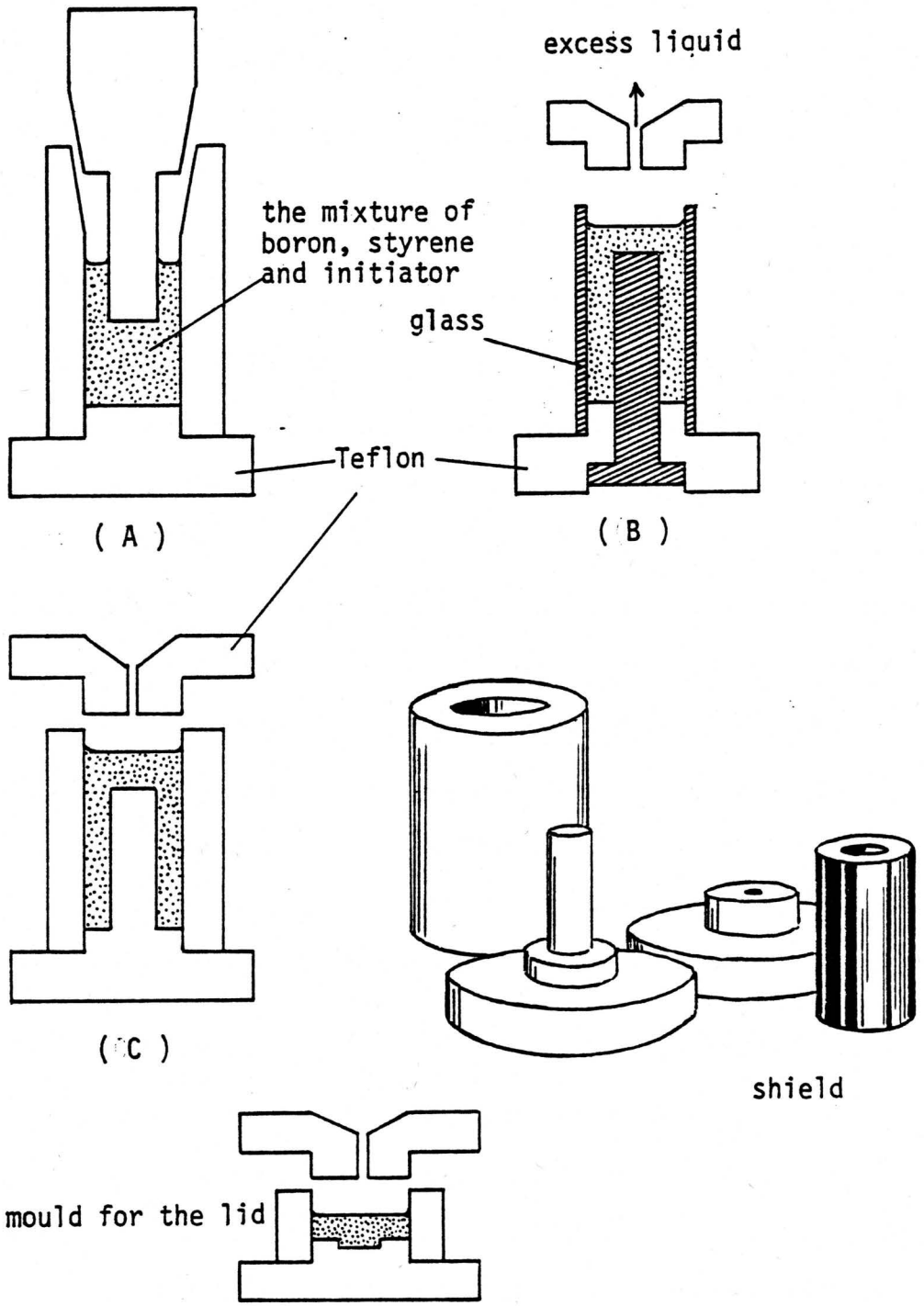

Figure VI-24. Moulds for the boron shield

(Fig. VI-24) which was entirely made of high-density Teflon and was found to be successful. By exposing the constructed boron shield using mould C to a saturated vapor of styrene monomer in a closed container at 60-70 ^{o}C, a smooth (both external and internal) finish was obtained.

2. Performance

With the design described above, the density of boron in the shield could be attained almost as high as the apparent density of boron in the powder. The thickness of the boron shield can be varied easily by changing the diameter of the central rod in the mould. In addition, high rigidity of the shield made the reduction of its wall thickness feasible down to a few millimeters for placing relatively large amounts of sample in the very limited space available, even in a small irradiation vial. This is particularly useful in the DUSR facility where the diameter of the normal irradiation vial is small (medium-size, 1.3 cm). By varying the thickness of the boron shield one could select a desired cut-off energy for neutrons.

Shields of three different thicknesses were made to study the effective thermal neutron shielding properties using uranium and vanadium. The standards containing 1 μg of uranium and 50 μg of vanadium were irradiated in these three shields and counted under similar conditions. Uranium and vanadium were selected because U has a high advantage factor (I/σ_{th} = 103) and V has a low advantage

factor (I/σ_{th} = 0.55) for epithermal neutrons. In addition, the extent of suppression of activity of ^{52}V was of interest in analysing oil and coal fly-ash containing large amounts of vanadium.

The effect of shield thickness on advantage factors for uranium with respect to vanadium is summarized in Table VI-23. The relative standard deviation of the measured activities of uranium and vanadium is less than 4% whereas that for the calculated advantage factor (in the worst case) is about 7%. Since the advantage factor is the final result calculated from 4 independent measurements a significant contribution to this deviation can come from counting statistics. Therefore, it is fair to state that the reproducibility of the composition of the flux obtained by using independently made shields of the same thickness is excellent. It should be noted (Table VI-23) that a little sacrifice of the advantage factor is necessary for obtaining a larger volume for sample inside the shield.

The variation of the advantage factor with the wall thickness is graphically shown in Fig. VI-25. Although a definitive conclusion cannot be made about the shape of the curve at wall thicknesses lower than 0.2 *cm* (the minimum wall thickness used), it appears that increasing the wall thickness beyond 0.4 *cm* might not be advantageous for the particular boron density (54% w/v) used. Nevertheless, increasing the wall thickness beyond 0.35 *cm* is not practical for shields made for the inner irradiation sites of the DUSR because of lack of space for the

Table VI-23. Effect of wall thickness of boron shield on advantage factor ($^{239}U/^{52}V$)

wall thickness[a] (cm)	sample capacity[b] of the shield (cm^3)	activity (A_o), cps/μg								advantage factor
		vanadium				uranium				
		shield 1	shield 2	shield 3	average	shield 1	shield 2	shield 3	average	$^{239}U/^{52}V$
0.0	3.05	194	210	215	206±11	840	804	824	823±18	1.00
0.25	1.16	6.05	5.93	6.22	6.07±0.15	550	543	569	554±14	22.84±1.5
0.30	0.885	4.57	4.69	4.82	4.69±0.13	520	538	530	529±9	28.23±1.9
0.35	0.650	3.97	3.73	3.75	3.82±0.13	490	470	465	475±13	31.12±2.3

[a] density of boron in the shield material = 54% w/v basis (g/cm^3)

[b] assuming the height of the cylindrical hole = 2.3 cm (≈ half of the height of the irradiation vial)

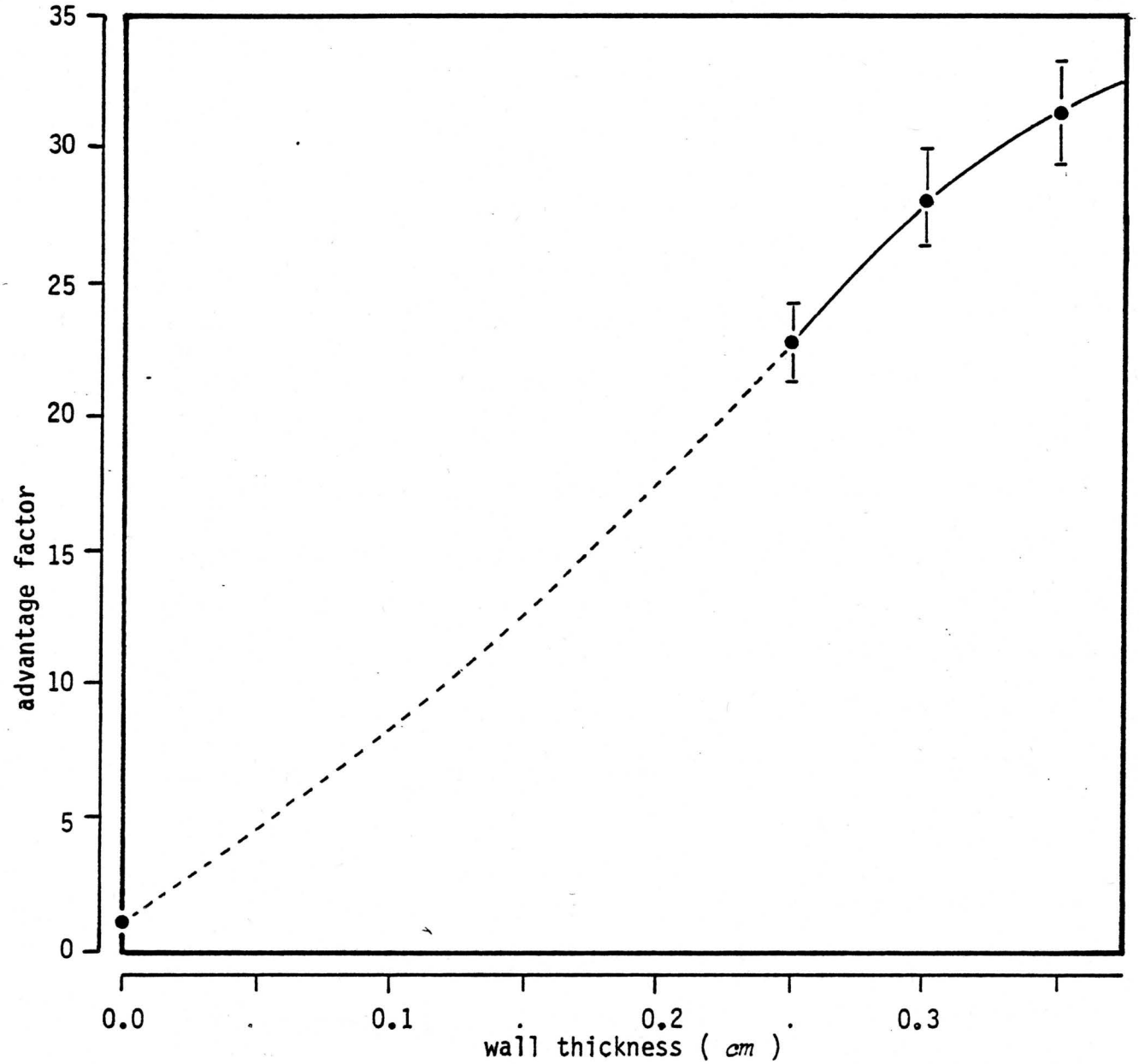

Figure VI-25. Variation of advantage factor of ^{239}U relative to ^{52}V with wall thickness of the boron shield

sample. However, the above observation becomes important in making larger shields, *e.g.* shields for outer sites of the DUSR (diameter ≃ 2.8 *cm*).

3. Applications

The developed boron shields were found to be very useful for the determination of several short- and medium-lived nuclides by EINAA. Owing to their high rigidity these shields can even be used in cyclic activations for the detection of short-lived nuclides without encountering any physical damage. In addition, even for medium- and long-lived nuclides the boron shields can be advantageously used over conventional Cd foils. Compared to Cd foils, since the boron shields themselves do not produce any appreciable radioactivity, they can be used for successive irradiations in a single day without any radiation hazard. The possibility of reusage of shields will provide an economical advantage over Cd foils when routine analyses involving a large number of samples are carried out.

If the samples are not wrapped properly with Cd foils, due to possible leakage of thermal neutrons, the effective composition of the neutron flux can vary from sample to sample, sample to standard and standard to standard. However, with the present design of the boron shields, such leaks are minimal, if any at all. Even if there is any leakage, the same neutron flux composition can be attained for each irradiation by using either the same shield or an identical

shield.

During EINAA with Cd foils, it is necessary to wash the sample thoroughly with acid before counting,for removing surface contamination by radio-cadmium, unless other special precautions are taken. The use of boron shields eliminates the above problem. In fact, if the shield is contaminated, it can be washed with aqueous solutions (but not with organic solvents) and reused. This is particularly useful in cyclic activation where the sample is counted along with the shield.

These boron shields were advantageously applied to EINAA of several environmental materials such as coal fly ash, oil fly ash and geological materials which are difficult to be analysed by conventional thermal neutron irradiations. Elemental concentrations determined through short-lived nuclides of a typical sample of coal fly ash collected from a local power plant are given in Table VI-24. It should be noted that the thermal neutron irradiations (*i.e.* without the shield) of these samples produced such high activities that no photopeaks other than those of interfering nuclides such as ^{28}Al and ^{52}V can be detected. The same coal fly ash samples were also analysed for other elements using medium-lived nuclides produced by irradiations of 10 - 15 *min* in the shield. Table VI-25 shows the advantage factors of several nuclides - short- and medium-lived - calculated relative to major interfering elements. The two gamma-ray spectra obtained by thermal and epithermal INAA of the same coal fly ash sample are shown

Table VI-24. Elemental content of a coal fly ash sample measured via short-lived nuclides by EINAA using a boron shield (t_i = 10 s, t_d = 10 s, t_s = 30 s)

element	nuclide	half-life (s)	gamma-ray energy (keV)	concentration (μg/g)	limits (μg/g)	
					L_D	L_Q
Ag	^{110}Ag	24.4	658	<29	29	102
Dy	^{165m}Dy	76	108	14.	4.3	12
Hf	^{179m}Hf	18.6	214	8.2	0.5	1.8
Rb	^{86m}Rb	62	556	160	140	540
Sc	^{46m}Sc	18.7	142	45	8	26
Se	^{77m}Se	17.4	162	<60	60	180

Table VI-25. Advantage factors for several nuclides under a boron shield[a]

nuclide	half-life	gamma-ray energy (*keV*)	Advantage factors relative to		
			^{52}V	^{28}Al	^{24}Na
^{110}Ag	20 *s*	658	9.6	7.5	4.5
^{76}As	26.8 *h*	559	17	14	8.2
^{20}F	11.2 *s*	1633	7.2	5.7	3.4
$^{116m_1}In$	54 *m*	417	8.6	6.9	4.1
^{56}Mn	2.58 *h*	847	2.0	1.6	0.94
^{86m}Rb	62 *s*	556	10	8.1	4.8
^{155}Sm	22 *m*	104	10	8.3	5.0
^{87m}Sr	2.8 *h*	388	10	8.1	4.9
^{239}U	23.5 *m*	74	28	24	14

[a]shield thickness = 0.3 *cm*, density of boron in the shield = 54% *w/v*

in Fig. VI-26. Although the irradiation time is 1 *min* for thermal neutron irradiation (compared to 15 *min* irradiation with the shield), the major interfering activity due to ^{52}V is much higher than that obtained by epithermal neutron irradiation. Photopeaks due to several other nuclides can be seen in the gamma-ray spectrum (Fig. VI-26) obtained by EINAA.

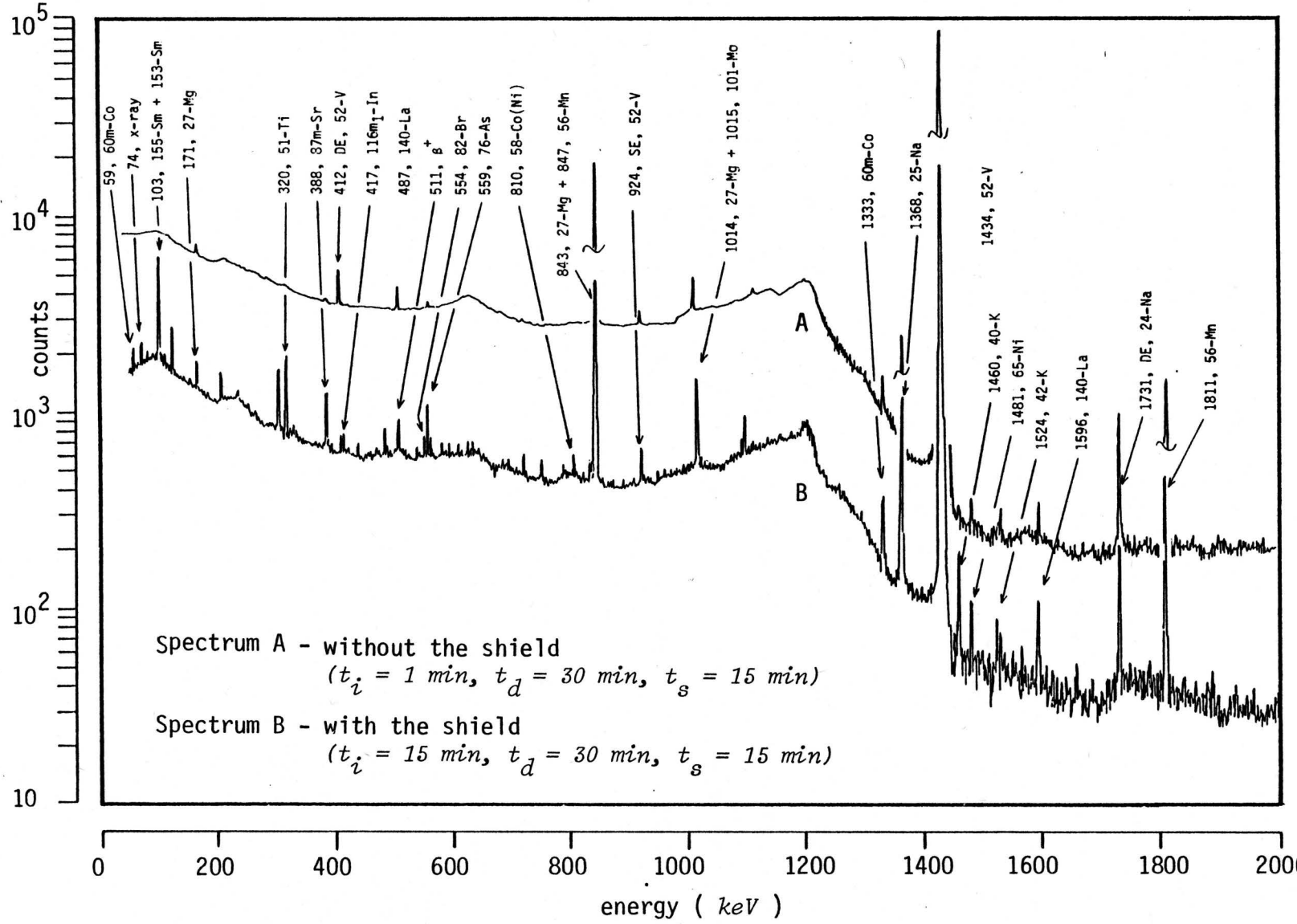

Figure VI-26. Gamma-ray spectra of a coal fly ash sample recorded after irradiation with thermal and boron-filtered neutons

G. Analysis of Biological and Environmental Materials

The INAA methods developed and described in this thesis were applied to analyse several biological and environmental materials of interest. Following CINAA of short-lived nuclides, the same samples were counted for a longer time to determine several other medium-lived nuclides. In some cases, the sensitivities of medium-lived nuclides were sufficient for their simultaneous measurement during CINAA. In addition, same samples were irradiated for several minutes to hours in order to measure elemental concentrations via other medium- and long-lived nuclides. These INAA methods were successfully applied to multielement analysis of size-fractionated oil fly ash and atmospheric particulate matter collected from the Halifax area, and to several other matrices. Elemental contents of few such matrices are given in Tables VI-26 and VI-27.

A human hair sample (IAEA Intercomparison Run, HH-1,1980) supplied by the International Atomic Energy Agency, Vienna, was analysed for certification purposes. Concentrations of several elements were determined using a combination of several INAA methods developed in this work. Results are given in Table VI-28 along with the non-certified interim values tabulated by the IAEA. The agreement between the measured value and the IAEA value is generally good indicating the reliability of the methods developed.

Table VI-26. Elemental content of oil fly-ash and bottom-ash collected from a power plant in Halifax area.

element	concentration range[a,b]	
	fly-ash	bottom-ash
As	29-830	4.1-8.2
Co	280-2140	340-410
Cr	32-870	1800-2090
Fe	9%-51%	3.9%-4.3%
Hg	n.d.-122	4.5-45
La	304-11%	450-640
Mn	1.6%-15%	1.0%-1.6%
Ni	5.3%-29%	6.2%-7.5%
Sb	2.4-67	n.d.
Sc	0.2-1.2	1.4-2.2
Sm	11-2500	17-25
V	41%-72%	11%-15%
Zn	0.1%-1.2%	170-260

[a] $\mu g/g$ unless otherwise mentioned

[b] range is given for 10 independent samples in each case

Table VI-27. Elemental content of an aerosol sample collected from the Halifax area

element	concentration[a]	element	concentration[a]
Al	860	In	0.011
As	2.2	K	270
Au	0.0022	La	1.5
Ba	15	Lu	0.025
Br	31	Mg	220
Ca	250	Mn	3.3
Ce	4.7	Na	880
Cl	280	Ni	11
Co	0.32	Rb	1.8
Cr	2.2	Sb	0.030
Cs	0.07	Sc	0.085
Cu	411	Se	1.2
Dy	2.3	Sm	0.12
Eu	0.04	Sr	3.2
Fe	460	Ti	26
Hf	0.060	V	28
Hg	0.077	Zn	11
I	0.57		

[a] concentration are given in ng/m^3

Table VI-28. Elemental content of a human hair sample (IAEA Intercomparison Run, HH-1, 1980)

element	concentration[a]	
	this work	overall mean of accepted laboratory averages[b]
Ag	0.16±0.04	...
Al	6.5±0.5	6.78±2.52
As	0.054±0.003	0.05±0.02
Au	0.016±0.004	0.02±0.00
Ba	4.7±2.5	0.38±0.22
Br	3.80±0.02	4.08±2.23
Ca	540±20	544.13±150.91
Cl	2000±50	2129.83±304.23
Co	5.87±0.13	5.88±1.32
Cr	<2	0.38±0.18
Cu	8.5±1.2	10.57±3.34
F	900±85	...
Fe	< 35	23.89±10.30
Hg	1.77±0.04	1.69±0.25
I	24.0±0.7	20.20±6.97
K	10±1	7.13±1.45
Mg	81±34	59.99±10.14
Mn	0.85±0.25	0.89±0.25
Na	23.5±0.6	12.41±2.55
S(%)	4.2±0.1	5.14±1.23
Sb	0.026±0.001	0.04±0.02
Sc	< 0.002	...
Se	0.29±0.05	0.34±0.05
V	0.045- < 0.032	...
Zn	177±2	171.47±25.97

[a] $\mu g/g$ unless otherwise mentioned

[b] ref. (80I2)

CHAPTER VII

CONCLUSIONS AND RECOMMENDATIONS

The results presented in this thesis demonstrate the effects of coincidence losses on measurement of short-lived activities and the validity of the correction method developed for rapidly decaying high count rates. Short-lived nuclides with half-lives longer than 10 *s* were measured by the developed pseudo-cyclic INAA (PCINAA) method. It was shown that the PCINAA method can simultaneously determine concentrations of both short- and medium-lived nuclides. In order to improve the sensitivity further and to detect nuclides with shorter half-lives (as short as a fraction of a second) an automated rapid cyclic transfer system was designed. This system was used to develop cyclic INAA (CINAA) methods. Both PCINAA and CINAA methods with the developed correction method were found to improve precision, accuracy and detection limits. A formula was derived to correct for coincidence losses in CINAA. The proposed formula considerably simplifies the data manipulation without sacrificing the accuracy of CINAA where corrections for coincidence losses are applicable.

Much of the interferences caused by thermal neutron activation products of V, Na, Mn, Cl, Al, *etc.* were significantly reduced by the developed epithermal INAA (EINAA) method. The EINAA method is particularly useful for measuring elemental contents through short-

and medium-lived nuclides in complex sample matrices. Compared to the conventional epithermal irradiations using Cd foils, the main advantages of the developed shield are that it can be used for short-lived nuclides and can be reused almost immediately for successive irradiations with virtually no radiation hazard.

In order to realize the full potential of the methods developed, several recommendations are made in the following paragraphs.

Incorporation of a pile-up rejector into the present analyser system should considerably improve the performance of the analyser and the correction method for coincidence losses. At high count rates, when a pile-up rejector is not used, a significant portion of the pulses processed by an ADC consists of unnecessary distorted pulses. These distorted pulses introduce unnecessary additional dead-time and distort the spectrum. Furthermore, the rejector can eliminate the pulses going above the upper discriminator level due to pile-up which in turn can significantly reduce possible errors in the estimation of total output count rate of the amplifier - a term which appears in the pile-up correction equation. However, as already mentioned, for the present correction method, LLD and ULD of the ADC had to be set at minimum and maximum possible levels. In some situations, one may be interested in only a particular energy region (energy window) defined by the LLD and ULD. Then the total pulse rate at the output of the amplifier can no longer be derived from "SCA OUT" of the ADC. The proposed method can be applied to such cases by incorporating a separate

single channel analyser, connected to the output of the amplifier, which can be used to directly record the total output count rate at the amplifier. Instead of a single channel analyser, any simple electronic circuit which gives out a logic pulse for each pulse coming out of the amplifier-pile-up rejector system would serve the same purpose.

Data processing procedure can be considerably simplified if the dead-time and pulse pile-up correction procedure were directly incorporated into the minicomputer of the multichannel analyser or by including additional software to carry out multichannel scaling internally. The present system at DUSR can be modified by suitably interfacing the two analysers. Moreover, since the ADC used in this study is operated at 50 *MHz*, use of a faster ADC (typically 100 *MHz*) would improve the capability of the system. At this point, one might ask whether it serves any purpose in improving a correction method to handle unlimited high count rates. One might also ask, given a perfect correction method, whether increasing count rates would necessarily continue to improve the counting statistics. If not, what is the limit?

It should be realized that, in a radioactive measurement, the fundamental purpose of using a high count rate is to increase the number of counts accumulated in the photopeak of interest, hence to improve counting statistics. Furthermore, the final result depends only on the undistorted pulses. However, the nature of a random process is such that the probability of arrival of multiple pulses within the resolving time of the amplifier-pile-up rejector system

increases as the count rate is increased. Similarly, probability of having a single pulse decreases. Then the question is; is there an optimum count rate?

In section IV.A two expressions for the output count rate of the amplifier system have been derived depending on whether or not a pile-up rejector is used. If a pile-up rejector is used, equation IV-8 gives the pulse rate, R_a, at the output of the amplifier-pile-up rejector as:

$$R_a(\textit{with rejector}) = R_o\, e^{-R_o\tau} \qquad \text{VII-1}$$

where R_o and τ are the absolute total count rate and pulse resolving time of the amplifier-rejector system. In this case R_a corresponds to undistorted pulses only.

When a pile-up rejector is not used, an expression for R_a can be obtained from equation IV-12 (section IV.A) where the average number of pulses (including distorted pulses), N_a, coming out of the amplifier within τ is given by:

$$N_a = 1 - e^{-R_o\tau} \qquad \text{IV-12}$$

Therefore,

$$R_a(\textit{without rejector}) = N_a / \tau$$

$$= \frac{1 - e^{-R_o\tau}}{\tau} \qquad \text{VII-2}$$

Using equation VII-1 and VII-2 one can calculate the output pulse rate of the amplifier for the two cases (with and without a pile-up rejector). In Fig. VII-1, R_a for the two cases are plotted for varying input count rates R_o at different values of the pulse resolving time. It shows how the R_a values in the two cases deviate from the ideal case where $\tau = 0$. The difference in the two curves for a particular resolving time is equal to the rate of distorted pulses when the rejector is not used.

However, in both cases the rate of useful (undistorted) pulses vary with R_o according to the curve obtained for the case with a rejector (which passes through a maximum). Therefore, it is important to note that beyond the maximum value of R_a (with the rejector) one *should not* increase the total count rate R_o, as a measure of increasing sensitivity, which results in an opposite effect. For example, if a 2 μs shaping time constant of the amplifier is selected the corresponding pulse resolving time will typically be around 8 μs. Then, at an input pulse rate of about 70,000 *cps*, one can attain about 90% of the maximum attainable undistorted pulse rate (corresponds to an input count rate of about 130,000 *cps*).

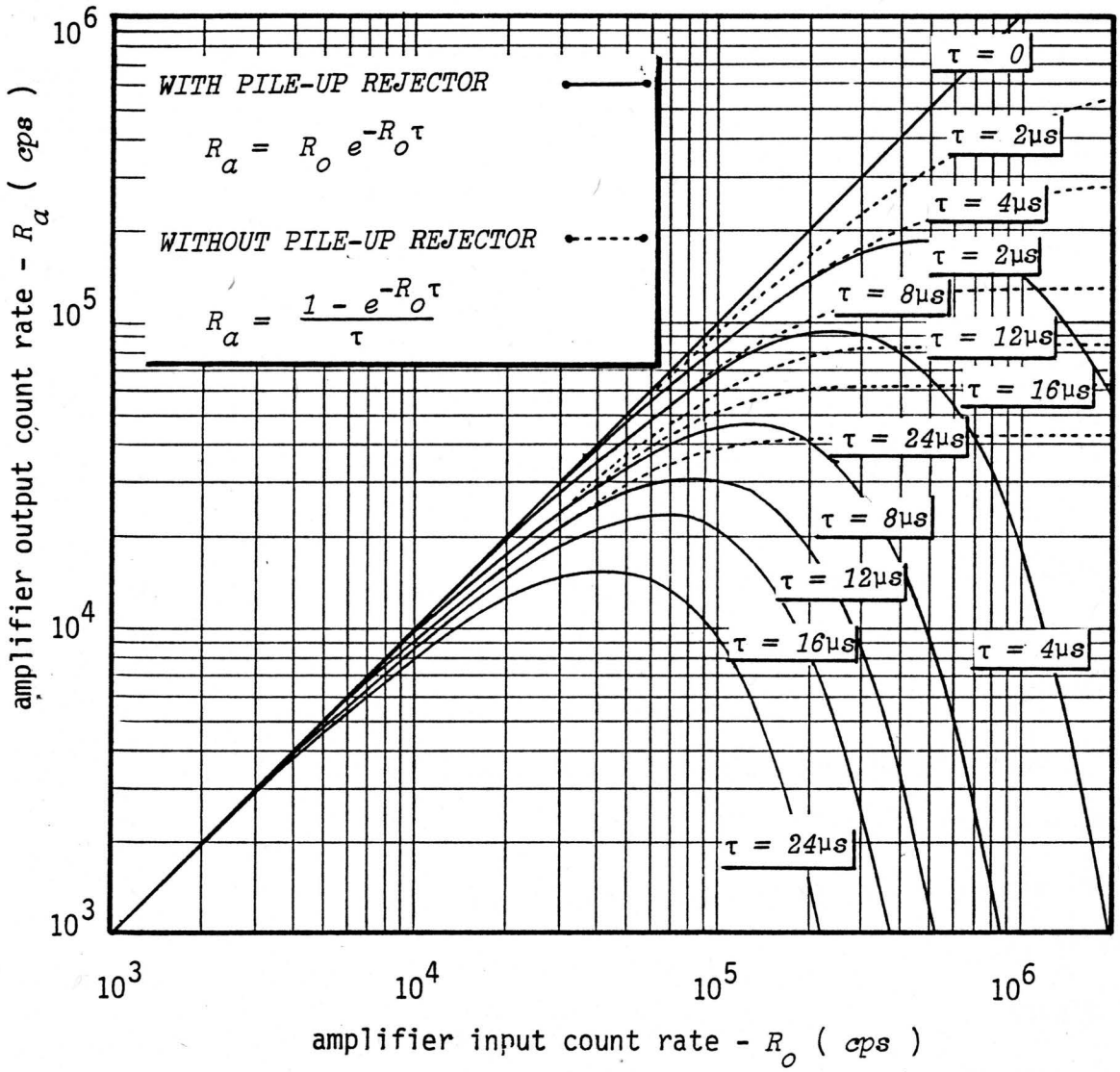

Figure VII-1. Total output count rate versus absolute total input count rate at different pulse resolving times of the amplifier

When a pile-up rejector is used, beyond the maximum region, any increase in coincidence losses will be mainly due to pulse pile-up losses and not due to the ADC dead-time. Thus, at high count rates, it is important to select an optimum pulse resolving time (typically the pulse resolving time is about four times the selected shaping time constant) and the total activity.

For the measurement of very short-lived activities, sensitivity is mainly restricted by the transfer time of the sample. A reduction of transfer time even by 0.1 *s* may yield a significant improvement of the sensitivities of very short-lived nuclides. Studies on the effect of sample weight on transfer time (section VI.C) have shown that sample weights beyond one gram have a significant effect on the transfer time of the present DUSR transfer system. This variation of sample weight was observed with a total weight of the irradiation capsule ranging from approximately 6.5 to 8.0 *g*. Therefore, it is likely that the use of smaller irradiation capsules with the same diameter may reduce the transfer time. With a simple modification (reduction of height) of the irradiation capsules currently being used at DUSR, the total capsule weight can be reduced to approximately 4.0 *g*. In addition to the reduction of the weight, shorter irradiation capsules would considerably facilitate the motion inside the pneumatic tube. From the experience gained with the present system, transfer times of samples are expected to reduce to $\simeq$ 200 *ms* with the above simple modification.

The construction procedure described for the boron shield allows one to change the composition of the shield material - hence the composition of the neutron flux - or to use any other material which can be obtained in powder form. In some cases, further thermalizing of neutrons may be of interest. For such purposes, a shield can be made by the developed procedure with a common neutron thermalizer such as graphite powder. This becomes useful in determining the contribution of interfering nuclear reactions where one nuclide is formed from two different elements: for instance, through (n,γ) and (n,p) reactions, *e.g.*, $^{27}Al(n,\gamma)^{28}Al$ and $^{28}Si(n,p)^{28}Al$. In some cases two elements are determined by measuring the difference of produced activities of a single nuclide when irradiated with thermal and epithermal neutrons. Determination of Si and Al via ^{28}Al nuclide is a typical example. Then by using the measured activities of ^{28}Al of the two analyses in two simultaneous equations Al and Si concentrations can be calculated. In such cases a neutron thermalizing shield can be used to obtain relatively epithermal neutron free conditions. This should improve the accuracy of determinations.

Finally, it is hoped that sufficient evidence has been presented to demonstrate the reliability and applicability of the INAA methods developed with an emphasis on the improvement of sensitivity of short-lived nuclides. Hopefully, the theoretical discussions, experimental results, and the suggestions, presented here will generate new applications of these methods.

REFERENCES

75A1. Al-Shahristani, H., Abbas, K., J. Radioanal. Chem., 27 (1975) 105.

60A1. Anders, O.U., Anal. Chem., 32 (1960) 1368.

61A1. Anders, O.U., Anal. Chem., 33 (1961) 1706.

69A1. Anders, O.U., Nucl. Instr. and Meth., 68 (1969) 205.

72A1. Anderson, J.L. and Spangler, G.W., J. Phys. Chem., 76 (1972) 3603.

72B1. Bartosek, J., Adams, F. and Hoste, J., Nucl. Instr. and Meth., 103 (1972) 45-47.

72B2. Bartosek, J., Masek, J., Adams, F. and Hoste, J., Nucl. Instr. and Meth., 104 (1972) 221.

72B3. Bartosek, J., Windels, G. and Hoste, J., Nucl. Instr. and Meth., 103 (1972) 43.

76B1. Becker, D.A., Proc. of Trace Substances in Environmental Health, Univ. of Missouri, Columbia, Mo., (1976).

70B1. Bolotin, H.H., Strauss, M.G. and McClure, D.A., Nucl. Instr. and Meth., 83 (1970) 1.

64B1. Brune, D. and Jirlow, K., Nuklenonik, 6 (1964) 242-244.

66C1. Caldwell, R.L., Mills, W.R., Jr., Allen, L.S., Bell, P.R. and Heath, R.L., Science, 152 (1966) 3721.

80C1. Chatt, A. and De Silva, K.N., Proceedings of the Fourth International Conference on Nuclear Methods in Environmental and Energy Research, Univ. of Missouri, Columbia, April 1980 (in press).

81C1. Chatt, A., De Silva, K.N., Holzbecher, J., Stuart, D.C., Tout, R.E. and Ryan, D.E., Can. J. Chem., (in press).

81C2. Chatt, A., De Silva, K.N. and Tout, R.E., J. Radioanal. Chem., (in press).

78C1. Chatt, A. and Katz, S.A., J. Radioanal. Chem., 46 (1978) 321-332.

74C1. Chattopadhyay, A., *Activation Studies of Toxic Heavy Metals in an Agricultural Ecosystem*, Ph.D. Thesis, Univ. of Toronto, Toronto (1974).

79C2. Chattopadhyay, A. and De Silva, K. Nimalasiri, Trans. Am. Nucl. Soc., 32 (1979) 185-186.

79C1. Chattopadhyay, A., Ellis, K.M. and De Silva, K. Nimalasiri, *Nuclear Activation Analysis in the Life Sciences, 1978*, IAEA, Vienna (1979).

74C2. Cohen, E.J., Nucl. Instr. and Meth., 121 (1974) 25-32.

60C1. Covell, D.F., Sandomire, M.M. and Eichen, M.S., Anal. Chem., 32 (1960) 1086.

70C1. Crouthamel, C.E., Adams, F. and Dams, R., *Applied Gamma-Ray Spectrometry*, 2nd Edition, Pergamon Press, Oxford, (1970) 261.

68C1. Currie, L.A., Anal. Chem., 40 (1968) 586.

32C1. Curtiss, L.F., J. Res. Nat. Bur. Stand., A8 (1932) 339.

72D1. Das, H.A. and Zonderhuis, J., Nucl. Instr. and Meth., 103 (1972) 45.

74D1. De Bruin, M., Then, S.S., Bode, P. and Korthoven, P.J.M., Nucl. Instr. and Meth., 121 (1974) 611-613.

71D1. Debertin, K., Atomkernenergie, 17 (1971) 97.

81D1. De Silva, K.N. and Chatt, A., to be published.

72D2. De Soete, D., Gijbels, R. and Hoste, J., *Neutron Activation Analysis, Vol. 34 on Chemical Analysis*, A Series of Monographs on Analytical Chemistry and Its Applications, Edited by P.J. Elving and I.M. Kolthoff, (1972).

78D1. Dryak, P., Kokta, L. and Novota, P., Radiochem. Radioanal. Lett., 32 (1978) 173-180.

76E1. Egan, A. and Spyrou, N.M., Anal. Chem., 48 (1976) 1959.

77E1. Ellis, K.M., *Multielement Neutron Activation Analysis of Suspended Matter in Estuary Water*, M.Sc. Thesis, Dalhousie Univ., Halifax (1977).

62E1. Evans, R.D., *The Atomic Nucleus*, McGraw-Hill, N.Y., (1962) Ch. 26-28.

64F1. Friedlander, G., Kennedy, J.W. and Miller, J.M., *Nuclear and Radiochemistry*, 2nd Edition, John Wiley & Sons, Inc., New York (1964).

74F1. Frigerio, N.A., Nucl. Instr. and Meth., 114 (1974) 175-177.

70G1. Givens, W.W., Mills, W.R. and Caldwell, R.L., Nucl. Instr. and Meth., 80 (1970) 95.

74G1. Gladney, E., *Trace Element Emissions of Coal Fired Power Plants: A Study of Chalk Point Electric Generating Station*, Ph.D. Thesis, Univ. of Maryland, (1974).

79G1. Gladney, E.S. and Perrin, D.R., Anal. Chem., 51 (1979) 2297-2300.

69G1. Golanski, A., J. Radioanal. Chem., 3 (1969) 161.

70G2. Gorner, W. and Hohnel, G., Nucl. Instr. and Meth., 88 (1970) 193.

70G3. Goulding, F.S. and Stone, Y., Science, 170 (1970) 280.

75G1. Grass, F., Atomkernenergie (ATKE), 25 (1975) 4.

78G1. Grass, F. and Niesner, R., Nucl. Instr. and Meth., 151 (1978) 589.

77G1. Grass, F. and Westphal, G.P., Nucl. Instr. and Meth., 140 (1977) 97.

77H1. Hanna, A.G. and Al-Shahristani, H., J. Radioanal. Chem., 37 (1977) 581-589.

67H1. Harms, J., Nucl. Instr. and Meth., 53 (1967) 192-196.

36H1. Hevesy, G. and Levi, H., Math-fys., Meddr. 14, No. 5 (1936).

74H1. Huysmans, K., Gijbels, R. and Hoste, J., J. Radioanal. Chem., 20 (1974) 51.

80I1. IAEA/RL/69, Report No. 2, *Intercomparison of Minor and Trace Elements in IAEA Animal Muscle (H-4)* (1980).

80I2. International Atomic Energy Agency, *Human Hair Intercomparison Run (HH-1)*, Interim Report (1980).

71J1. Janezyszyn, J. and Gorski, L., Radiochem. Radioanal. Lett., 8 (1971) 297.

79J1. Jones, J.D., Kaufman, P.B. and Rigot, W.L., J. Radioanal. Chem., 50 (1979) 261-275.

74J1. Junod, E., J. Radioanal. Chem., 20 (1974) 113.

80K1. Kulathilake, A.I., Ph.D. Thesis, Dalhousie Univ., Halifax, (1980).

78L1. Lederer, C.M. and Shirley, V.S., Eds., *Table of Isotopes*, Wiley Interscience, Torontom 7th Edition, (1978).

64L1. Low, K., Nucl. Instr. and Meth., 26 (1964) 216.

76M1. Miller, D., *Instrumental Neutron Activation Analysis Using Short-Lived Nuclides*, Ph.D. Thesis, Univ. of California, Irving, Ca., (1976).

76M2. Miller, D.A. and Guinn, V.P., J. Radioanal. Chem., 32 (1976) 179-188.

71N1. Nagy, A.Z., Csoke, A. and Szabo, E., J. Radioanal. Chem., 7 (1971) 365.

76N1. National Bureau of Standards, Certificate of Analysis, Standard Reference Material 1575, Pine Needles, Washington, D.C., (1976).

77N1. National Bureau of Standards, Certificate of Analysis, Standard Reference Material 1577, Bovine Liver, Washington, D.C., (1977).

79N2. National Bureau of Standards, Certificate of Analysis, Standard Reference Material 1566, Oyster Tissue, Washington, D.C., (1977).

77N3. National Bureau of Standards, Certificate of Analysis, Standard Reference Material 1648, Urban Paritculate Matter, Washington, D.C., (1977).

77N4. National Bureau of Standards, Report of Investigation Research Material 50, Albacore Tuna, Washington, D.C., (1977).

65N1. Nowlin, C.H. and Blakenship, J.L., Rev. Sci. Instr., 36 (1965) 1830.

75P1. Paciga, J.J., *Trace Element Characterization and Size Distributions of Atmospheric Particulate Matter in Toronto*, Ph.D. Thesis, Univ. of Toronto, Toronto, (1975).

69R1. Roberts, R.M., Gilbert, J.C., Rodewald, L.B. and Wingrove, A.S., *An Introduction to Modern Experimental Organic Chemistry*, Holt, Rinehart and Winston, Inc., N.Y. (1969).

77R1. Roscoe, B.A. and Furr, A.K., Nucl. Instr. and Meth., 140 (1977) 401-404.

72R1. Rositto, F., Terrani, M. and Terrani, S., Nucl. Instr. and Meth., 103 (1972) 77.

77R2. Rowe, J.J. and Steinnes, E., J. Radioanal. Chem., 37 (1977) 849.

10R1. Rutherford, E. and Geiger, H., Phil. Mag., 20 (1910) 698.

78R1. Ryan, D.E., Stuart, D.C. and Chattopadhyay, A., Anal. Chim. Acta, 100 (1978) 87-93.

66S1. Schonfeld, E., Nucl. Instr. and Meth., 42 (1966) 213.

05S1. von Schweidler, E., Congress Intern. de Radiologie, Leige (1905).

74S1. Spyrou, N.M., Ingle, K. and Ozek, F., Proc. 2nd Intern. Conf. on Nuclear Methods in Environmental Research, J.R. Vogt and W. Meyer, Eds., Univ. of Missouri, Columbia, Mo. (1974) 151.

79S2. Spyrou, N.M. and Kerr, S.A., J. Radioanal. Chem., 48 (1979) 169-183.

71S1. Steinnes, E., *Epithermal Neutron Activation of Geological Materials in Activation Analysis in Geochemistry and Cosmochemistry*, A.O. Brunfelt and E. Steinnes, Eds., Universitets Forlaget, Oslo, Norway, (1971) 113-128.

76S1. Steinnes, E. and Rowe, J.R., Anal. Chim. Acta, 87 (1976) 451.

68S1. Strauss, M.G., Sifter, L.L., Lenkszus, F.R. and Brenner, R., IEE Trans. Nucl. Sci., NS-15, 3 (1968) 518.

67S1. Strauss, M.G., Sherman, I.S., Brenner, R., Rudnik, S.J., Larsen, R.N. and Mann, H.M., Rev. Sci. Instr., 38 (1967) 725.

79S1. Sanderman, M., M.Sc. Thesis, Dalhousie Univ., Halifax, (1979).

79T1. Tominaga, H. and Tachikawa, N., Radiochem. Radioanal. Lett., 37 (1979) 55-60.

79T2. Tout, R., private communication.

81T1. Tout, R. and Chatt, A., Anal. Chim. Acta, in press, (1981).

73T1. Tracor Northern-ADC Manual, Northern Scientific Inc., Middleton, Wisconsin, U.S.A., (1975).

80T1. Tse, C.S., Ph.D. Thesis, Dalhousie Univ., Halifax, (1980).

80V1. van der Sloot, H.A., Walls, G.D., Weers, C.A. and Das, H.A., Anal. Chem., 52 (1980) 112.

65V1. Vogt, J.R. and Ehmann, W.D., Proc. 1965 Intern. Conf. on Modern Trends in Activation Analysis, College Station, Texas, April 19-22 (1965) 82.

78W1. Walpole, R.E. and Myers, R.H., *Probability and Statistics for Engineers and Scientists*, 2nd Edition, (1978).

71W1. Wiernik, M., Nucl. Instr. and Meth., 95 (1971) 13-18.

71W2. Wiernik, M., Nucl. Instr. and Meth., 96 (1971) 325.

69W1. Wiernik, M. and Amiel, S., J. Radioanal. Chem., 3 (1969) 245.

79W1. Westphal, G.P., Nucl. Instr. and Meth., 163 (1979) 189-196.

68W1. Williams, C.W., IEEE, Trans. Nucl. Sci., NS-15 (1968) 297.

79W2. Woittiez, J.R.W., Zonderhuis, J., Faanhof, A. and Das, H.A., J. Radioanal. Chem., 53 (1979) 191-201.

71W3. Wyttenbach, A., J. Radioanal. Chem., 8 (1971) 335.

APPENDIX-A. Electronic circuit for measurement of ADC dead-time

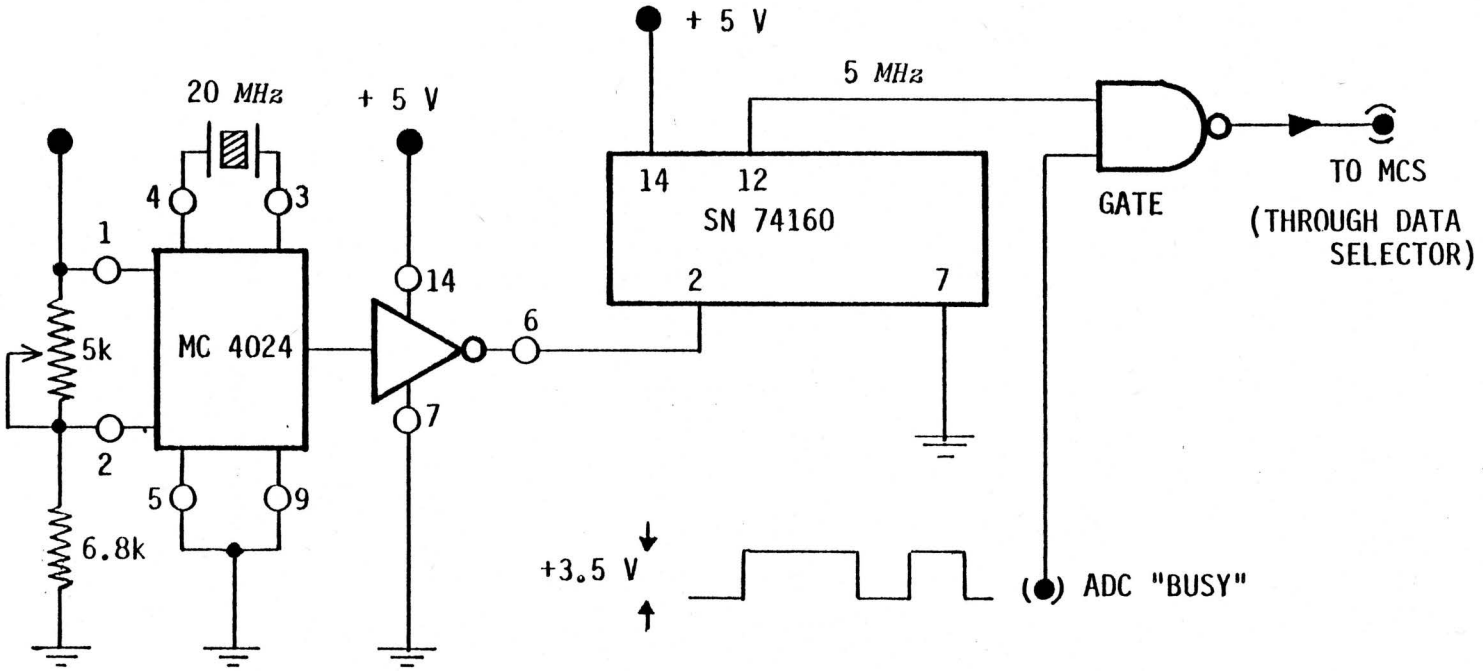

APPENDIX B. Data selector circuit for alternate measurements of ADC "BUSY" and "SCA OUT" signals

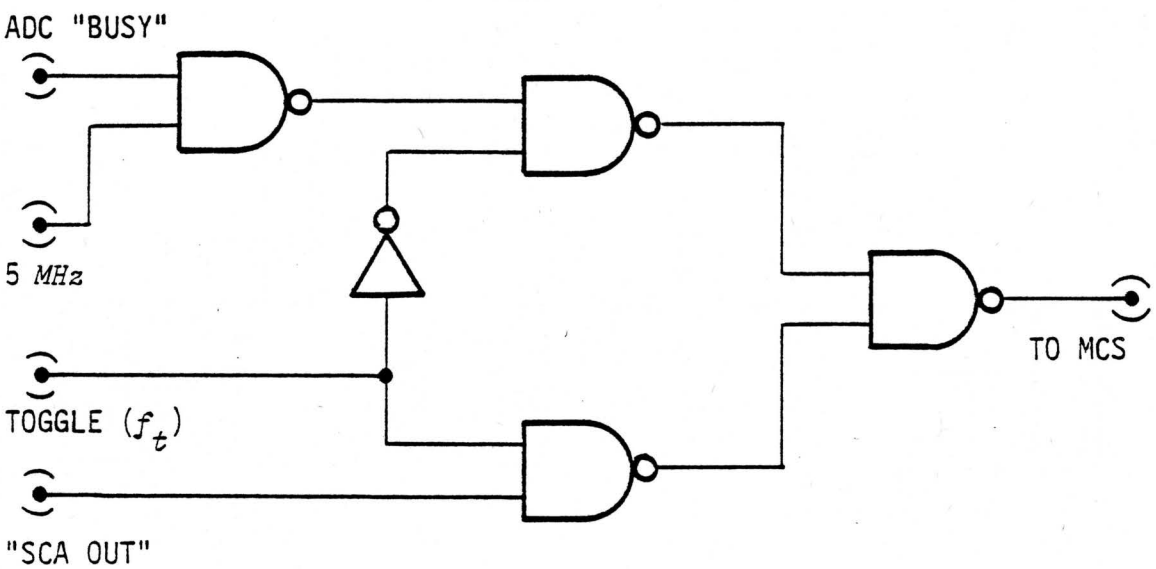

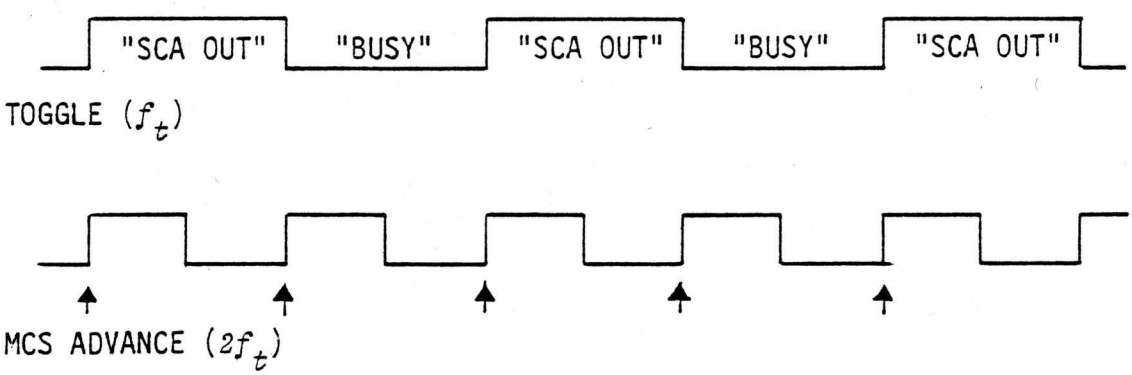

APPENDIX C. The circuit diagram of the delay timer for automatic recycling of the sample

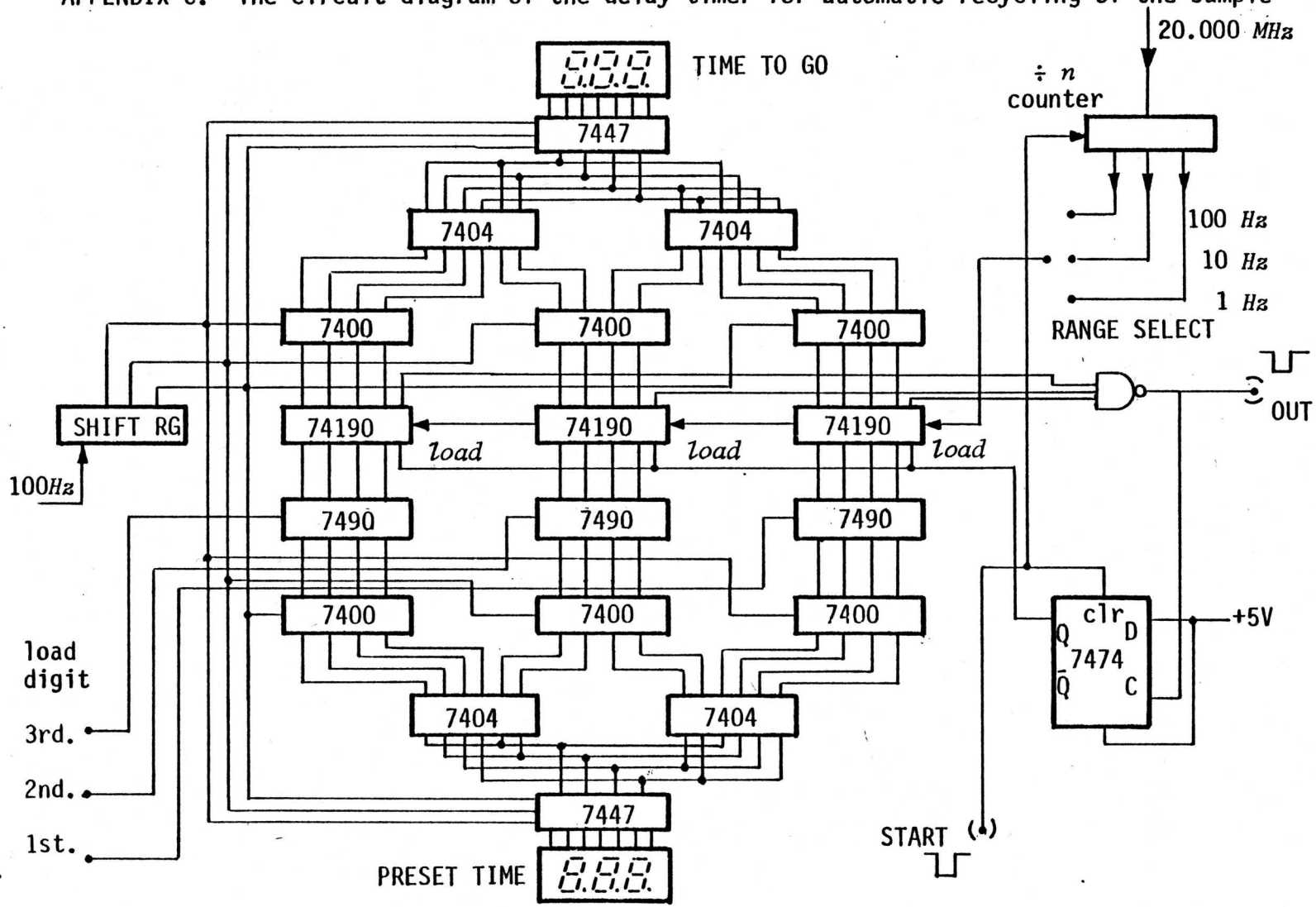

APPENDIX D. The circuit for electronic triggering of TN-11 Multichannel Analyser

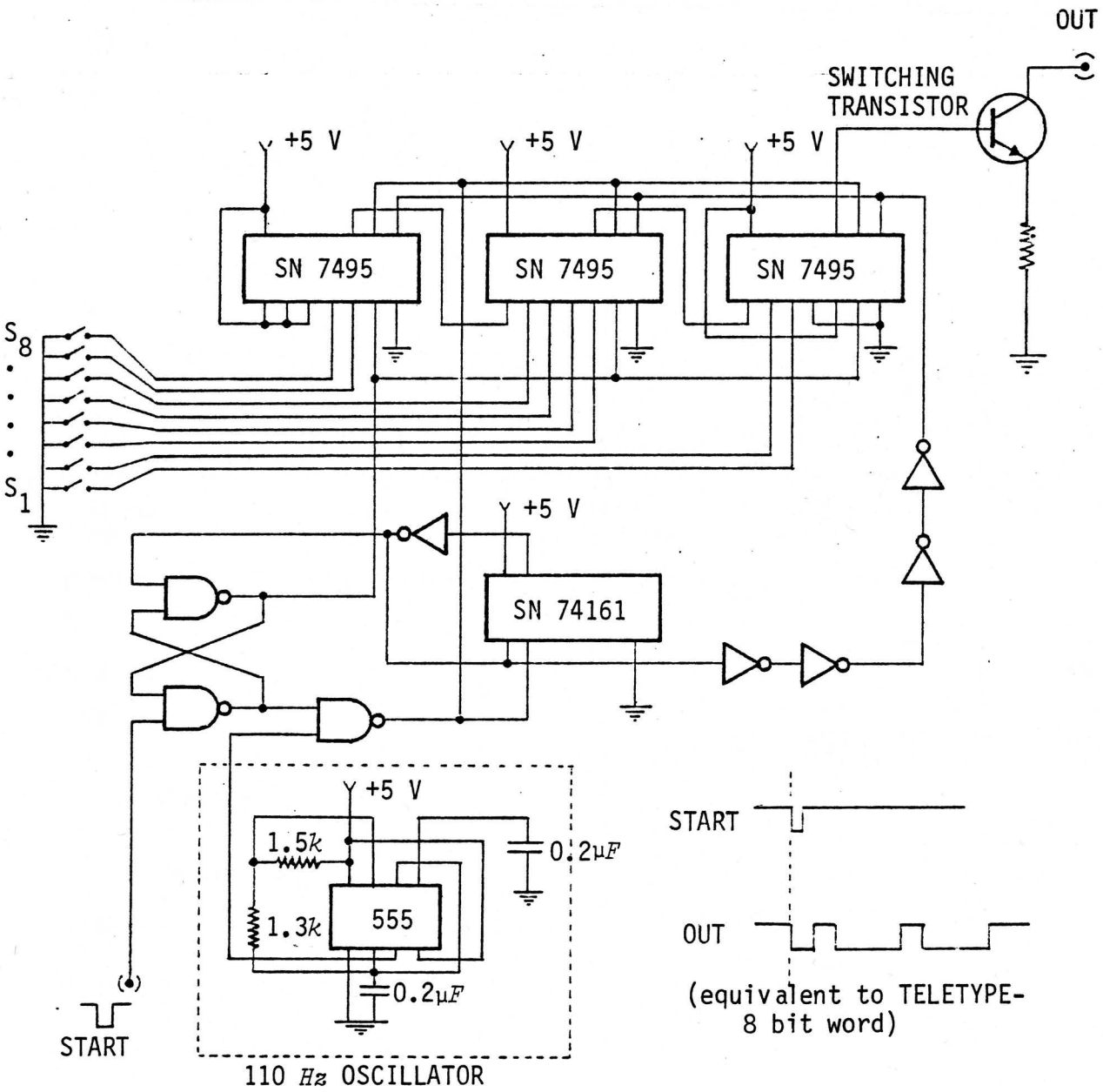

APPENDIX E. Circuit diagram of the electronic regular pulser